University of Naples Federico II

Department of Chemical, Materials and Production Engineering
(DICMaPI)

PhD Program

"INDUSTRIAL PRODUCT AND PROCESS ENGINEERING"

XXIX cycle

"Design and Synthesis of Hybrid Ceramic Foams with Tailored Porosity"

Tutors

Prof. B. Liguori

Prof. D. Caputo

Dr. L.Verdolotti

Dr. M. Lavorgna

PhD student

Ilaria Capasso

To the ones who dream,

foolish as they might seem.…

"Men love to wonder, and that is the seed of science"

R.W. Emerson

Summary

Introduction 1
1. Ceramic Foams: definition, production and properties 3
1.1 Ceramic materials 3
1.2 Cellular solids 6
1.3 Ceramic Materials with Tailored Porosity 10
1.4 Manufacturing of ceramic foams 12
Influence of processing on structure, properties and other characteristics 12
Processing methods 13
Replica technique 15
Sacrificial Template Method 18
Direct Foaming 22
Bibliography 28
2. Geopolymers: innovative eco-sustainable binders 34
2.1 Geopolymer definition and hystorical background 34
2.2 Reaction of geopolymerization 36
2.3 Raw materials 40
Aluminosilcate sources 40
Alkali activators 43
2.4 Properties and application of geopolymers 44
Mechanical properties 47
2.5 Geopolymer as sustainbale binders: comparison with Portland cement 49
2.6 Geopolymer as chemically bonded ceramics 51
Bibliography 53
3. Design and synthesis of hybrid geopolymeric foams 61
3.1 Foaming techniques 62
Chemical foaming 62
Mechanical foaming 63
Evaluation of foaming properties 64
3.2 Materials 66
Metakaolin 66
Sodium silicate solution 70
Sodium hexafluorosilicate 70
Metal Silicon 71
Vegetable surfactant 72

3.3 Design of geopolymeric foams ... 73
3.4 Preparation of geopolymeric foams ... 74
3.5 Optimization of process parameters affecting final foam properties ... 76
Bibliography ... 80
4. Characterization of hybrid ceramic foams ... 83
4.1 Mechanical characterization ... 83
4.2 Morphological characterization ... 87
4.3 Porosimetric characterization ... 91
4.4 Chemical characterization (FTIR spectroscopy) ... 92
Bibliography ... 97
5. Hybrid ceramic foams with hierarchical porosity: addition of different levels of porosities ... 98
5.1 Use of diatomite as nanometric porosity source ... 99
Diatomite and its characterization ... 99
Production of foams with diatomite addition ... 104
5.2 Properties of the produced ceramic foams ... 105
Mechanical characterization ... 105
Morphology of hybrid foams ... 110
Porosity characterization ... 115
Mercury intrusion porosimetry ... 119
Chemical and mineralogical characterization ... 120
Acoustic characterization ... 123
Thermal stability ... 124
Fire behavior ... 128
Thermal conductivity ... 132
5.3 Use of 3D printing inverse replica method to create macroporosity ... 133
Additive manufacturing and 3D printing process ... 133
Stereolithography Process ... 134
Autodesk Ember 3D-Printer ... 135
Design and printing of templates ... 137
5.4 Production of hybrid ceramic foams using 3D printing inverse replica ... 138
Microstructural characterization of ceramic foams produced ... 139
Influence of template geometry ... 142
Bibliography ... 145
Conclusions ... 149

Introduction

Geopolymers are alkali-bonded ceramics belonging to the class of chemically bonded materials, produced at low temperatures using chemical reactions. Alkali-bonded ceramics constitute a family of materials with properties varying between those characteristic of ceramics, cements, zeolites or refractories, depending on formulation. These characteristics arise from a number of beneficial features, including rapid development of mechanical strength, fire resistance, dimensional stability, acid resistance, excellent adherence to aggregates and reinforcements, thermal and acoustic insulation, etc. So geopolymers proved to be appealing for an increasing number of innovative applications, such as catalysis [1], filter, biomaterials [2], heat exchangers and thermal insulation

The goal of designing tailored geopolymers is pursued intensively, allowing exploitation of the full technological potential of these materials. Reticulated porous ceramics characterized by high porosity (70–95%) are expected to be applied in many different technological fields thanks to their high gas permeability, large surface area, high temperature stability, and thermal shock resistance [3]. Industrial uses include structural lightened parts, insulator panels, filters, and membranes (for micro- and ultra-filtration, separation, particulate environmental clean-up and reuse and molten metal filters), radiant burners, gas or chemical sensors, and support materials for catalysis or adsorbents [3]. For all the above-mentioned applications, it is absolutely necessary to control the pore structure (shape, morphology, orientation, surface properties), as well as the texture, the total porosity, and the pore size distribution. Several ways to produce macroporous ceramics have been reported including sacrificial template, replica and direct foaming methods [4]. Processing methods that rely on the template-free direct deposition of materials, such as three-dimensional (3D) printing, extrusion, and spinning processes complete the most important set of techniques available for the creation of macroporous materials [5]. The macroporous structures obtained via these approaches can be further modified to incorporate additional pores at smaller length scales, leading to truly hierarchical porous architectures [5].

The aim of this PhD research activity is the design and synthesis of hybrid foams with hierachical porosity starting from a ceramic matrix based on alkali activated alumino-silicate structures. Alkali-bonded ceramic foams have already very interesting

applications as thermal and acoustic insulators, catalysts, filters, which can be extended by tailoring their porosity in the nano-to-ultramacro range. In fact, materials with tailored porosity exhibit special properties and features that usually cannot be achieved by their conventional dense counterparts. Moreover chemical consolidation by geopolymerization can be considered a sustainable alternative to produce ceramic foams with 3D porous architectures without using high temperatures treatments (such as burnout of organics and sintering).

Alkali activated ceramic foams have been produced by using metakaolin and/or diatomite as aluminosilicate source, an aqueous sodium silicate solution as alkali activator and Na_2SiF_6 as a catalyst that promotes the gelification of the entire system. Two different techniques of direct foaming have been coupled, one based on chemical reactions with gas production and the other one based on a mechanical foaming. Then, other levels of hierarchical porosity (nanometric and macrometric scale) have been added to the produced expanded ceramic systems. This approach allows to tailor the chemical–physical properties and density of the resulted hybrid foams. The produced foams have been mechanically, chemically, physically and morphologically characterized. Moreover, their acoustic and thermal properties, in terms of thermal stability and conductivity, and also their fire behavior have been investigated.

References

[1] P. Sazama, O. Bortnovsky, J. Dedecek, Z. Tvaruzkov, Z. Sobalik, Geopolymer based catalysts—new group of catalytic materials, Catalysis Today, 164, (2011), 92–99.

[2] H. Oudadesse, A.C. Derrien, M. Lefloch, J. Davidovits, MAS-NMR studies of geopolymers heat-treated for applications in biomaterials field, Journal of Materials Science, 42, (2007) 3092–3098.

[3] P. Colombo, Conventional and novel processing methods for cellular ceramics, Philosophical Transactions of the Royal Society of London, Series A 364, (2006) 109–124.

[4] A.R. Studart, U.T. Gonzenbach, E. Tervoort, L.J. Gauckler, Processing routes to macroporous ceramics: a review, J. Am. Ceram. Soc.89 (2006) 1771–1789.

[5] A.R Studart, Additive manufacturing of biologically-inspired materials, Chem. Soc. Rev, 45, (2016) 359-376

1. Ceramic Foams: definition, production and properties

1.1 Ceramic materials

The word *"ceramic"* comes from the Greek word κεραμικός (*keramikos*), which derives from κέραμος (*keramos*) which means "potter's clay" or "pottery". Its origin is a Sanskrit term meaning "to burn". The early Greeks used the word "keramos" for describing products obtained by heating clay-containing materials. The term has long included all products made from fired clay, like, for example, bricks, fireclay, refractories, sanitary ware and tableware. So the earliest ceramics made by humans were pottery objects, including 27,000-year-old figurines, made from clay, either by itself or mixed with other materials, like silica, hardened, sintered in fire. Later ceramics were glazed and fired to create smooth, colored surfaces, decreasing porosity through the use of glassy, amorphous ceramic coatings on top of the crystalline ceramic substrates [1]. In 1822, silica refractories were first made; although they contained no clay, the traditional ceramic process of shaping, drying and firing was used to make them. So the term "ceramic", while retaining its original sense of a product made from clay, began to include other products made by the same manufacturing process [1]. Modern ceramics include domestic, industrial and building products, as well as a wide range of ceramic art. In the 20th century, new ceramic materials were developed for use in advanced ceramic engineering, such as in semiconductors.

The field of ceramics, broader than the materials themselves, can be defined as the art and science of making and using solid articles that contain as their essential component a ceramic. This definition covers the purification of raw materials, the study and production of the chemical compounds concerned, their formation into components, and the study of structure, composition, and properties [1].

Ceramics are usually associated with "mixed" bonding, a combination of covalent, ionic, and sometimes metallic. They consist of arrays of interconnected atoms; there are no discrete molecules. This characteristic distinguishes ceramics from molecular solids, such as iodine crystals, and paraffin wax (composed of long-chain alkane molecules). The majority of ceramics are compounds of metals or metalloids and nonmetals. Most frequently they are oxides, nitrides, and carbides. Richerson [2] says, "most solid materials that are not metal, plastic, or derived from plants or animals are ceramics". The most widely accepted definition of a ceramic is given by Kingery et al. [3]: "A ceramic

is a nonmetallic, inorganic solid". Thus all inorganic semiconductors are ceramics. By definition, a material ceases to be a ceramic when it is melted.

Ceramics generally have some specific properties such as:

- *Brittleness*. The reason that the majority of ceramics are brittle is the mixed ionic-covalent bonding that holds the constituent atoms together. At high temperatures (above the glass transition temperature) glass no longer behaves in a brittle manner; it behaves as a viscous liquid. That is why it is easy to form glass into intricate shapes.
- *Poor electrical and thermal conduction*. The valence electrons are tied up in bonds, and are not free as they are in metals. In metals it is the free electrons, the electron gas, that determines many of their electrical and thermal properties. Diamond, which is classified as a ceramic has the highest thermal conductivity of any known material.
- *Compressive strength*. Ceramics are stronger in compression than in tension, whereas metals have comparable tensile and compressive strengths. This difference is important when we use ceramic components for load-bearing applications. It is necessary to consider the stress distributions in the ceramic to ensure that they are compressive. An important example is in the design of concrete bridges—the concrete, must be kept in compression. Ceramics generally have low toughness, although combining them in composites can dramatically improve this property.
- *Chemical insensitivity*. A large number of ceramics are stable in both harsh chemical and thermal environments. Pyrex glass is used widely in chemistry laboratories specifically because it is resistant to many corrosive chemicals, stable at high temperatures (it does not soften until 1100 K), and is resistant to thermal shock because of its low coefficient of thermal expansion (33×10^{-7} K^{-1}). It is also widely used in bakeware.
- *Transparency*. Many ceramics are transparent because they have a large *E*g. Examples include sapphire watch covers, precious stones, and optical fibers. [1]

Although it is always possible to find at least one ceramic that shows atypical behavior, the properties mentioned above are in many cases different from those shown by metals and polymers and so can be considered typical of this category of materials.

Considering the large number of materials the can be considered ceramics, the applications for these materials are very diverse, from bricks and tiles to electronic and magnetic components. These applications use the wide range of properties exhibited by ceramics. Some of these properties are listed in Table 1.1 together with examples of specific ceramics and applications. The functions of ceramic products are dependent on their chemical composition and microstructure, which determines their properties. It is the interrelationship between structure and properties that is a key element of materials science and engineering [1].

Table 1.1.Properties and applications for ceramic materials [1]

Property	*Example*	*Application*
Electrical	$Bi_2Ru_2O_7$	Conductive component in thick-film resistors
	Doped ZrO_2	Electrolyte in solid-oxide fuel cells
	Indium tin oxide (ITO)	Transparent electrode
	SiC	Furnace elements for resistive heating
	$YBaCuO_7$	Superconducting quantum interference devices (SQUIDs)
	SnO_2	Electrodes for electric glass melting furnaces
Dielectric	α-Al_2O_3	Spark plug insulator
	$PbZr_{0.5}Ti_{0.5}O_3$ (PZT)	Micropumps
	SiO_2	Furnace bricks
	$(Ba,Sr)TiO_3$	Dynamic random access memories (DRAMs)
	Lead magnesium niobate (PMN)	Chip capacitors
Magnetic	γ-Fe_2O_3	Recording tapes
	$Mn_{0.4}Zn_{0.6}Fe_2O_4$	Transformer cores in touch tone telephones
	$BaFe_{12}O_{19}$	Permanent magnets in loudspeakers
	$Y_{2.66}Gd_{0.34}Fe_{4.22}Al_{0.68}Mn_{0.09}O_{12}$	Radar phase shifters
Optical	Doped SiO_2	Optical fibers
	α-Al_2O_3	Transparent envelopes in street lamps
	Doped $ZrSiO_4$	Ceramic colors
	Doped (Zn,Cd)S	Fluorescent screens for electron microscopes
	$Pb_{1-x}La_x(Zr_zTi_{1-z})_{1-x/4}O_3$ (PLZT)	Thin-film optical switches
	Nd doped $Y_3Al_5O_{12}$	Solid-state lasers
Mechanical	TiN	Wear-resistant coatings
	SiC	Abrasives for polishing
	Diamond	Cutting tools
	Si_3N_4	Engine components
	Al_2O_3	Hip implants
Thermal	SiO_2	Space shuttle insulation tiles
	Al_2O_3 and AlN	Packages for integrated circuits
	Lithium-aluminosilicate glass ceramics	Supports for telescope mirrors
	Pyrex glass	Laboratory glassware and cookware

It is common to classify ceramic materials as traditional or advanced. Traditional ceramics include high-volume items such bricks and tiles, toilet bowls (white wares), and pottery. Advanced ceramics include newer materials such as laser host materials, piezoelectric ceramics, ceramics for dynamic random access memories (DRAMs), etc., often produced in small quantities with higher prices. There are other characteristics that separate these categories. Traditional ceramics are usually based on clay and silica. There

is sometimes a tendency to equate traditional ceramics with low technology, however, advanced manufacturing techniques are often used. Competition among producers has caused processing to become more efficient and cost effective. Complex tooling and machinery is often used and may be coupled with computer-assisted process control. Advanced ceramics are also referred to as "special," "technical," or "engineering" ceramics. They exhibit superior mechanical properties, corrosion/oxidation resistance, or electrical, optical, and/or magnetic properties. While traditional clay-based ceramics have been used for over 25,000 years, advanced ceramics have generally been developed within the last 100 years [1].

It is well known that ceramic materials offer many distinct advantages over other materials such as polymers or metals; particularly the properties of hardness, chemical inertness, thermal shock resistance, corrosion and wear resistance and low density are the qualities that are essential to many applications [4, 5]. In particular, there is a specific class of ceramic materials, the advanced porous ceramics, also called ceramic foams, which are being utilized in a broad range of applications in order to mitigate several environmental, biological and transportation related issues facing society [6]. The presence of porosity in the material is often viewed as problematic, but there are, however, many applications in which the use of porous materials can be advantageous, e.g., refractories, high temperature filters, catalytic substrates, thermal insulation, gas burner materials, etc. Although the primary function of these materials may not be structural, many of these applications require a high degree of mechanical reliability.

1.2 Cellular solids

Cellular solids – ceramics, polymers, metals – have properties that depend on both topology and material. Of the three classes, polymer foams are the most widely investigated, and it is from these studies that much of the current understanding derives. Recent advances in techniques for foaming metals has led to their intense study, extending the understanding. Of the three classes, ceramic foams are the least well characterized. Their rapidly growing importance as filters, catalyst supports, membranes, and scaffolds for cell growth has stimulated much recent scientific works. The underlying principles that influence cellular properties are common to all three classes.

Mainly three factors dominate (Figure 1):

- The properties of the solid of which the foam is made.
- The topology (connectivity) and shape of the cells.
- The relative density ρ/ρ_s of the foam, where ρ is the density of the foam and ρ_s that of the solid of which it is made [7].

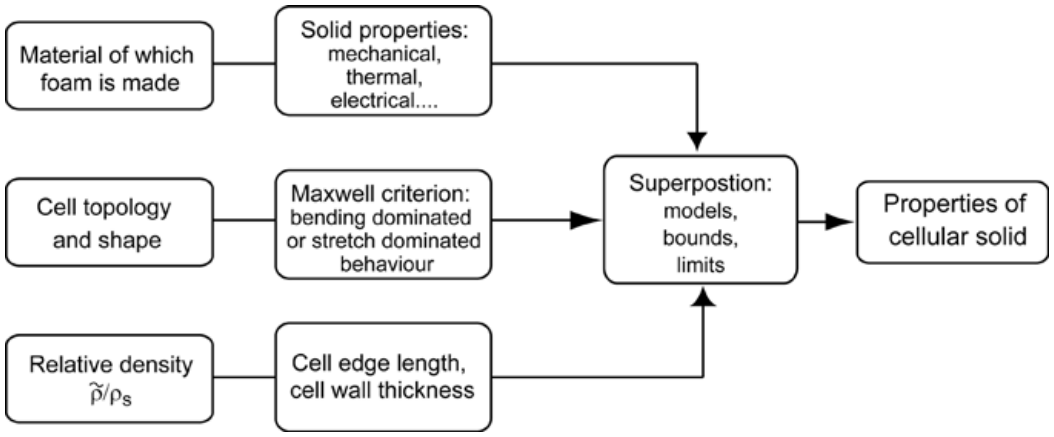

Figure 1.1 Schematic summary of the factors influencing the properties of cellular solids [7]

Cellular ceramics constitute a specific class of materials containing a high level of porosity (greater than 60 vol%) which are characterized by the presence of a recognizable 'cell', that is an enclosed empty space possessing faces and solid edges [4]. Cellular ceramics are comprised of various arrangements of a space-filling polygons (cells) and can be classified into two broad groups:

- Foams
- Honeycombs

In honeycombs the cells form a two-dimensional array (Figure 1.2), whereas foams are comprised of a three dimensional array of hollow polygons [8]. An example of the microstructure of ceramic foam is reported in Figure 1.3.

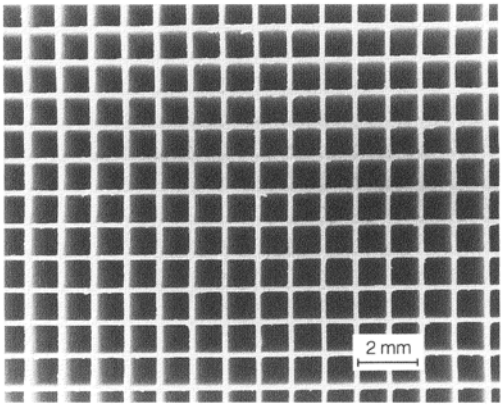

Figure 1.2 Microstructure of ceramic honeycomb consisting of square prismatic cells.

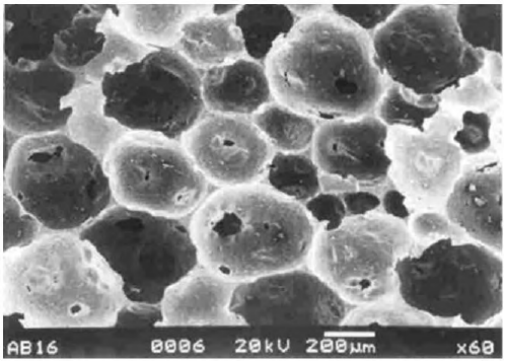

Figure 1.3 Microstructure of ceramic foam (alumina foam) consisting of three-dimensional array of hollow polygons.

The common feature of all the above cellular materials is a combination of solid and gaseous elements that are structured by more or less defined regular geometric shapes and positions. Cellular materials differ from the "conventional" materials by the combination of a solid phase with closed or open regularly structured voids, tubes, or any other type of inhomogenities, such as pores. These inhomogenities change the mechanical, thermal, acoustic and electrical properties of cellular materials drastically if they differ from the ceramic. The most common inhomogenities are pores in a great variety of shapes and sizes. The general effects of porosity, such as dilution of one material, and the specific effects of porosity, which include effects determined by shape and distribution, are interlinked [7].

Cellular ceramics are divided into two general categories consisting of either open or closed cells. In particular foams are usually sub-divided into two further categories, depending on whether or not the individual cells possess solid faces [8]. Some foams have *closed cells* (like a soap foam), in this case the solid material is distributed in little plates

which form the faces of the cells; other foams have *open cells* (like a sponge), it means that the solid material is distributed in little columns or beams which form the cell edges. The mechanical properties reflect, to some extent, this distribution. In reality, most man-made foams, even those with closed cell faces, behave like open-celled foams because surface tension draws much of the solid material into the cell edges during manufacture [9]. The microstructure of the two different kinds of cellular ceramic are reported in Figure 1.4.

Figure 1.5 shows in detail the specific nomenclature of the corresponding structural elements typical of porous materials.

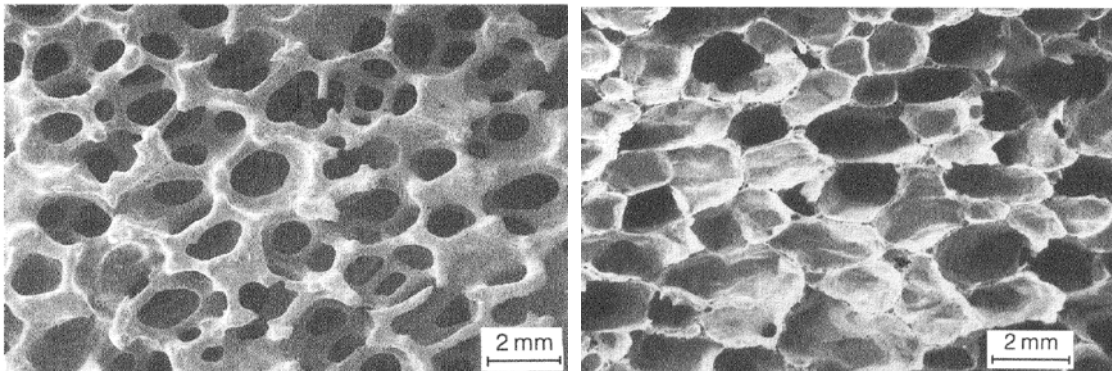

(a) (b)

Figure 1.4 Microstructure of three dimensional cellular ceramic with open cells (a) and closed cells (b)

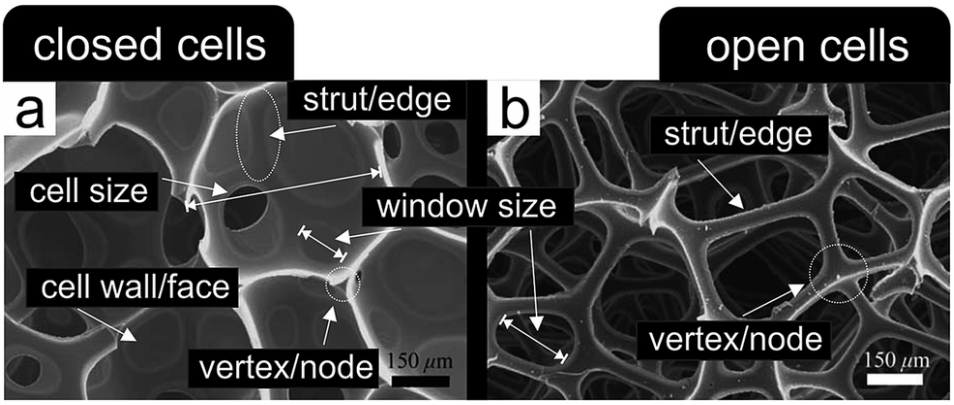

Figure 1.5 Nomenclature of the structural elements building up cellular porous materials [10].

Because of their structure, cellular materials possess a number of favorable properties, like low density, low thermal conductivity, thermal stability, high specific strength and high resistance to chemical attack, which make them suitable for a variety of applications [11]. In fact, porous ceramics can be used in exhaust filters, molten metal and hot gases filtration, catalyst supports, refractories, thermal insulation, heat exchangers, porous implants in the area of biomaterials and lightweight structures [12-17]. Each application needs specific features and properties of porous ceramics; they may differ in terms of porosity, strength, pore size distribution, pore morphology and pore connectivity. For effective thermal insulation, for example, it is favorable to have closed porosity whereas for filters and membranes open porosity is a must. In the bioceramics field it is desirable to use porous ceramic implants with certain porosity to promote integration with biological tissues [18].

So, over the past few years, there has been a significant increase in interest in the production and use of highly porous ceramic materials.

1.3 Ceramic Materials with Tailored Porosity

As already mentioned above, contrary to metallic and polymeric porous structures, pores have been traditionally avoided in ceramic components because of their inherently brittle nature. However, an increasing number of applications that require porous ceramics have appeared in the last decades, especially for environments where high temperatures, extensive wear and corrosive media are involved. [5]

Ceramic foams are cellular structures composed of a three-dimensional network of struts. Figure 1.6 (a) shows the typical structure of a ceramic foam and Figure 1.6 (b) shows an example of ceramic foam microstucture.

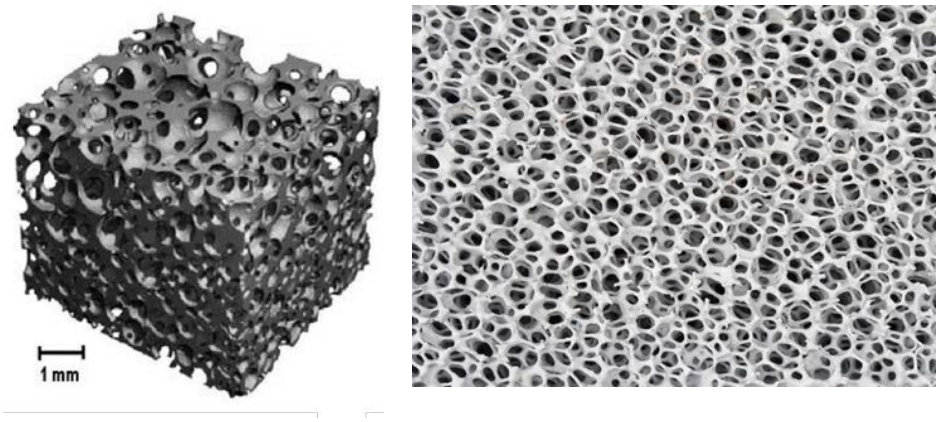

(a) (b)

Figure 1.6 Structure (a) and microstructure (b) of a ceramic foam

In Figure 1.7, some pictures of different kinds of commercial ceramic foams are reported.

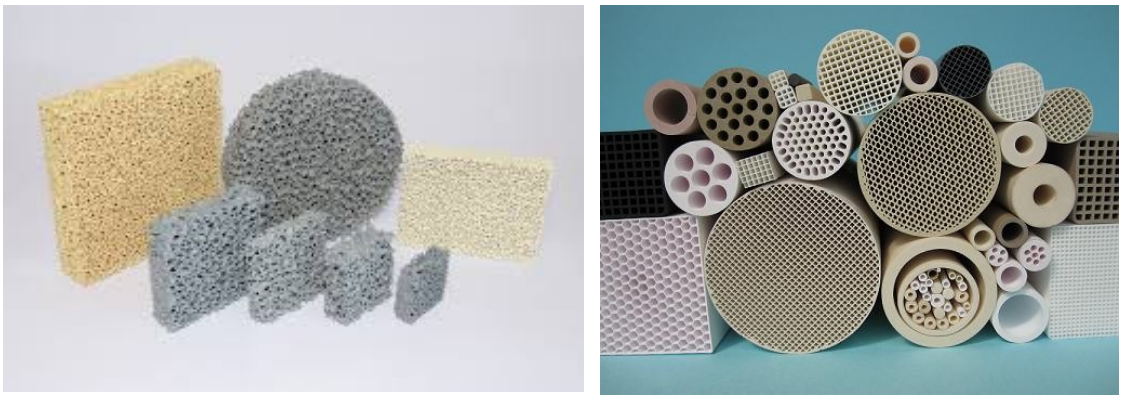

Figure 1.7 Different kinds of ceramic foams

The properties of this category of materials can be tailored for each specific application by controlling the composition and microstructure of the porous ceramic. Changes in open and closed porosity, pore size distribution, and pore morphology can have a major effect on a material's properties. All of these microstructural features are in turn highly influenced by the processing route used for the production of the porous material [5].

Parameters relating to the pore structure, such as pore size, shape, distribution, and connectivity all play into the resulting functionality of the porous ceramic material. For instance, the pores may offer insulating properties at high temperature, capture impurities in a filter, facilitate tissue growth in a bio-scaffold, or provide the architecture for reinforcement in a ceramic–metal composite. So, these materials may be designed to

possess the required properties for a particular application through the modification and optimization of processing techniques, and they can be tailored to possess the desired properties through the control of the microstructure [5, 19].

1.4 Manufacturing of ceramic foams

Influence of processing on structure, properties and other characteristics

A wide range of processing routes have been proposed for the production of cellular ceramics, employing raw materials of various nature and leading to a variety of morphologies. The fabrication processes for porous ceramics have been subject to much consideration in order to accommodate and satisfy the wide range of property demands for specific applications [19]. It is important to point out that processing can strongly influence various characteristics of cellular ceramics. Concerning the macrostructure, for instance, closed cell materials or components with graded or anisotropic porosity can be obtained only through specific manufacturing processes [4]. Furthermore, each fabrication method is best suited for producing a specific range of cell sizes, cell size distribution and overall amount of porosity [20], as well as influencing the level of interconnectedness among the cells and the presence, amount, thickness and orientation of the cell walls. The thickness of the struts is also influenced by the fabrication procedure and this parameter, together with the relative density of the material, directly affects the strength of the components. The maximum size of the part and the range of shapes achievable depend also on the processing route.

Microstructural effects include the presence of hollow struts in ceramic foams produced by the replica technique and the development in extruded honeycombs of preferred orientation in the ceramic grains after sintering, due to the use of specific raw materials, as discussed by

Lachman et al. [21]. Surface finish, the composition of the grain boundaries and, especially, the flaw population (amount, size and morphology of the defects) in the ceramic material are also all dependent on the processing method used. Furthermore, for cost constraints as well as for limiting shrinkage during firing, the ceramic material comprising the ligaments and the cell walls of the cellular structure is often not fully sintered, leading to additional micro-porosity. Performance and properties depend naturally on the macro- and microstructure of the cellular ceramic component: the

presence of cell walls influences both permeability and strength, while compositional purity affects chemical and oxidation resistance, as well as high-temperature creep, electrical resistivity and thermal properties [4].

Compositional purity depends strongly on the processing method, with only some methods (e.g. chemical vapor deposition (CVD)) allowing the production of very pure materials. For some applications, high purity, stoichiometric ceramic materials are necessary, because they typically have higher strength and corrosion resistance than lower grade materials. Finally, each fabrication method differs in terms of overall cost, making some of them of interest for the production of a large number of low cost, single use components (e.g. filters for liquid metals), while others are more suited specifically for the development of high performance, high added value products (e.g. for the aerospace industry) [4].

As different applications usually require materials with different characteristics, it is strongly advisable to select the fabrication procedure according to the specific features needed in the final component.

Processing methods

Pores can be incorporated into the structure of a ceramic through many processing techniques. The most straightforward processing route for the preparation of porous ceramics is the partial sintering of initially porous powder compacts or the sintering of powder mixtures which undergo solid state reactions that lead to pore formation [22, 23]. This method often results in a relatively low porosity (<60 vol%), with pores homogeneously distributed within the microstructure.

In addition to such a straightforward approach, many novel methods for the preparation of porous ceramics with controlled microstructure have been developed in response to the increasing number of new potential applications for cellular ceramics [7]. Versatile techniques that allow one to deliberately tune the porosity, pore morphology and size distribution, and that can additionally be applied to ceramic materials of many different chemical compositions are especially demanded. Novel applications where specific chemical compositions and tailored microstructures are required include electrodes and supports for batteries and solid oxide fuel cells, scaffolds for bone replacement and tissue engineering, heating elements, chemical sensors, solar radiation conversion, among others.

Other traditional methods of fabricating porous ceramics can be divided into three basic processing techniques, schematically reported in Figure 1.8:

- Replica technique
- Sacrificial template
- Direct foaming

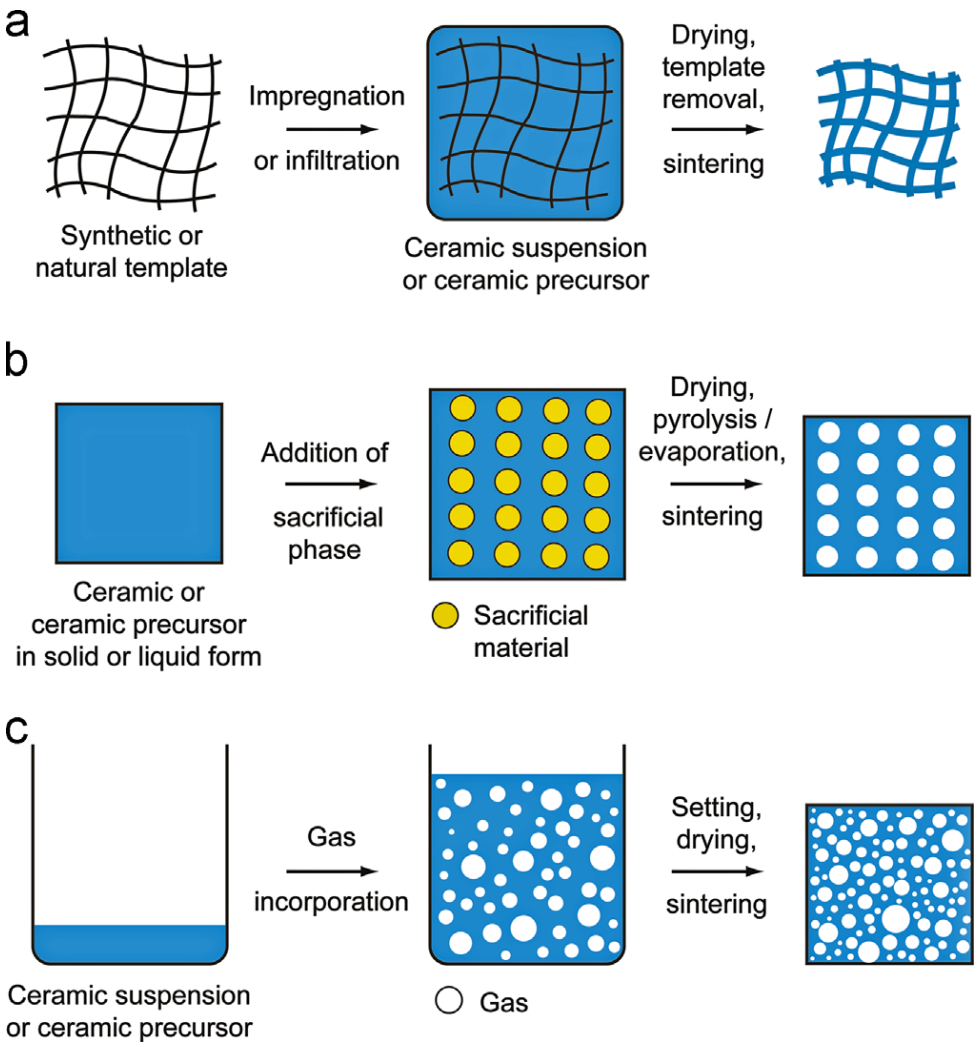

Figure 1.8 Typical processing methods for the production of macroporous ceramics:(a) replicatechnique;(b)sacrificial template technique and(c)direct foaming technique [5]

Depending on the processing method used, the final ceramic product obtained will have some specific features in terms of pore dimensions and, as a consequence, of final properties. Figure 1.9 shows the typical porosity and average pore size achieved via the replica, sacrificial templating, and direct foaming processing routes [5].

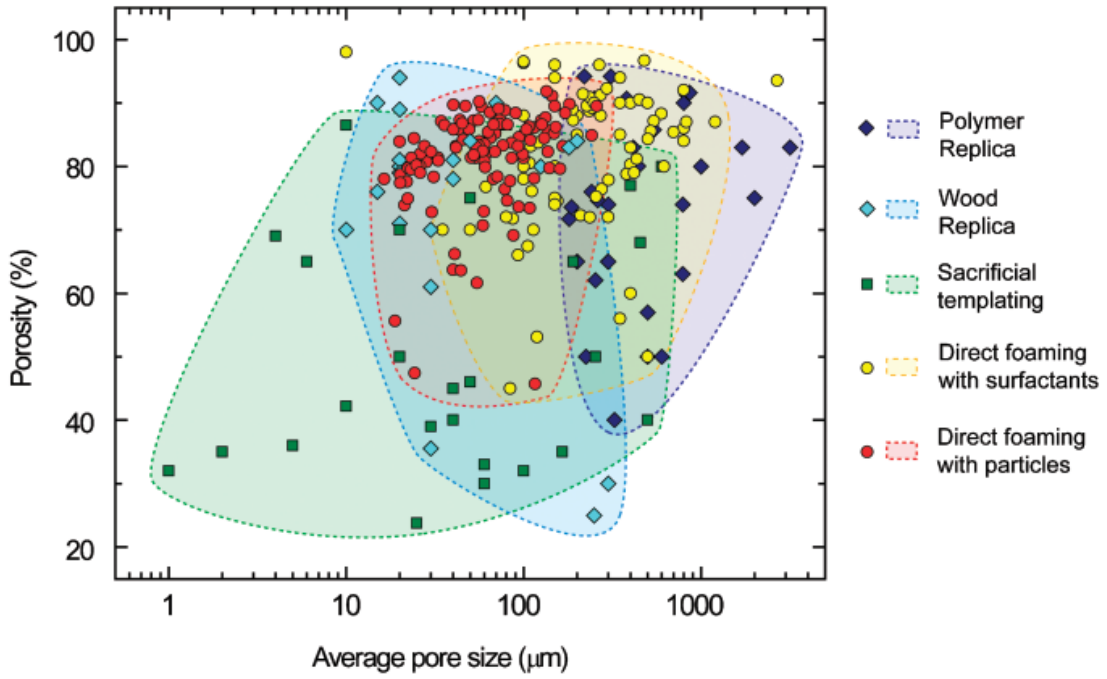

Figure 1.9 Typical porosity and average pore size achieved via the replica, sacrificial templating, and direct foaming processing routes.

Replica technique

The replica method is based on the impregnation of a cellular structure with a ceramic suspension or precursor solution in order to produce a macroporous ceramic exhibiting the same morphology as the original porous material (Fig. 1.8 (a)). Many synthetic and natural cellular structures can be used as templates to fabricate macroporous ceramics through the replica technique [5]. The replica technique is in fact considered as the first method deliberately used for the production of macroporous ceramics. The original invention dates back to the early 1960s, when Schwartzwalder and Somers [24] started using polymeric sponges as templates to prepare ceramic cellular structures of various pore sizes, porosities, and chemical compositions. Since then the sponge replica technique has become the most popular method to produce macroporous ceramics and is today extensively used in industry to prepare ceramic filters for molten metal filtration [25] and other applications. This success is primarily attributed to the simplicity and flexibility of the method. In the polymer replica approach, a highly porous polymeric sponge, typically polyurethane, but other polymers such as polyvinyl chloride, polystyrene, cellulose and latex have been tested successfully as well [4], is initially soaked into a ceramic

suspension until the internal pores are filled in with ceramic material. The organic foam must possess reproducible and suitable properties, such as the ability to regain its shape after squeezing, limited tolerances for the cell size and size distribution and complete and clean burn-out during sintering [4]. The impregnated sponge is then passed through rollers to remove the excess suspension and enable the formation of a thin ceramic coating over the struts of the original cellular structure. At this stage, the slurry has to be sufficiently fluid to be partially removed under the shearing conditions applied by the rollers, but the remaining ceramic wet coating should be viscous enough to avoid dripping. Therefore, ceramic suspensions exhibiting shear-thinning behavior are needed to efficiently coat the polymeric template [5]. The ceramic-coated polymeric template is subsequently dried and pyrolysed through careful heating between 300°C and 800°C [26]. Heating rates usually lower than 1°C/min are required in this step to allow for the gradual decomposition and diffusion of the polymeric material, avoiding the build-up of pressure within the coated struts [26]. Binders and plasticizers are added to the initial suspension in order to provide ceramic coatings sufficiently strong to prevent cracking the struts during pyrolysis. Typical binders used are colloidal aluminum orthophosphate, potassium and sodium silicates, magnesium orthoborate, hydratable alumina, colloidal silica, polyvinyl butyral with polyethylene glycol as plasticizer, and polymerizable monomers [26-29]. After removal of the polymeric template, the ceramic coating is finally densified by sintering in an appropriate atmosphere at temperatures ranging from 1100° to 1700°C depending on the material.

Only open-cell foams can be obtained through this process; in fact porous ceramics obtained with the sponge replica method can reach total open porosity levels within the range 40%–95% and, also because of limitations in the efficiency of infiltration and excess slip removal, they are characterized by a reticulated structure of highly interconnected pores with sizes between 200 mm and 3 mm [5]. Relative density ranges typically between 5 and 30% theoretically [4]. A disadvantage of the sponge replica technique is the fact that the struts of the reticulated structure are often cracked during pyrolysis of the polymeric template, markedly degrading the final mechanical strength of the porous ceramic [20]. Figure 1.10 shows that the strut flaws reduce the compressive strength of replica-derived porous ceramics to levels usually lower than the strength theoretically predicted for open cell structures.

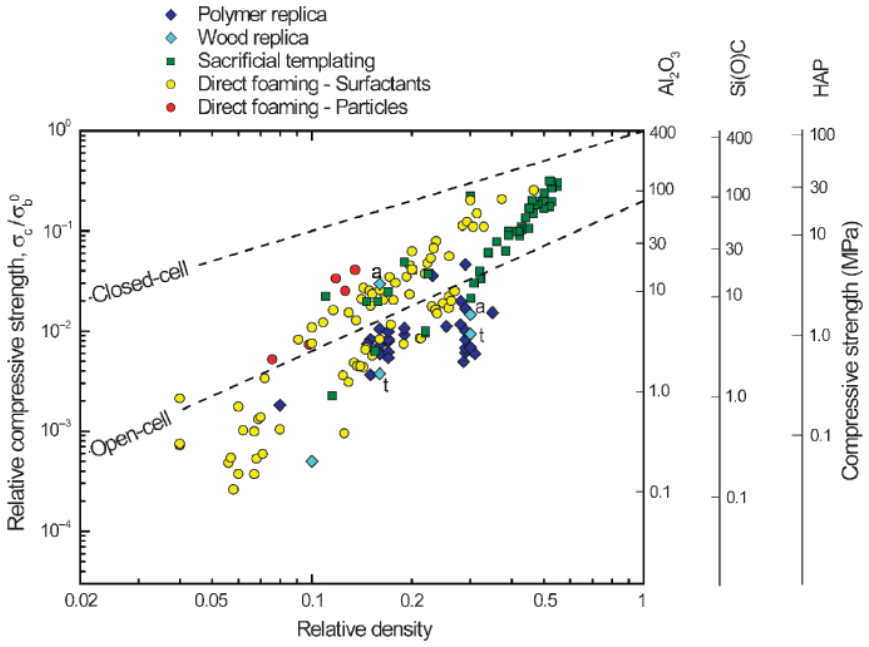

Figure 1.10 Relative compressive strength as a function of the relative density of macroporous ceramics produced via replica, sacrificial template and direct foaming methods.

A variation of the replication technique described previously is a process where the polymeric template is not burned out but pyrolysed to yield a pyrolytic carbon skeleton that can then be coated by a ceramic material, generally using the chemical vapor deposition [30]. The resulting structure is completely open cell with struts which are dense and multi layered, being comprised of a carbon core and an external layer—typically 10–1000 mm thick—of the chosen material (oxide, nitride, carbide ceramics as well as borides, silicides and metals). The carbon core is eliminated if the ceramic foam is employed in an oxidizing environment at elevated temperature, leading to a gradual modification mainly of the mechanical properties during use.

It has also been shown that, by repeating the impregnating of the polymeric template and drying steps several times, it is possible to increase the strut size and, thus, the strength of a ceramic foam, while only moderately increasing its bulk density or reducing permeability [31]. Alternatively, it is possible to recoat the reticulated ceramic foam after the sintering step [32, 33]; by coating with a low viscosity slurry, thicker struts are obtained, and the occurrence of large flaws is minimized by the recoating process. Additionally, low cost, low strength reticulated ceramic foams can be coated using CVD, resulting in a very large increase in strength, as well as an improvement in corrosion resistance [4].

In addition to synthetic polymer foams, other cellular structures have been used as templates for the fabrication of macroporous ceramics through the replica approach. Cellular structures available in nature are particularly interesting as natural replica templates, due mainly to their special pore morphology and intricate microstructures, which might be difficult to produce artificially [5]. For example, many investigators have studied the transformation of wood cellular structures into macroporous ceramics. The presence of oriented vessels in the structure of wood enables the preparation of macroporous ceramics with highly anisotropic aligned pores which cannot be achieved with the other replica techniques [34].

In Figure 1.11 an example of a synthetic hierarchical porous structure obtained using the replica method is reported, in particular the porous structure of rattan palm is the selected template. Typically, synthetic building blocks in the form of suspended particles, precursor sols, or molten phases are incorporated into the chosen porous template through an infiltration process. In this example, the infiltrated silicon partly reacts with carbon from the template to form a silicon–silicon carbide (SiSiC) porous structure [35].

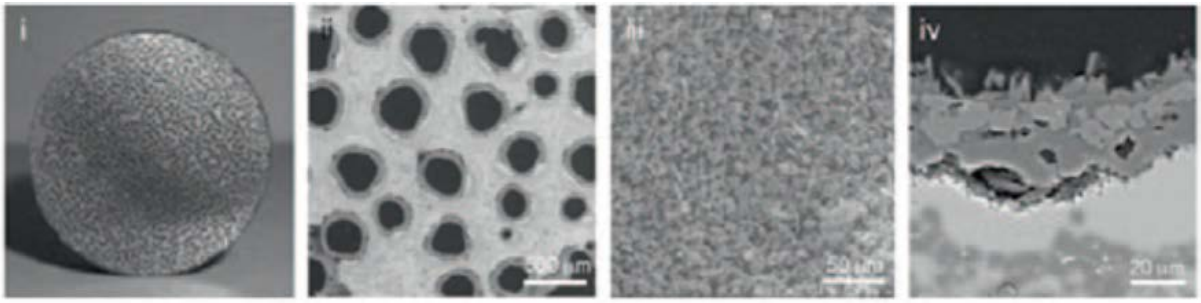

Figure 1.11 Rattan-derived silicon–silicon carbide (SiSiC) porous structure: (i) Transversal cross section of the structure. (ii) Closer view of the macropores generated after infiltration and pyrolysis of the original wood template at 1550°C. (iii) Microporous zeolite particles deposited on the macropore walls. (iv) Detailed lateral view of the zeolite layer on the surface of each macropore [35]

Sacrificial Template Method

The sacrificial template technique usually consists of the preparation of a biphasic composite comprising a continuous matrix of ceramic particles or ceramic precursors and a dispersed sacrificial phase that is initially homogeneously distributed throughout the matrix and is ultimately extracted to generate pores within the microstructure (Figure 1.8) [5]. In particular, hollow cells are produced when the solid material that occupies that

space within the volume of the component disappears during heating at high temperature. The way that the sacrificial material is extracted from the consolidated composite depends primarily on the type of pore former employed. A wide variety of sacrificial materials have been used as pore formers, including natural and synthetic organics, salts, liquids, metals, and ceramic compounds, some of the most used are listed in Table 1.2 [5]. Starch, wax, polymeric beads (polymethyl methacrylate, polystyrene, polyvinyl chloride), carbon black, sawdust have all been used with various degrees of success [36-38]. Synthetic and natural organics are often extracted through pyrolysis by applying long thermal treatments at temperatures between 200° and 600°C [39-41]. The long periods required for complete pyrolysis of the organic component, the extensive amount of gaseous by-products generated during this process and the mismatch in thermal expansion coefficient between the organic and inorganic phases that can also induce cracks within the porous structure during pyrolysis, are the main disadvantages of using organic materials as sacrificial phase [5].

Additionally, a dual-phase mixing approach can be adopted to create an open interconnected porosity [42]. Pore size and shape is obviously controlled by the characteristics of the sacrificial filler, and graded structures can be obtained by layering using fillers with varying dimensions.

Table 1.2 Examples of Sacrificial Template Methods Reported in the Literature [5]

Sacrificial template				
Synthetic organics	*Natural Organics*	*Salts*	*Metals/ceramics*	*Liquids*
PVC beads	Gelatine	NaCl	Nickel	Freeze-drying
PS beads	Peas and seeds	$BaSO_4$ and $SrSO_4$ K_2SO_4	Carbon (graphite, fiber, nanotubes)	Camphene
PEO or PVB beads	Cellulose/cotton		SiO_2 (particles, fibers)	Water
PMMA or PMMA-PEG beads	Glucide		ZnO	Emulsions-Oils
Phenolic resin	Sucrose			
Nylon	Dextrin			
Cellulose acetate	Wax			
Polymer gels	Alginate			
Naphtalene	Starch			

In order to produce a truly high porosity, cellular structure, a large volume of the porogen agent needs to be mixed with the ceramic phase [4]. This generally leads to the

development of a large amount of gas during sintering, and, thus, the process needs to be carefully controlled to avoid the formation of cracks in the ceramic body. The resulting foams can possess closed or open cells, depending on the volume fraction and nature (amount of gas generated and temperature at which gas development occurs) of the fugitive pore former. Non-fugitive inorganic phases, such as expandable perlite, have also been proposed as porogen agents [43], but their influence on the composition of the resulting ceramic phase needs to be taken into account. Recently [39, 44] using this approach and commercially available polymeric microbeads it has been possible to produce microcellular ceramic foams, both from preceramic polymer precursors and a conventional ceramic powder slurry, with cell size ranging from ca 1 to 100 mm and possessing enhanced mechanical properties.

The main drawback connected to the use of organic templates, can be partially overcome by using for example liquid pore formers such as water and oils or a solid phase that can be easily sublimated; Sacrificial materials such as salts, ceramic and metallic particles, on the other hand, are usually extracted by chemical rather than thermal means. The extraction of salts has been easily accomplished by repeatedly washing the composite with water [45, 46]. Ceramic and metallic particles or fibers require more aggressive agents and are in most cases removed by acidic leaching [47-49].

It is important to underline that, in all of these processes, the continuous matrix phase has to be partially consolidated before removal of the sacrificial material, so that the porous structure does not collapse during the extraction step [5].

One of the main advantages of the sacrificial template method in comparison with the other fabrication routes is the possibility to deliberately tailor the porosity, pore size distribution, and pore morphology of the final ceramic component through the appropriate choice of the sacrificial material. The range of porosity and pore sizes that can be achieved with this technique is very broad (20%–90% and 1–700 mm respectively), as reported in Figure 1.9, as they only depend on the volume fraction and size of the sacrificial template used [5].

The sacrificial template method leads to porous materials displaying a negative replica of the original sacrificial template, as opposed to the positive morphology obtained from the replica technique described previously. So, since in this method the ceramic component corresponds to the negative of the original template, the removal of the sacrificial phase does not lead to flaws in the struts as in the case of the positive replica techniques

described earlier. Therefore, the mechanical strength of sacrificial-templated porous structures is usually considerably higher than that of porous materials produced via positive replica, as it is shown in Figure 1.10. Macroporous ceramics obtained with the template method display compressive strengths typically within the range predicted for open and closed-cell structures [5].

Figure 1.12 depicts an example of hierarchical ordered porous structure generated from a sacrificial template. In particular, it is possible to see a porous structure created using oil droplets as templates in a suspension of silica particles [50]. Interconnected macropores are generated upon drying of the suspension and evaporation of the oil droplets. The solid particles of the initial suspension form the walls between the macropores. A wide variety of templates can be exploited using this technique, ranging from ice crystals to immiscible phases to solid particles [5]. The possibility to predefine the level of porosity and pore size/morphology of the final structure by changing, respectively, the initial concentration and size/shape of the template phase is a major advantage of this processing route. Figure 1.12(iv) shows two possible approaches to create pores at smaller length scales within this structure. These can arise from the interstitial openings between partially sintered packed particles (Figure 1.12(iv), left) or from the nanopores formed upon infiltration and removal of packed templating particles (Figure 1.12(iv), right).

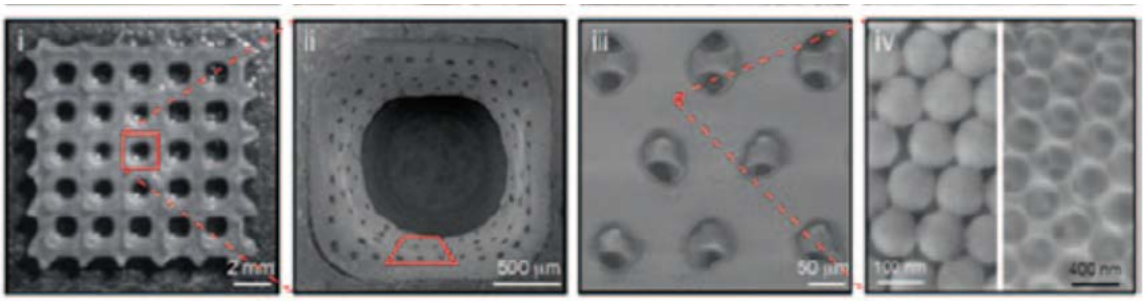

Figure 1.12 Hierarchical ordered porous structure generated from sacrificial templates: (i) Glass scaffold with periodic millimeter-sized holes used as substrate for the deposition of suspensions with templating droplets. (ii) Single hole that was coated with particles and oil droplets to generate macropores upon evaporation of the oil phase. (iii) Closer view of the interconnected macropores created after removal of the templating droplets. (iv, left) Packed particles between the macropores that are only partially sintered to generate interstitial pores at smaller length scales. (iv, right) Fine, ordered porosity created by infiltrating templating polymer particles with sol–gel precursors followed by pyrolysis of the template [50]

Direct Foaming

Direct foaming consists in the generation of bubbles inside a liquid slurry containing ceramic powders or inside a ceramic precursor solution to create a foam which then needs to be set in order to maintain its porous morphology and keep the structure of air bubbles created (Figure 1.8 c). In most cases, the consolidated foams are afterwards sintered at high temperatures to obtain high-strength porous ceramics [4,5]. The total porosity of directly foamed ceramics is proportional to the amount of gas incorporated into the suspension or liquid medium during the foaming process. The blowing agent can be a volatile liquid (such as a low boiling point solvent) or solid (such as $CaCO_3$ powder which decomposes upon heating), or gas can be developed in situ by chemical reactions, for instance, cross-linking reactions in silicone resins leading to the formation of water, or oxidation of a solid C or SiC filler forming CO_2 gas, or can be added to the liquid mixture by mechanical stirring or bubbling (gas injection). Nucleation of the gas bubbles inside the liquid slurry is influenced by the presence of suspended particles, and the bubbles initially have a spherical shape and later grow as polyhedral cells [4].

Differently to foams obtained by a replica method, direct foaming allows manufacturing of both closed and open-cell foams. In comparison to reticulated ceramics, it generally leads to a wider range of cell dimensions; however, there are some limitations for obtaining large cells, due to liquid foam stability issues. Furthermore, a wider range of relative densities (amount of porosity) can be achieved. Generally speaking, there is a decrease in cell size with increasing relative density. These materials typically possess cell walls containing interconnecting pores (cell windows), thus displaying a different permeability behavior from reticulated foams and allowing for a finer adjustment of fluid transport within the structure [51]. With direct foaming techniques, it is also easy to produce foams with a graded porosity along one direction and the process allows for a good versatility in terms of final part shapes, as the solution can be cast in any mould making it possible to shape components without additional machining. Conversely, it is more difficult to produce a material with a narrow distribution of cell sizes, and occasionally both closed and open cells are present in the material. Also, in cellular materials produced by direct foaming sometimes some unwanted anisotropy in the structure can be found, due to differing expansion in the rise direction versus the lateral directions during foaming [4].

The pore size that can be obtained with this processing method is determined by the stability of the wet foam before its setting takes place. In fact, wet foams are thermodynamically unstable systems which undergo continuous Ostwald ripening and coalescence processes in order to decrease the foam overall free energy. These destabilization processes significantly increase the size of incorporated bubbles, resulting in large pores in the final cellular microstructure. Therefore, the most critical issue on direct foaming methods is the approach used to stabilize the air bubbles incorporated within the initial suspension or liquid media [5]. Two main approaches can be found in literature to stabilize air bubbles within the ceramic matrices, one based on the stabilization with surfactants and the other one that provides stabilization with particles adsorbed at the gas-liquid interface.

In particular, several long-chain amphiphilic molecules and biomolecules such as lipids and proteins can be used as surface-active agents to stabilize wet aqueous foams. These molecules slow down the coalescence and disproportionation of bubbles by adsorbing at the air bubble surface and reducing the air–water interfacial energy. However, due to the low adsorption energy of surfactants at the gas–liquid interface, long-chain surfactants and biomolecules cannot prevent the long-term destabilization of foams. Wet foams stabilized with long-chain surfactants collapse within a few minutes after foaming, whereas those stabilized by proteins exhibit bubble disproportionation within a few hours [5].

Therefore, direct foaming based on surfactants requires a setting agent to consolidate the foam microstructure before extensive coalescence and disproportionation take place. The ultimate pore size of the porous ceramic depends on a balance between the kinetics of bubble disproportionation and the speed of liquid/suspension setting. Small pore sizes (~50 mm) can only be achieved by using efficient surfactants and by rapidly setting the wet foam. Table 1.3 depicts some examples of surfactants used for the stabilization of foams in direct foaming methods. Numerous processing routes have been developed in the last decades to prepare porous ceramics using direct foaming methods based on surfactants. Several methods have been addressed in previous review articles by Sepulveda [20] and Saggio - Woyansky et al. [26]. Some of these direct foaming methods were adapted from conventional techniques used for the production of polymer foams; the most used ones are reported in Table 1.4.

Table 1.3 Examples of Surfactants Used for the Stabilization of Foams in Direct Foaming Methods

Surfactant	
Type	*Molecule*
Nonionic	PEG-8 octyl phenyl ether PEG-11 nonyl phenyl ether PEG-11 C10 oxo-alcohol PEG-20 sorbitane oleate Cocoalkyldimethylamine oxide Poly(dimethylsiloxane) copolymer
Anionic	Sodium dodecyl sulfate (SDS)
Cationic	Benzethonium chloride
Protein	Albumin

Table 1.4 Examples of the most common direct foaming methods based on surfactants [5]

Foam setting		
In situ polymer blowing/setting	*Sol-gel setting*	*Gel cast setting*
Thermosetting (condensation) of polyols and isociantes (polyurethane precursors) in the presence of catalyst	Condensation of metal hydroxide and alkoxides specie or gelling reaction between metal oxides and surfactants	Free radical polymerization
Soldification of the thermoplastic polymer polystyrene upon cooling		Coss-linking of polyvinyl alchol with organotitanates and epoxy with ethylene imine
Thermosetting (condensation) of preceramic silicone-based polymers		Temperature-induced setting of polysaccharides: sucrose, carrageenan gum
		Temperature or pH-induced setting of proteins: gelatine, ovalbumin, bovine serum albumin
		Cement hydration

By controlling the foam stability and the setting kinetics, pore sizes within the range of 35 μm to 1.2 mm have been achieved using the above surfactant-based direct foaming methods. Figure 1.9 also shows that the porosity of cellular structures produced via

surfactant-based direct foaming can be tuned from approximately 40% up to 97%. The pores obtained with this method are typically spherical and can be either closed or opened depending on the foam wet processing. Open pores exhibiting interconnecting windows are obtained if particles segregate at the plateau borders of the foam because of bubble disproportionation. Closed pores, on the other hand, are typically achieved when the particles are distributed uniformly around the gas bubbles upon setting. These conditions can be controlled in the process by adjusting the foam stability, air content, particle concentration, and setting kinetics [5].

As opposed to the replica techniques, the direct foaming methods usually lead to dense flawless struts after sintering which markedly increase the mechanical strength of the porous ceramic in comparison with the replica derived structures. For porosities higher than 90% (relative density <10%) the cell walls are markedly thin, leading to lower mechanical strength than that theoretically estimated for open-cell structures. However, by decreasing the porosity (increasing density) pores gradually change from a highly open to a completely closed morphology, increasing the strength towards the level predicted for closed-cell structures.

The second approach of direct foaming is based on the use of solid particles with tailored surface chemistry which have lately been shown to efficiently stabilize gas bubbles upon adsorption at the air–water interface [52–55]. Particles adsorbed at the gas–liquid interface were observed to impede the destabilization mechanisms responsible for bubble coalescence and disproportionation for several days, as opposed to the few minutes typically required for the collapse of foams prepared with long-chain surfactants [55]. Some of these methods involves also a surface modification of particles. For example, one method uses colloidal particles as foam stabilizers in order to produce macroporous ceramics with smaller pore sizes than those obtained with surfactant-based foaming techniques; the attachment of colloidal particles at the air–water interface is promoted by deliberately changing the wettability of the particle upon adsorption of short-chain amphiphilic molecules on the surface [55, 56]. After the surface modification of particles, air can be easily incorporated by mechanical frothing, injection of gas stream, or initiation of a chemical reaction that releases gaseous by-products directly into the initially fluid suspension. The stability of particle-stabilized foams prepared with this method is compared in Figure 1.11 with that of a surfactant stabilized shaving foam known to be extremely resistant against coalescence and Ostwald ripening. The particle-stabilized

foam is completely stable against drainage, coalescence and disproportionation for more than 4 days, as opposed to the approximately fourfold increase in average bubble size observed in the shaving foams after only 4 h. The outstanding stability achieved with this novel direct foaming method relies on the irreversible adsorption of colloidal particles at the air–water interface of the gas bubbles, as opposed to the continuous adsorption–desorption experienced by conventional surfactant molecules [52-55]. Particles irreversibly adsorbed at the interface sterically impede the coalescence of neighboring bubbles and also form a coating layer that restrict bubble shrinkage and expansion in such a way that Ostwald ripening is strongly hindered [55].

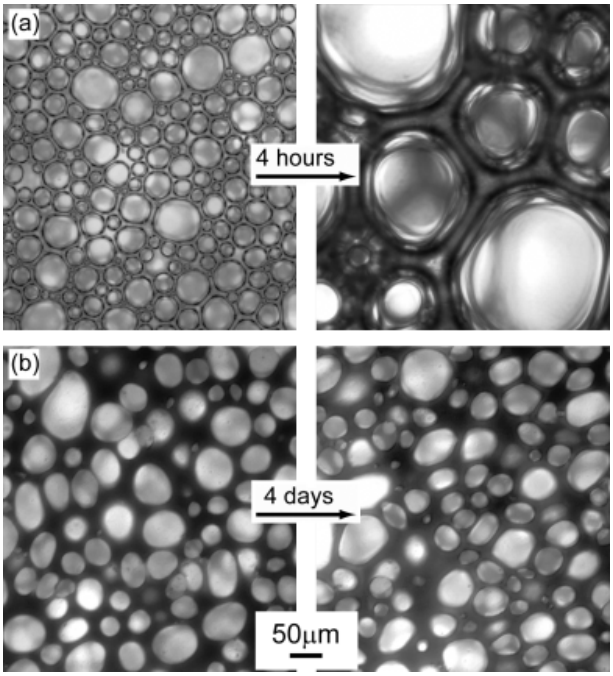

Figure 1.13 Stability of particle-stabilized foams (b) as compared with a well-established shaving foam stabilized with long-chain surfactants (Gillette™ a).

Because of its remarkable stability, particle-stabilized foams do not necessarily require a setting step and can thus be directly dried and sintered to obtain the macroporous ceramic. The porosity of foams produced with this method vary typically between 40% and 93%, whereas the average pore sizes can be tuned from approximately 10 to 300 μm. As the air bubbles in the wet foam can be completely covered with a layer of surface modified particles, porous ceramics with closed pores can be easily prepared with this method [5]. Moreover, macroporous ceramics produced from particle-stabilized foams exhibit

remarkable mechanical strength (Figure 1.10) at very high porosity levels (87%–90%) and small pore sizes (e.g., 30 μm). This strength level is achieved by tailoring the foaming conditions to produce porous structures with closed cells and flawless walls. Porous ceramics exhibiting open porosity has also been prepared with this technique by simply decreasing the concentration of stabilizing particles or by adding minor amounts (<1 wt%) of a sacrificial phase into the initial suspension (e.g., graphite particles). Using this simple, cheap, and environmentally-friendly method, we have fabricated porous ceramics of various porosity levels and pore size ranges (Figure 1.9) with many different chemical compositions. Figure 1.14 shows a typical example of a macroporous structure generated by direct foaming of a polysiloxane resin. In this case, foaming is driven by the evaporation of a physical blowing agent (azodicarbonamide) from the resin while the mixture is heated up to 250 °C. Simultaneous cross-linking of the resin during heating enables consolidation of the foam structure before coalescence of the bubbles (Figure 1.14(i), (ii)) [57, 58]. The obtained foam can then be pyrolyzed under argon above 1350°C to promote the in situ formation of SiC nanowires (Figure 1.14(iii), (iv)). Together with macropores resulting from the foaming process, the interstitials created between the nanowires ultimately lead to a SiOC-based hierarchical porous ceramic.of a hierarchical porous ceramic made by direct foaming of a poly(siloxane) [57, 58].

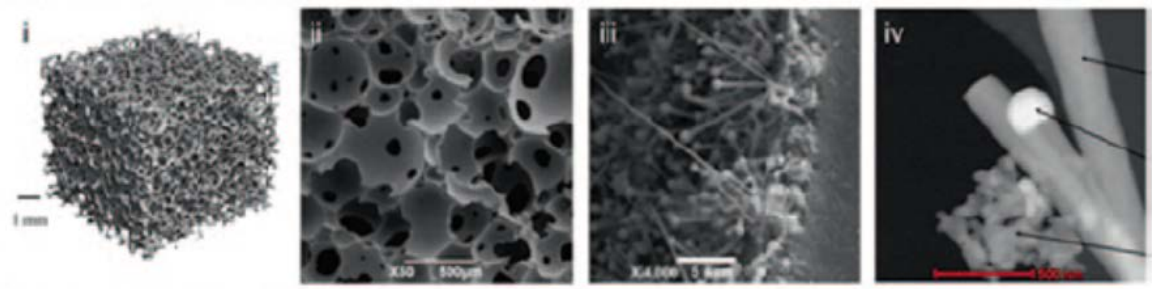

Figure 1.14 Hierarchical porous ceramic made by direct foaming of a poly(siloxane) resin followed by in situ precipitation of nanowires at 1350 °C: (i) Typical 3D macroporous structure of the polysiloxane foam. (ii) Interconnected macropores within the foam. (iii) Detailed view of the macropore wall, depicting the nanowires grown from the wall surface. (iv) Nanowires and nanoparticles that give rise to the second hierarchy of pores [57, 58].

In addition to the template-based techniques described above, hierarchical porous structures have also been produced using template-free, top-down fabrication technologies such as 3D printing (direct writing) and electrospinning [59, 60]. These processing routes typically involve the formation and deposition of filaments that are

assembled into ordered or random cellular structures. Proper formulation of the ink or precursor solution is key to reach the rheological behavior required during the deposition process and to enable consolidation of the cellular structure. In conclusion, taking into account the decisive influence of the processing method on the material's microstructure and properties, the selection of the processing route for the production of porous ceramics depends primarily on the final properties and application aimed.

Bibliography

[1] C. B Carter, M. G. Norton, Ceramic materials: Science and engineering. Springer. (2007) pp. 3-4. ISBN 978-0-387-46271-4.

[2] D.W. Richerson, The Magic of Ceramics, The American Ceramic Society, Westerville, OH. (2000).

[3] W.D. Kingery, H.K. Bowen and D.R. Uhlmann, Introduction to Ceramics, 2nd edition, Wiley, New York. (1976).

[4] P. Colombo, Conventional and novel processing methods for cellular ceramics, Philos. rans. R. Soc. A364 (2006) 109–124.

[5] A.R. Studart, U.T. Gonzenbach, E. Tervoort, L.J. Gauckler, Processing routes to macroporous ceramics: a review, J. Am. Ceram. Soc.89 (2006) 1771–1789.

[6] J. Luyten, S. Mullens, I. Thijs, Designing with pores – synthesis and applications, Kona 28 (2010) 131–142.

[7] M. Scheffler, P. Colombo (Eds.), Cellular Ceramics: Structure, Manufacturing, Properties and Applications. John Wiley & Sons (2006). ISBN: 3-527-31320-6.

[8] R. Brezny, D. J. Green, Mechanical behavior of cellular ceramics, Materials science and technology (1991).

[9] M.F. Ashby, R.F.M. Medalist, The mechanical properties of cellular solids, Metallurgical Transactions A 14.9 (1983), 1755-1769.

[10] Y.J. Lee, K. B. Yoon, Effect of composition of polyurethane foam template on the morphology of silicalite foam, Microporous Mesoporous Mater. 88 (2006), 176–186.

[11] P. Colombo, M. Griffoni, M. Modesti, Ceramic foams from a preceramic polymer and polyurethanes: preparation and morphological investigations. Journal of sol-gel science and technology, 13.1-3 (1998), 195-199.

[12] E.J.A.E. Williams, J.R.G. Evans, Expanded ceramic foam, J. Mater. Sci. 31, 559(3), (1996) 559–563.

[13] Z.R. Ismagilov, R.A. Shkrabina, N.A. Koryabkina, A.A. Kirchanov, H. Veringa, P. Pex, Porous alumina as a support for catalysts and membranes. Preparation and study, React. Kinet. Catal. Lett. 60(2), (1997) 225-231.

[14] S. Wood, A.T. Harris, Porous burners for lean-burn applications, Prog. Energ. Combust. 34(5), (2008) 667-684.

[15] A.L. Ahmad, C.P. Leo, S.R.A. Shukor, Tailoring of a γ-Alumina Membrane with a Bimodal Pore Size Distribution for Improved Permeability, J. Am. Ceram. Soc. 91, (2008) 246-251.

[16] A. Norris, R.A. Olson, Kiln furnitures, Cellular Ceramics: Structure, Manufacturing, Properties and Applications, ed. by M. Scheffler, P. Colombo. Wiley-VCH, Weinheim, (2005), p. 439

[17] L.L. Hench, Bioceramics, J. Am. Ceram. Soc. 81, (1998) 1705-1728.

[18] W. Frieb, J. Warner, Biomedical applications, Handbook of Porous Solids, ed. by F. Schüth, K.S.W. Sing, J. Weitkamp. Wiley-VCH, Weinheim, (2002), p. 2946.

[19] E. C. Hammel, OL-R. Ighodaro, O. I. Okoli, Processing and properties of advanced porous ceramics: an application based review, Ceramics International 40(10), (2014) 15351-15370.

[20] P. Sepulveda, Gelcasting foams for porous ceramics, Am. Ceram. Soc. Bull. 76, (1997) 61–65.

[21] I. M. Lachman, R. D. Bradley, R. M. Lewis, Thermal expansion of extruded cordierite Ceramics, Am. Ceram. Soc. Bull. 60, (1981) 202–205.

[22] S. Y. Shan, J. F. Yang, J. Q. Gao, W. H. Zhang, Z. H. Jin, R. Janssen, and T. Ohji, Porous Silicon Nitride Ceramics Prepared by Reduction–Nitridation of Silica, J. Am. Ceram. Soc., 88 [9], (2005) 2594–6.

[23] I. H. Arita, V. M. Castano, D. S. Wilkinson, Synthesis and Processing of Hydroxyapatite Ceramic Tapes with Controlled Porosity, J. Mater. Sci.—Mater. Med., 6 [1], (1995) 19–23.

[24] K. Schwartzwalder, A. V. Somers, Method of Making Porous Ceramic Articles, US Pat. No. 3090094, May 21, (1963).

[25] L. J. Gauckler, M.M. Waeber, C. Conti, M. Jacobduliere, Ceramic Foam for Molten-Metal Filtration, J. Metals, 37 [9], (1985) 47–50.

[26] J. Saggio-Woyansky, C. E. Scott, W. P. Minnear, Processing of Porous Ceramics, Am. Ceram. Soc. Bull., 71 [11], (1992) 1674–82.

[27] X. W. Zhu, D. L. Jiang, S. H. Tan, Z. Q. Zhang, Improvement in the Strut Thickness of Reticulated Porous Ceramics, J. Am. Ceram. Soc., 84 [7], (2001) 1654–6.

[28] L. Montanaro, Y. Jorand, G. Fantozzi, A. Negro, Ceramic Foams by Powder Processing, J. Eur. Ceram. Soc., 18 [9], (1998) 1339–50.

[29] H. R. Ramay and M. Q. Zhang, Preparation of Porous Hydroxyapatite Scaffolds by Combination of the Gel-Casting and Polymer Sponge Methods, Biomaterials, 24 [19], (2003) 3293–302.

[30] A. J. Sherman, R. H. Tuffias, R. B. Kaplan, Refractory ceramic foams: a novel, new high temperature structure, Am. Ceram. Soc. Bull. 70, (1991) 1025–1029.

[31] K. Yoshihisa, F. Masashi, Ceramic foam. British Patent 2 (1986) 168 337.

[32] X. Zhu, D. Jiang, S. Tan, Z. Zhang, Improvement in the strut thickness of reticulated porous ceramics. J. Am. Ceram. Soc. 84, (2001) 1654–1656.

[33] X. Pu, X. Liu, F. Qiu, L. Huang, Novel method to optimize the structure of reticulated porous ceramics. J. Am. Ceram. Soc. 87, (2004) 1392–1394.

[34] T. Ota, M. Takahashi, T. Hibi, M. Ozawa, S. Suzuki, Y. Hikichi, H. Suzuki, Biomimetic Process for Producing SiC ‘‘Wood’’, J. Am. Ceram. Soc., 78 [12], (1995) 3409–11.

[35] A. Zampieri, H. Sieber, T. Selvam, G.T.P. Mabande, W. Schwieger, F. Scheffler, M. Scheffler, P. Greil, Biomorphic cellular SiSiC/zeolite ceramic composites: from Rattan palm to bioinspired structured monoliths for catalysis and sorption, Adv Mater, 17(3), (2005) 344-349.

[36] S.Komarneni, L. Pach, R. Pidugu, Porous-alumina ceramics using bohemite and rice flour, Mater. Res. Soc. Symp. Proc. 371, (1995) 285–290.

[37] R. A. Lopes, A. M. Segadaes, Microstructure, permeability and mechanical behavior of ceramic foams, Mater. Sci. Eng. A209, (1996) 149–155.

[38] A. F. Lemos, J. M. F. Ferreira, Porous bioactive calcium carbonate implants processed by starch consolidation, Mater. Sci. Eng. C11, (2000) 35–40.

[39] P. Colombo, E. Bernardo, L. Biasetto, Novel Microcellular Ceramics from a Silicone Resin, J. Am. Ceram. Soc., 87 [1], (2004)152–4.

[40] Y. Hotta, P. C. A. Alberius, L. Bergstrom, Coated Polystyrene Particles as Templates for Ordered Macroporous Silica Structures with Controlled Wall Thickness, J. Mater. Chem., 13 [3], (2003) 496–501.

[41] J. M. Bouler, M. Trecant, J. Delecrin, J. Royer, N. Passuti, G. Daculsi, Macroporous Biphasic Calcium Phosphate Ceramics: Influence of Five Synthesis Parameters on Compressive Strength, J. Biomed. Mater. Res., 32 [4], (1996) 603–9.

[42] S. H. Li, J. R. de Wijn, P. Layrolle, K. de Groot, Novel method to manufacture porous hydroxyapatite by dual-phase mixing, J. Am. Ceram. Soc. 86, (2003) 65–72.

[43] H. Maier, C. Aneziris, High strength fired porous ceramic structure production. German Patent 19 605 149 (1997).

[44] F. Tang, H. Fudouzi, T. Uchikoshi, Y. Sakka, Preparation of porous materials with controlled pore size and porosity. J. Eur. Ceram. Soc. 24, (2004) 341–344.

[45] T. J. Fitzgerald, V. J. Michaud, A. Mortensen, Processing of Microcellular Sic Foams. 2. Ceramic Foam Production, J. Mater. Sci., 30 [4], (1995) 1037–45.

[46] E. S. Toberer, J. C. Weaver, K. Ramesha, R. Seshadri, Macroporous Monoliths of Functional Perovskite Materials Through Assisted Metathesis, Chem. Mater., 16 [11], (2004) 2194–200.

[47] H. Wang, I. Y. Sung, X. D. Li, D. Kim, Fabrication of Porous SiC Ceramics with Special Morphologies by Sacrificing Template Method, J. Porous Mater., 11 [4], (2004) 265–71.

[48] H. Kim, C. da Rosa, M. Boaro, J. M. Vohs, R. J. Gorte, ‘‘Fabrication of Highly Porous Yttria-Stabilized Zirconia by Acid Leaching nickel from a Nickel–Yttria-Stabilized Zirconia Cermet, J. Am. Ceram. Soc., 85 [6], (2002) 1473–6.

[49] N. Miyagawa, N. Shinohara, Fabrication of Porous Alumina Ceramics with Uni-Directionally-Arranged Continuous Pores Using a Magnetic Field, J. Ceram. Soc. Jpn., 107 [7], (1999) 673–7.

[50] A. R. Studart, J. Studer, L. Xu, K. Yoon, H. C. Shum, D. A. Weitz, Hierarchical porous materials made by drying complex suspensions, Langmuir, 27(3), (2010)955-964.

[51] M. D. M. Innocentini, P. Sepulveda, V.R. Salvini, V.C. Pandolfelli, Permeability and structure of cellular ceramics: a comparison between two preparation techniques. J. Am. Ceram. Soc. 81, (1998) 3349–3352.

[52] Z. P. Du, M. P. Bilbao-Montoya, B. P. Binks, E. Dickinson, R. Ettelaie, B. S. Murray, Outstanding Stability of Particle-Stabilized Bubbles, Langmuir, 19 [8], (2003) 3106–8.

[53] E. Dickinson, R. Ettelaie, T. Kostakis, B. S. Murray, Factors Controlling the Formation and Stability of Air Bubbles Stabilized by Partially Hydrophobic Silica Nanoparticles, Langmuir, 20 [20], (2004) 8517–25.

[54] B. P. Binks, T. S. Horozov, Aqueous Foams Stabilized Solely by Silica Nanoparticles, Angewandte Chemie—Int. Ed., 44 [24], (2005) 3722–5.

[55] U. T. Gonzenbach, A. R. Studart, E. Tervoort, L. J. Gauckler, Ultrastable particle-stabilized foams, Angew. Chem. Int. Ed., 45, (2006) 3526 –3530.

[56] U. T. Gonzenbach, A. R. Studart, E. Tervoort, L. J. Gauckler, Macroporous Ceramics from Particle. Stabilized Wet Foams, J. Am. Ceram. Soc. 90[1], (2007) 16-22.

[57] J. Zeschky, F. Goetz-Neunhoeffer, J. Neubauer, S. J. Lo, B. Kummer, M. Scheffler, P. Greil, Preceramic polymer derived cellular ceramics. Composites Science and Technology, 63(16), (2003) 2361-2370.

[58] C. Vakifahmetoglu, E. Pippel, J. Woltersdorf, P. Colombo, Growth of One-Dimensional Nanostructures in Porous Polymer-Derived Ceramics by Catalyst-Assisted Pyrolysis. Part I: Iron Catalyst, Journal of the American Ceramic Society, 93(4), (2010) 959-968.

[59] J. L. Simon, S. Michna, J.A. Lewis, E. D. Rekow, V. P. Thompson, J. E. Smay, J. L. Ricci, In vivo bone response to 3D periodic hydroxyapatite scaffolds assembled by direct ink writing, Journal of Biomedical Materials Research Part A, 83(3), (2007) 747-758.

[60] H. Chen, J. Di, N. Wang, H. Dong, J. Wu, Y. Zhao, L. Jiang, Fabrication of hierarchically porous inorganic nanofibers by a general microemulsion electrospinning approach, small, 7(13), (2011) 1779-1783.

2. Geopolymers: innovative eco-sustainable binders

2.1 Geopolymer definition and hystorical background

Geopolymers are inorganic materials introduced by Davidovits in the early 1970s, they are a class of largely X-ray amorphous alumosilicate materials, generally synthesized at ambient or slightly elevated temperature by reaction of a solid aluminosilicate powder with a concentrated alkali metal silicate or hydroxide solution [1]. The reaction process of this system can be considered as an alkaline activation, that is a chemical process in which a powder material of an aluminosilicate nature is mixed with an alkaline activator to produce a paste that is able to set and harden in a short time [2, 3]. These inorganic polymeric materials can be considered as the amorphous equivalent of geological feldspars, but synthesized in a manner similar to thermosetting organic polymers. For this reason, these materials are termed as ‘‘geopolymers’’[4]. They are in fact named because of the similarities with the organic condensation polymers as far as their hydrothermal synthesis conditions are concerned [1]. Study of the literature and patents demonstrated, that before 1978, the idea of using this mineral chemistry for the development of a mineral polymer had been totally neglected. As a function of chemical composition of initial materials, the alkaline cements are classified into two groups:

- Binders synthesized from materials rich in calcium, such as blast furnace slag that produces calcium silicate hydrate (CSH) gel when activated with alkaline solution.
- Materials synthesized with raw materials low in calcium and rich in SiO_2 and Al_2O_3 such as metakaolin. These materials when activated with alkaline solution, formation of an amorphous material (alkaline aluminosilicate) that develops high mechanical strength at early ages after a soft thermal curing [5].

These materials differ substantially from ordinary Portland cement, as they use totally different reaction pathway in order to attain structural integrity. Pozzolanic cement depends on the presence of calcium-silicate hydrate for matrix formation and strength whereas geopolymers utilize the polycondensation of silica and alumina precursors (fly ash, kaolin, metakaolin) and a high alkali content to attain structural strength [6].

Geopolymers were accidentally discovered by Purdon in 1940 [7]. He studied the sodium hydroxide on a variety of minerals and glasses containing silicon and/or aluminum and summarized it in two steps:

(1) liberation of silica, alumina and lime
(2) formation of hydrated calcium silicates, aluminates as well as regeneration of caustic solution.

Purdon proposed that the hardening mechanism of alkali-activated alumino silicate binder involves dissolution of Si or Al in the presence of sodium hydroxide, and precipitation of calcium silicate or aluminum hydrate with the generation of sodium hydroxide. Similarly, in the 1950s Glukhovsky identified both CSH and calcium and alumino-silicate hydrate as solidification product on the alkali activation of slag binders and concluded that clay mineral reacts during alkali treatment to form aluminosilicate hydrate. And proposed a general mechanism for the alkali activation of materials primarily comprising silica and reactive alumina [8]. The Gluhhovsky model divides the process into three stages: (a) destruction–coagulation; (b) coagulation–condensation; (c) condensation–crystallization. More recently, different authors have elaborated on and extended the Glukhovsky theories and applied the accumulated knowledge about zeolite synthesis in order to explain the geopolymerization process as a whole [9-13]. Finally, in the 1970s, Davidovits [14] developed a kind of mineral polymer material with 3D cross-linked polysialate chain, which resulted from the hydroxylation and polycondensation reaction of natural minerals such as clay, slag, fly ash and pozzolan on alkaline activation below 160°C. This inorganic polymer was first named polysialate, in fact in 1976 Davidovits introduced the 'sialate' nomenclature to describe aluminosilicate structures [15]. The linkage type Si-O-Al was named a sialate bond, and Si-O-Si a siloxo bond. This provided a means of describing the composition of geopolymers according to their Si/Al ratio, with a ratio of 1.0 being a poly(sialate), 2.0 being a poly(sialate-siloxo), and 3.0 a poly(sialate-disiloxo), later the term "Geopolymer" was coined [14]. In 1980 the setting reaction of alkali activated slag cement was explained [7, 16].

Recently, Deventer [6, 7, 16-26] has widely contributed towards the development and applications of geopolymers.

Although the term 'geopolymer' is generically used to describe the amorphous to crystalline reaction products from synthesis of alkali aluminosilicates from reaction with alkali hydroxide/alkali silicate solution, geopolymeric gels and composites are also commonly referred to as 'low-temperature aluminosilicate glass'[27], 'alkali-activated cement' [28] 'geocement' [29], 'alkali-bonded ceramic' [30], 'inorganic polymer concrete' [31], and 'hydroceramic' [32]. Despite this variety of nomenclature, these

terms all describe materials synthesized utilizing the same chemistry, which can be described as a complex system of coupled alkali mediated dissolution and precipitation reactions in an aqueous reaction substrate.

2.2 Reaction of geopolymerization

Geopolymerization is a geosynthesis (reaction that chemically integrates minerals) that involves naturally occurring silico-aluminates [33]. Any pozzolanic compound or source of silica and alumina, that is readily dissolved in the alkaline solution, acts as a source of geopolymer precursor species and thus lends itself to geopolymerization [17]. The alkali component as an activator is a compound from the element of first group in the periodic table, so such material is also called as alkali activated aluminosilicate binders or alkali activated cementitious material [34]. Figure 2.1 shows schematically the starting materials needed for geopolymer production process. Silicon and aluminum atoms react to form molecules that are chemically and structurally comparable to those building natural rocks [33].

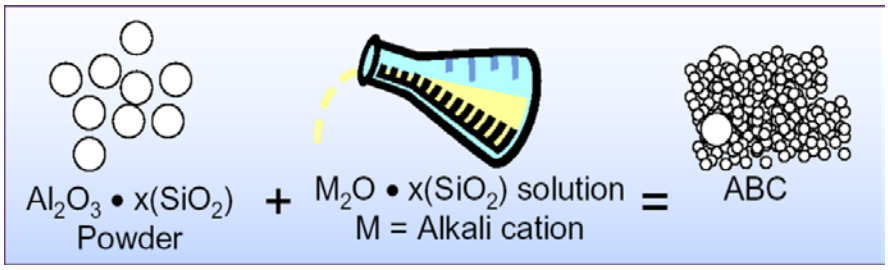

Figure 2.1 Starting materials for the production of geopolymers

Mechanism of geopolymerization involves the polycondensation reaction of geopolymeric precursors i.e. alumino-silicate oxide with alkali polysialates, yielding:

$$M_n[-(Si\text{-}O_2)_z\text{-}Al\text{-}O]_n \cdot wH_2O$$

where M is the alkaline element, z is 1,2, or 3 and n is the degree of polycondensation [35].

The exact mechanism of geopolymerization is not yet fully understood, but it is believed to consist of four main stages:

(1) Surface dissolution of Al and Si in a highly alkaline solution that produces aluminate and silicate species (most likely in monomeric form)

(2) Diffusion of the dissolved species through the solution

(3) Polycondensation of the Al and Si complexes with the added silicate solution and formation of a gel, as the oligomers in the aqueous phase form large networks by condensation. This process releases the water that was nominally consumed during dissolution.

(4) Hardening of the gel that results to the final geopolymeric product: after gelation the system continues to rearrange and reorganize, as the connectivity of the gel network increases, resulting in the three-dimensional aluminosilicate network commonly attributed to geopolymers.

Stages (2) to (4) cannot be monitored since the procedures cannot be stopped and the products cannot be isolated. Therefore, the dissolution stage is the only one that can be quantitatively studied [36]. The formation of geopolymers cab be illustrated with the two chemical reactions reported in Figure 2.2.

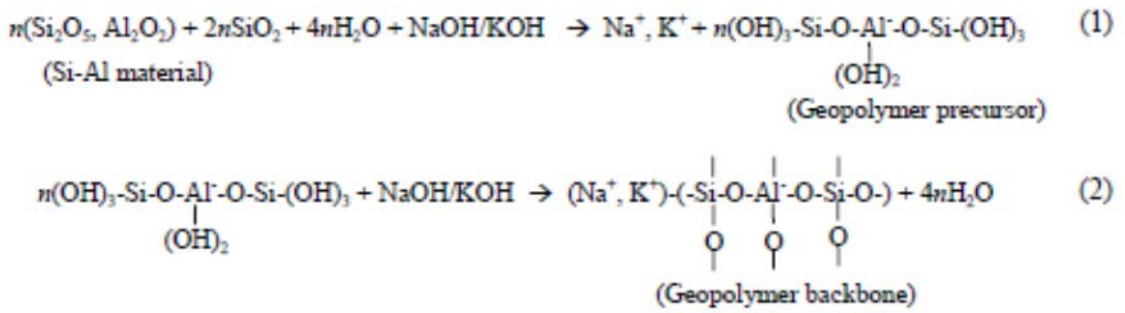

Figure 2.2 Reactions of geopolymer formation [16]

Moreover, the mechanism of geopolymerization is graphically reported and schematically summarized respectively in Figures 2.3 and 2.4.

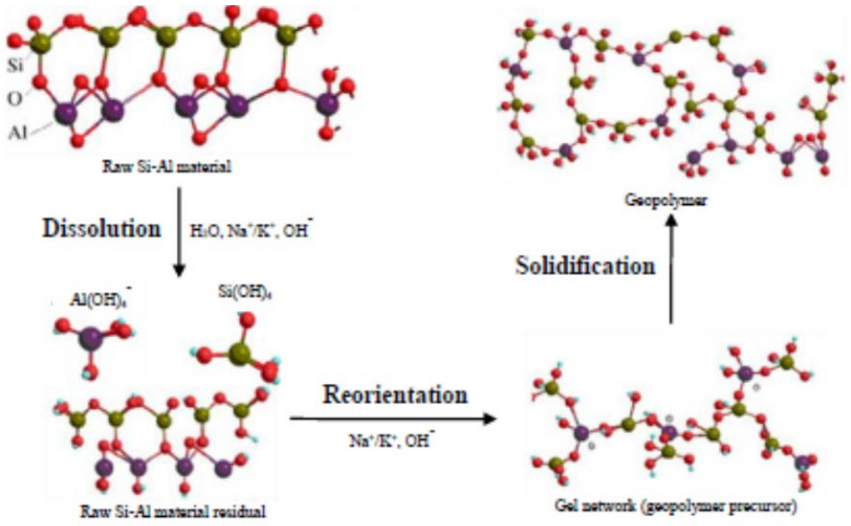

Figure 2.3 Graphical representation of the mechanism of geopolymerization

Geopolymers consist of aluminum (Al^{3+}) and silica (Si^{4+}) tetrahedrally interlinked alternately by sharing all the oxygen atoms. A polymeric structure of Al–O–Si formed constitutes the main building blocks of geopolymeric structure (Figure 2.5). Alkali metal salts and/or hydroxide are necessary for the dissolution of silica and alumina as well as for the catalysis of the condensation reaction. The gel phase is thought to be highly reactive and produced by co-polymerization of individual alumina and silica from their source, dissolved by the alkali metal. Some cations must be present to keep the structure neutrality (since aluminum is four fold). Na, K, Ca and other metallic cations maintain this neutrality. In fact, the negative charge on the AlO^{4-} group is charge-balanced by alkali cations (typically Na^{+} and/or K^{+}). Geopolymers derived from different combinations of raw materials can easily be synthesized containing multivalent cations [37]. It is still not clear whether these ions simply play a charge-balancing role or are actively bonded into the matrix. The mechanism of immobilization is expected to be the combination of chemical and physical interaction. Cation is either bonded into the matrix via Al–O or Si–O bond or present in the framework cavities to maintain electrical charge balance.

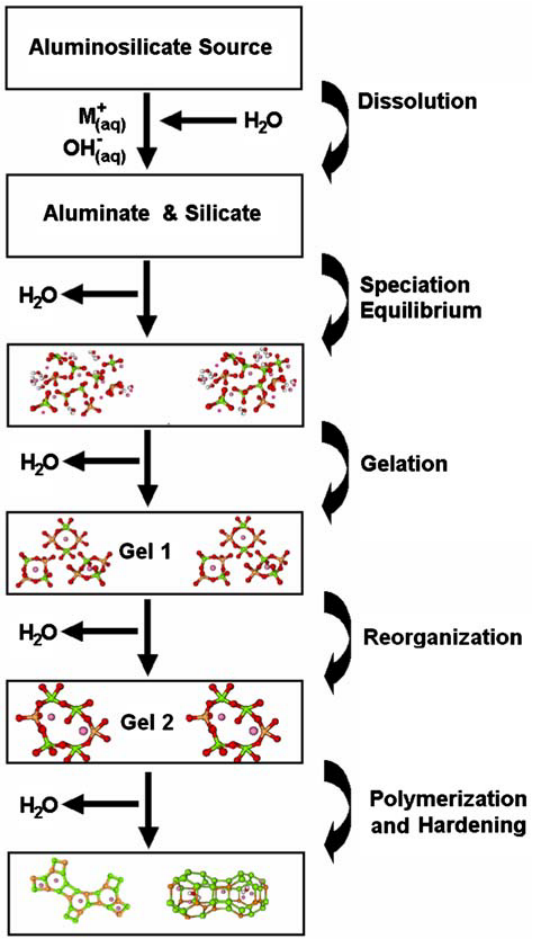

Figure 2.4 Summary of the different stages of geopolymeric reaction

A physically encapsulated cation should be substituted by another cation if its surrounding allows the diffusion process to occur [7].

Some examples of possible molecular structures for geopolymeric chains are reported in Figure 2.6

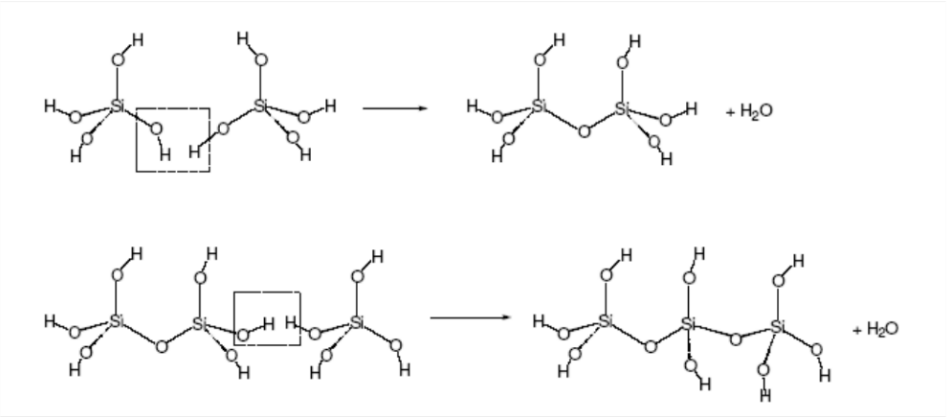

Figure 2.5 Schematic molecular structure of geopolymers

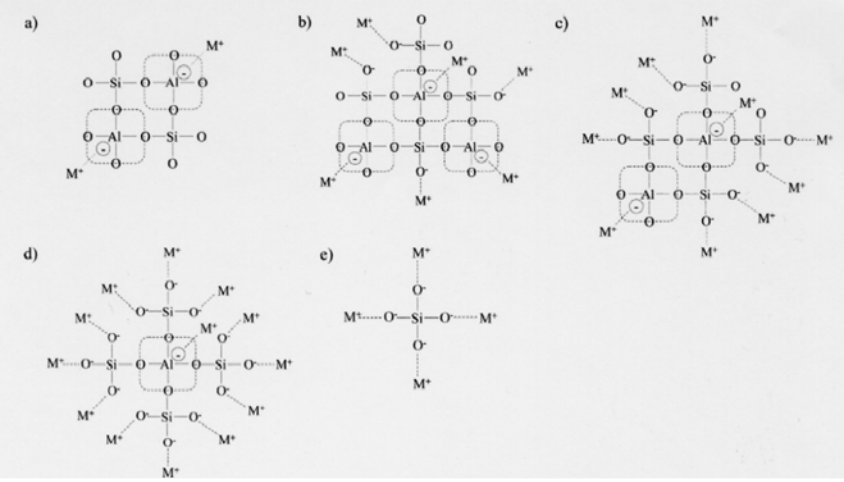

Figure 2.6 Different kinds of geopolymeric molecular structures

2.3 Raw materials

Starting material plays an important role in the formation of geopolymer. Several studies have been conducted in order to develop various methods to improve the durability of the geopolymeric cement and concrete. Wide range of materials is presently being used for geopolymerization [38]. These include various pozzolanic, supplementary cementitious materials, chemicals and mineral additives [39]. Materials rich in Si (like fly ash, slag and rice husk) and materials rich in Al (clays like kaolin, bentonites) are the primary requirement to undergo geopolymerization. Some other materials can also be utilized as a reactive filler material or a setting additive like ordinary Portland cement, kiln dust etc. which helps in the development of good mechanical properties.

The coordination number of the silica and alumina in the source material is of great importance. Some of the water and NaOH are expelled out during hardening of the gel phase. It is believed that the alkali metal hydroxide acts as a catalyst and leach out from the hardened alkali activated binder in more or less the same amount as that was added during synthesis. Ions such as metal cations that are incorporated into the matrix in one way or another influence the final structure stability and therefore leaching characteristics [7].

Aluminosilicate sources

The three most common raw material classes used in geopolymerization are slags, calcined clays and coal fly ashes.

Metakaolin

Metakaolin is ideally synthesized by dehydroxylation of phase pure kaolin. While the temperature and calcination time of kaolin affect the ultimate surface area, degree of dihydroxylation and reactivity, the base structure is that of a highly disrupted phyllosilicate structure containing silicon and aluminum only. Although most commercial metakaolin contains levels of impurities, primarily muscovite and titanium dioxide, the effect of these impurities is limited by both their low dissolution and the inability of the products of their dissolution to affect the formation mechanism. In general, the knowledge gained by investigation of metakaolinbased geopolymers may be applied to all metakaolin supplies in the world. Metakaolin-based geopolymers can be manufactured consistently, with predictable properties both during preparation and in property development. The particle size of metakaolin varies to some degree, but is generally smaller than 5 μm, with the intrinsic size of the clay being in the order of 20 nm [37]. Although the dispersion of particles during mixing will affect the rheological behavior and degree of reaction somewhat, it has been shown that there is little difference in the reaction of metakaolin-based geopolymer with variation in raw material surface area [40], although the amount of soluble silicate and alkali cation in the activating solution affects the extent of reaction [26].

Fly ash

Fly ash is one of the important source materials for geopolymer. It is available worldwide yet its utilization is still limited. Fly ash consists of finely divided ashes produced by burning pulverized coal in power stations. The chemical composition depends on the mineral composition of the coal gangue (the inorganic part of the coal). Silica usually varies from 40 to 60 % and alumina from 20 to 30%. The iron content varies quite widely. When the content of CaO is greater than 20% then it can be categorized as cementitious material. When CaO varies between 10% and 20% categorized as cementitious and pozzolanic material. The particles in fly ash are generally spherical, but inhomogeneous, and comprise glassy as well as crystalline (often mullite and quartz) phases. The particle size distribution can be very broad, and different size fractions will differ in elemental and phase composition. This degree of inhomogeneity means that more care is required when working with fly ash to ensure that the optimal mix design is obtained for a given ash if a consistent product is to be obtained, and this area is the subject of much ongoing work worldwide [10, 41-43]. In any case, in a pioneering investigation the main characteristics of fly ashes were ranged in order to establish their potential to be alkali

activated [44]. The fly ashes that are most widely used in geopolymer synthesis are low in Ca, i.e. Class F according to ASTM C618. Published work on higher-Ca (Class C) ashes is scarcer, possibly due to the rapidity with which setting may occur in systems of 'standard' geopolymer design [45]. One of the most important aspects related to the use of fly ash as starting material for the production of geopolymer, is the possibility to re-use secondary raw materials considered as industrial waste in a new production process.

Blust furnace slag

Blast furnace slag (abbreviated GGBFS, for 'ground granulated blast furnace slag') is broadly described as a mixture of poorly crystalline phases with compositions resembling gehlenite ($2CaO{\cdot}Al_2O_3{\cdot}SiO_2$) and akermanite ($2CaO{\cdot}MgO{\cdot}2SiO_2$), as well as depolymerized calcium silicate glasses. The degree of depolymerization largely controls reactivity. As slag is generated at high temperature as a liquid in the blast furnace during iron production and subsequently quenched, its composition is essentially that of an overcharge-balanced calcium aluminosilicate framework – i.e., there is more than sufficient calcium available to charge-balance aluminium, with the remainder contributing to depolymerizing the glass network [46]. In the context of geopolymer synthesis from slag glasses, the key glass network forming cations are Al^{3+} and Si^{4+}; the divalent Ca^{2+} and Mg^{2+} act as network modifiers along with any alkalis present. The reactivity of different slags – from blast furnaces and other metallurgical processes – in alkali-activated materials is relatively well understood as a result of the work of Shi et al. [47]. It is also well known that the reactions of slag are dominated by small particles. Particles above 20 μm in size react only slowly, while particles below 2 μm react completely within approximately 24 hours in blended cements and in alkali-activated systems [48, 49]. Clearly, when using slag in geopolymerization, careful control of particle size distribution can be utilized to control the strength development profile, as is done in OPC blends [48].

Pozzolan

Natural pozzolans, which are almost similar to aluminosilicate materials, are geological deposits with a wide range of chemical compositions which vary from batch to batch, but they are usually high in available SiO_2, that, when combined with suitable alkali activators, can be converted to geopolymer cement for concrete production. Possible deficiencies in the SiO_2, Al_2O_3 and CaO content in a natural pozzolan might be compensated for by adding mineral additives, such as kaolinite or lime enabling them to

be used as a geopolymer cement [50]. In fact, it is possible to activate natural-pozzolan and to produce geopolymer cement using a proportioned mixture of sodium hydroxide and sodium silicate as an alkali-activator. In that case, the quality of natural pozzolan-based geopolymer cement depends on the composition of alkali activator, on the water/cement ratio used, in addition to the quality of natural pozzolan (its chemical composition and glass phase content) [51].

Calcined clay

The burning of certain clays (kaolin, bentonites, montmorillonite etc) and oil shales produces ashes, that harden when mixed with lime and water. Clay mineral, such as Kaolin, gains a distinct pozzolanic activity when burned at temperature between 600°C and 900°C. These artificial pozzolanas are mostly composed of silica and alumina. The loss of combined water due to the thermal treatment causes the crystalline network of the clay mineral to be destroyed, while silica and alumina remains in a messy, unstable amorphous state, that reacts with CH [33]. The pozzolanic activity depends on the clay mineral content and thermal treatment conditions. Hardening results from the presence of cementitious compounds such as C_2S and CS.

In recent years a new scenario is going to delineate, the use of waste materials as starting raw materials for geopolymer production. In particular, among the silicoaluminate wastes, reservoir sediments are worthy of consideration. In fact, most of these contain a diverse set of clay minerals, mostly illites, smectites, chlorites and kaolinites, and must be periodically removed to avoid the progressive reduction in reservoir capacity. The nature of the parent rocks strongly affects that of the clay minerals [52, 53]. Once removed, the sediments must be managed, and their recycling for the manufacture of geopolymer based materials can be of great interest [52].

Alkali activators

Strong alkalis are required to activate the silicon and aluminum present in the raw materials and setting additives, that allows transforming glassy structure partially or totally into a very compacted composite [2, 42]. The common activators are NaOH, Na_2SO_4, waterglass, Na_2CO_3, K_2CO_3, KOH, K_2SO_4 or a little amount ofcement clinker [10]. Sodium silicate has been used formore than a century for the production of commercial products such as special cements, coatings, molded articles and catalysts. Sometimes silica fume is used as an alternative to the sodium silicate, which normally

forms part of the reactant solution [43]. The soluble silicate is mixed with fly ash, cement, lime, slag or other source of multivalent metal ions that promotes the gelation and precipitation of silicates. More the NaOH get in contact with the reactive solid material the more silicate and aluminate monomers are released.

2.4 Properties and application of geopolymers

Geopolymeric materials constitute a unique family of materials of a mixed nature, with properties varying from those characteristic of cements, ceramics and zeolites (depending on formulation) [37]. These characteristics arise from their excellent mechanical, chemical and thermal properties [54, 55]. Owing to their lower Ca content, they are more resistant to acid attack than materials based on Portland cement [56].

Most considerable properties of geopolymers can be summarized and listed as follows:

1. Excellent mechanical strength due to high degree of polycondensation and fast setting time,in fact geopolymer obtain 70% of the final compressive strength in the first 4 h of setting [57];
2. Good resistance to abrasion [49];
3. High fire resistance: geopolymer can withstand 1000 °C to 1200 °C without losing function and without harmful gas emissions [1];
4. Excellent resistance to different chemical reagents [58] and long-term durability: geopolymer concrete or mortars withdraw thousands of years weathering attack without much function loss;
5. Low thermal conductivity [59];
6. Good adhesion properties to concrete, glass, steel and ceramic [60];
7. Lack of unwanted reactions between the matrix and aggregates [61];
8. Excellent surface finishing and ability to replicate complicate shapes with moulding processes [1];
9. Low production costs of about 10-30% compared to OPC, especially if wasting materials are used as raw materials [61].

In addition, they are of great interest because of the reduced energy requirement for their manufacture, in fact they are also known as ‘‘Green materials’’ for their low energy consumption and low waste gas emission during manufacture. Thermal processing of natural alumino-silicates at relative low temperature provides suitable geopolymeric raw

material, resulting in 3/5 less energy assumption than Portland cement. In addition, greenhouse gas emission can be reduced up to 80% in comparison to traditional cement based materials [62]. Depending on the raw material selection and processing conditions, geopolymers can exhibit a wide variety of properties and characteristics. Despite this wide variety of commonly boasted attributes, these properties are not necessarily inherent to all geopolymeric formulations. Inorganic polymers should not be considered a universal panacea for all material selection problems, but rather a solution that may be tailored by correct mix and processing design to optimize properties and/or reduce cost for a given application [37]. In Figure 2.7 are reported different possible geopolymer applications in relation to Si/Al ratios, which are a consequence of the raw materials selected; this means that it is possible to choose the more suitable starting material depending on the desired final properties of the product.

Geopolymer technology is gaining interest because of the successful application of products in various fields, driven by the superior properties of geopolymers relative to currently used materials. In addition, the environmental impact of the production process of Portland cement will drive active consideration of alternatives, including geopolymers. For construction applications in particular, new materials must meet a set of highly prescriptive standards and validation procedures, which is extremely expensive and time-consuming for manufacturers [63].

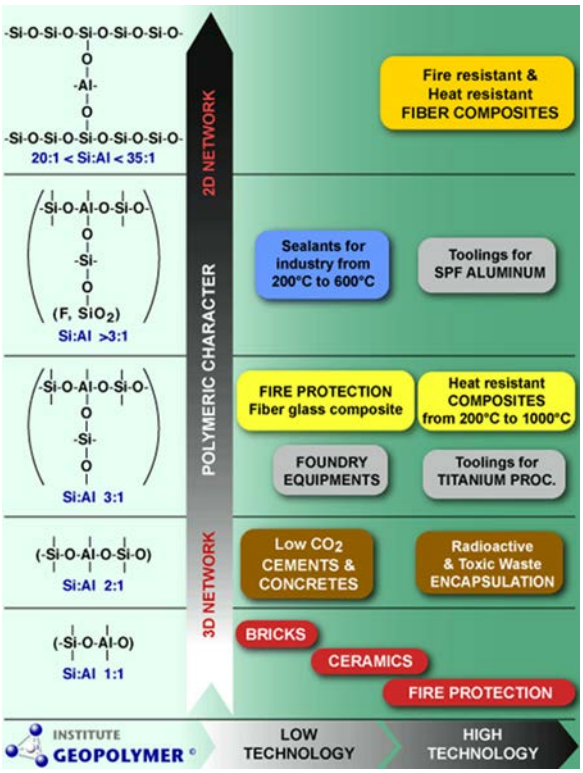

Figure 2.7 Different possible geopolymer applications in relation to Si/Al ratios

Although the lack of knowledge, especially on the long-term behaviour of geopolymers, cannot be neglected, an important reason for the slow development of markets for geopolymers is this conservative view of new materials. Consequently, it is not anticipated that geopolymers will supply a significant amount of the global need for cements in a near future. However, a geopolymer industry is forming and an increasing number of geopolymer supplier companies are becoming established based on research activities in universities and research institutes. Although there is no firm data on the market size, geopolymer concrete is now used in the transport sector in the USA and more recently in Australia. Moreover, the short setting time of geopolymer cement makes it an ideal solution for repairing highways and airport runways for example [63].

The ability of geopolymer matrixes to immobilize toxic materials and form an isolating coating for radioactive materials has been widely tested and appears to be accepted. In 1998 a pilot-scale experiment was successfully carried out in the Wismut mine water treatment facility at Schlema-Alberoda, Germany [64]. In another successful application, a geopolymeric shelter has been applied to encapsulate high level waste from the failed Chernobyl reactor 4 [63]. So there are many studies that showed geopolymer matrixes to

be a mature and cost-efficient solution to many problems where hazardous residues must be treated and stored under critical environmental requirements [63-65].

Another promising application of geopolymers is advanced fire resistant geopolymer composites. Geopolymers reinforced with carbon or glass fibres exhibit extraordinary mechanical properties at elevated temperatures and are ideal materials for aerospace applications [63]. In 1994, a geopolymer matrix composite was successfully used in a Formula 1 racing car, replacing titanium parts in exhaust system, and subsequently these composites have been widely adopted in racing cars where their thermal properties are effective [66]. Carbon fiber reinforced geopolymer composites do not ignite, burn or release any smoke after exposure to severe heat flux, which makes them appropriate materials for aircraft cabin fire protection, substituting for ordinary polymer matrix composites. The US Air Force is now uses bombers equipped with geopolymer composites as fire resistant materials [63].

Mechanical properties

Mechanical behavior is a basic property in assessing an engineering material for a specific application. For geopolymers as novel cementitious materials, compressive strength is an important factor. Ever since their invention in the 1950s, the better compressive strength, setting time and durability of geopolymers over conventional cements have been perceived as advantages. However, the compressive behavior of geopolymers varies according to the raw materials and processing method used. In order to produce a geopolymer with a high compressive strength, source materials with a high reactivity [23], a high strength gel phase and high ratio of gel to non-polymeric phases are required [63]. These factors relate directly to the type and molar ratios of oxides in the Al–Si source, type and pH of alkali solution and solubility of raw materials in the activator solution [19, 67]. Davidovits [68] introduced three ‘key parameters’ for producing high strength geopolymers. Based on research on kaolinite-based geopolymers, he defined the following ratios:

$$0.2 < Na_2O/SiO_2 < 0.28$$

$$3.5 < SiO_2/Al_2O_3 < 4.5$$

$$15 < H_2O/Na_2O < 17.5$$

In view of the importance of the dissolution of Al–Si species in alkali solution and of the polymerization reaction, it is unsurprising that the characteristics of the alkali solution directly affect the microstructural reorganization of the calcined clay and so the final mechanical properties of the product. In fact, although dissolution of Al–Si species increases on increasing the concentration of alkali solution [69], excessive amounts of NaOH or KOH in the aqueous phase decrease the SiO_2/Na_2O ratio and so inhibit polycondensation. Therefore, there is a limit for alkali hydroxide concentration in the activator solution to obtain a high strength gel phase.

Other important factors that affect mechanical strength of geopolymer are [38]:

- Curing temperature: curing at elevated temperature is effective (in the range of 30°C to 90°C) and has significant contribution to geopolymeric reactions, in fact, for example, at ambient temperature, the reaction of fly ash is extremely slow [70]. Initial curing at elevated temperature catalyzes formation in appropriate system chemistry [71].
- Curing time: experiments [38] reveal that prolonged curing time improve the polymerization process resulting in higher compressive strength. However, increase in strength for curing periods beyond 48 hours was not very significant [72, 58, 73]. Geopolymers developed compressive strength of 45 MPa in just 24 h. [28].
- Silicate and hydroxide ratio of activating solution: M_2O/SiO_2 ratio shows a positive effect on compressive strength. By the increase in concentration of alkali M_2O (M represents Na/K/metallic ions) or decrease in added silicate SiO_2, increase in compressive strength is expected [72, 23, 39]. This is because excess sodium silicate hinders water evaporation and structure formation [74]. The geopolymeric matrices activated with potassium silicate/KOH had the greatest compressive strength, while sodium silicate/NaOH activated matrices are generally weaker [38]. This is a consequence of the fact that K^+ is more basic and so it allows higher rate of solubilized polymeric ionization and dissolution, leading to dense polycondensation reaction that provides greater overall network formation and an increase in the compressive strength of the matrix.
- Aluminum source: Geopolymer containing clays (Kaolin and metakaolin) were found to be the strongest under compressive strength testing while fly ash alone lacked considerable strength alone [75]

- Liquid/solid ratio: strength decreases as the ratio of water-to-geopolymer solid by mass increases. This trend is analogous to water-to-cement ratio in the compressive strength in OPC. Although chemical processes involved in the formation of binders of both are entirely different [35, 19].
- Calcination of source materials: calcined fly ash, slag and metakaolin display a higher reactivity during geopolymerization than non-calcined material. Calcination activates material by changing their crystalline structure into amorphous structure to store extra energy and increase their activity [23] and increasing compressive strength [39]
- Relative humidity/curing conditions: experiment showed that samples cured at higher humidity (in sealed bags) do not improve strength; this behavior is in contrast with what expected from the curing of cementitious products.

2.5 Geopolymer as sustainbale binders: comparison with Portland cement

Availability of raw materials and its ease of production and application have made Portland cement concrete the most popular and widely used building material. The application of concrete in infrastructure and transport has unquestionably improved the development of civilisation, economic progress and the quality of life [76]. However, some inherent disadvantages of Portland cement remain difficult to overcome. Perhaps the most important of these is the high 'carbon content', in fact 1 t of CO_2 per tonne ordinary Portland cement (OPC) is released to the atmosphere and ~1,5 t per tonne of raw materials. This makes production of OPC extremely resource and energy intensive. Calculations [77] indicate that the total energy required to produce Portland cement is ~3630 MJ/t, compared with an energy consumption for geopolymer cement production of 990 MJ/t. The difference is mainly due to the lower calcination temperature for geopolymers (800 versus 1450°C). It has been estimated that total CO_2 emission for production of geopolymer cements is only 0,184 t per tonne of cement, about one-sixth that of Portland cement [78]. Considering global warming and international attempts to reduce greenhouse gas emissions, and government commitments under the Kyoto protocol, geopolymers as an alternative to Portland cements may potentially have a remarkable impact on CO_2 emission reduction strategies.

It is important to underline that geopolymeric cements present a different molecular structure compared to traditional cements based on Portland. In fact they show a more

complex structure characterized by a three-dimensional and cross-linked structure deriving from a multiphase chemical reaction of polycondensation. Traditional OPC are characterized by a different hardening method based, as it is well known, on hydration of silicate phases present in the raw materials that leads to a much less reticulated molecular structures. In Figure 2.8 are schematically reported these differences.

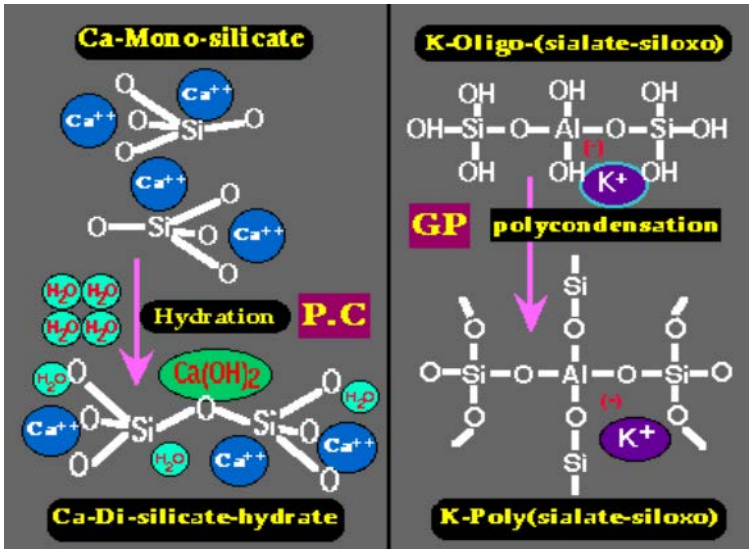

Figure 2.8 Comparison of the molecular structures of OPC and geopolymeric cement

In addition, the poor resistance of OPC concrete to corrosion and chemical attacks is a concern for designers, since OPC can deteriorate when exposed to severe environments. In contrast, geopolymers have shown superior resistance against chemical attacks. Song et al. [79] compared the durability of geopolymer and Portland cement concretes against sulphuric acid attack, concluding that the geopolymer concrete was highly resistant to sulphuric acid with a very low mass loss, < 3%.

Therefore, owing to their outstanding mechanical behaviour and environmentally friendly production, geopolymers have potential to substitute ordinary cements in construction applications or at least can decrease demand for Portland cement production. As discussed below, cost considerations also apply. Nevertheless, geopolymers are an ideal material for sustainable development, being characterised by [80]:

- abundant raw materials resources
- energy saving and environment protection

- simple preparation technique
- good volume stability
- short setting time
- ultra-high durability
- high fire resistance and low thermal conductivity
- ability to immobilize toxic atoms
- superior resistance to chemical attack.

All these properties make geopolymers a good substitute for ordinary materials in fields of industry such as civil engineering, automotive and aerospace, non-ferrous foundries, waste management and art and decoration.

2.6 Geopolymer as chemically bonded ceramics

Alkali-bonded ceramics constitute a family of materials with properties varying from those characteristic of ceramics, cements, zeolites or refractories, depending on formulation. These characteristics arise from a number of beneficial features, including rapid development of mechanical strength, fire resistance, dimensional stability, acid resistance, excellent adherence to aggregates and reinforcements [81].

These materials are called also chemically bonded ceramics (CBCs). This definition refers to the fact that they are produced through a chemical reaction at low temperature, in opposition to the traditional ceramic materials that usually are produced using fusion or sintering processes at elevated temperature. The bonding present in such CBCs, is a mixture of ionic, covalent, and van der Waals bonding, with the ionic and covalent dominating, like in ceramic materials, while in the traditional cement hydration products, van den Walls and hydrogen bonding dominate [82]. In fact, in hydraulic cements, hydrogen bonds are formed by chemical reaction when water is added to the powders. These bonds are distinct from the bond in ceramics in which high temperature interparticle diffusion leads to consolidation of powders. So, the main distinction between cements and ceramics is how they are produced, the first ones are obtained through a chemical reaction at room temperature, the other ones need to go through intense heat treatment for their consolidation. There exist products that are made like cements but exhibit a structure and properties like that of ceramics, because the mechanism bonding in them is covalent and ionic. To define such intermediate products, the name chemically bonded ceramic (CBCs) was coined by Roy [82].

Therefore, these CBCs show some of the typical properties of ceramic materials such as hardness, chemical and thermal stability, good resistance to acid attack and excellent corrosion resistance with the great advantage to be obtained at low temperature.

In the production of geopolymers, a chemical reaction is employed to produce a hard-ceramic like products and, though these products are produced like cements, their properties are more like a sintered ceramic [83]. So, geopolymers can be classified as chemically bonded ceramics.

Bibliography

[1] J. Davidovits, Geopolymers: Inorganic polymeric new materials. Journal of Thermal Analysis, 37, (1991) p. 1633-1656.

[2] P. Duxson, A. Fernandez-Jimenez, J.L Provis, G. C. Lukey, A. Palomo, J. S. J. van Deventer, Geopolymer technology: the current state of the art, Journal of Materials Science, 42, (2007) p. 2917-2933.

[3] P. Steins, A. Poulesquen, O. Diat, F. Frizon, Structural evolution during geopolymerization from an early age to consolidated material, Langmuir, 2012, 28, p. 8502-8510.

[4] J.P. Hos, P.G. Mccormick, L. T. Byrne, Investigation of a synthetic aluminosilicate inorganic polymer, J Mater Sci, 37(11), (2002) 2311-2316.

[5] S. Alonso, A. Palomo, Alkaline activation of metakaolin and calcium hydroxide mixtures: influence of temperature, activator concentration and solids ratio, Mater Lett 47, (2001) 55-62.

[6] J.G.S. Van Jaarsveld, J.S.J. Van Deventer, G.C. Lukey, The effect of composition and temperature on the properties of fly ash- and kaolinite-based geopolymers, Chem Eng J., 89, (2002) 63-73.

[7] J.S.G. Van Jaarsveld, J.S.J. Van Deventer, L. Lorenzen, Factors affecting the immobilization of metals in geopolymerized fly ash, Metal Mater Trans B 29, (1998) 283-291.

[8] V.D. Glukhovsky, Soil silicates, Gosstroyizdat, Kiev, (1959) pp 154.

[9] A. Fernández-Jiménez , A. Palomo, M. Criado, Microstructure development of alkali-activated fly ash cement: a descriptive model, Cem Conc Res, 35, (2005) 1204-1209.

[10] A. Fernández-Jiménez , A. Palomo, I. Sobrados, J. Sanz, The role played by the reactive alumina content in the alkaline activation of fly ashes, Micropor Mesopor Mater, 91, (2006) 111-119.

[11] J.L. Provis, G.C. Lukey, J.S.J. Van Deventer, Do Geopolymers Actually Contain Nanocrystalline Zeolites? A Reexamination of Existing Results, Chem Mater, 17, (2005) 3075-3085.

[12] J.L. Provis, P. Duxson, J.S.J. Van Deventer, G.C. Lukey, The Role of Mathematical Modelling and Gel Chemistry in Advancing Geopolymer Technology, Chem Eng Res Des, 83, (2005) 853-860.

[13] J.SJ. Van Deventer, J.L. Provis, P. Duxson, G.C. Lukey, Reaction mechanisms in the geopolymeric conversion of inorganic waste to useful products, J Hazard Mater, 139(3), (2006) 506–513.

[14] J. Davidovits, J.L. Sawyer, Early high-strength mineral polymer (1985) US Patent, No. 4509985.

[15] J. Davidovits, The need to create a new technical language for the transfer of basic scientific information. Transfer and Exploitation of Scientific and Technical Information, EUR 7716. Luxembourg, Commission of the European Communities, (1982).

[16] J.G.S. Van Jaarsveld, J.S.J. Van Deventer, L. Lorenzen, The potential use of geopolymeric materials to immobilise toxic metals: Part I. Theory and applications, Miner Eng, 10, (1997) 659-669.

[17] H. Xu, J.S.J. Van Deventer, The geopolymerisation of alumino-silicate minerals, Int J Miner Process, 59, (2000) 247-266.

[18] H. Xu, J.S.J. Van Deventer, Microstructural characterisation of geopolymers synthesised from kaolinite/stilbite mixtures using XRD, MAS-NMR, SEM/EDX, TEM/EDX, and HREM, Cement Concrete Res 32, (2002) 1705-1716.

[19] J.G.S. Van Jaarsveld, J.S.J. Van Deventer, G.C. Lukey, The characterisation of source materials in fly ash-based geopolymers, Mater Lett 57, (2003)1272-1280.

[20] J.G.S. Van Jaarsveld, J.S.J. Van Deventer, A. Schwartzman, The potential use of geopolymeric materials to immobilise toxic metals: Part II. Material and leaching characteristics, Miner Eng 12, (1999) 75-91.

[21] J.W. Phair, J.S.J. Van Deventer, Effect of silicate activator pH on the leaching and material characteristics of waste-based inorganic polymers, Miner Eng, 14, (2001) 289-304.

[22] J.W. Phair, J.S.J. Van Deventer, J.D. Smith, Mechanism of Polysialation in the Incorporation of Zirconia into Fly Ash-Based Geopolymers , Eng Chem Res 39, (2000) 2925-2934.

[23] H. Xu, J.S.J. Van Deventer, Geopolymerisation of multiple minerals, Miner Eng 15, (2002) 1131-1139.

[24] D. Feng, H. Tan, J.S.J. Van Deventer, Ultrasound enhanced geopolymerisation, J Mater Sci 39, (2004) 571-580.

[25] W.K.W Lee, J.S.J. Van Deventer, Effects of Anions on the Formation of Aluminosilicate Gel in Geopolymers, Ind Eng Chem Res 41, (2002) 4550-4558.

[26] P. Duxson, G.C. Lukey, F. Separovic, J.S.J. Van Deventer, Effect of Alkali Cations on Aluminum Incorporation in Geopolymeric Gels Ind Eng Chem Res, 44, (2005) 832-839.

[27] H. Rahier, B. Van Mele, M. Biesemans, J.Wastiels, X. Wu, Low-temperature synthesized aluminosilicate glasses, J Mater Sci 3, (1996) 71-79.

[28] A. Palomo, J.I.L. De La Fuente, Alkali-activated cementitous materials: Alternative matrices for the immobilisation of hazardous wastes: Part I. Stabilisation of boron, Cem Conc Res, 33, (2003) 281-288.

[29] P.V. Krivenko, Proceedings of the first international conference on alkaline cements, concretes. VIPOL Stock Company, Kiev, Ukraine, (1994) pp 11– 129.

[30] S. Mallicoat, P. Sarin, W.M. Kriven, Novel, alkali-bonded, ceramic filtration membranes, Ceram Eng Sci Proc, 26, (2005) 37.

[31] M. Sofi, J.S.J. Van Deventer, P.A. Mendis, G.C. Lukey, Bond performance of reinforcing bars in inorganic polymer concrete (IPC) J Mater Sci, 42, (2006), 3107–3116.

[32] Y. Bao, M.W. Grutzeck, C.M. Jantzen, Preparation and Properties of Hydroceramic Waste Forms Made with Simulated Hanford Low-Activity Waste, J Am Ceram Soc, 88, (2005) 3287-3302.

[33] E. Hermann, C. Kunze, R. Gatzweiler, G. Kiebig, J. Davitovits In: Proceedings of Geopolymers, (1999) p 211.

[34] C.J. Xiong, C.H. Ban, X. Pei, Z. Fang In: International workshop on sustainable development and concrete technology. Beijing, (2004) p 299.

[35] D. Hardjito, S.E. Wallah, D.M.J Sumajouw, B.V. Rangan, Brief Review Of Development Of Geopolymer Concrete, Invited Paper, George Hoff Symposium, American Concrete Institute. Las Vegas, USA, (2004).

[36] C. Panagiotopoulou, E. Kontori, T. Perraki, G. Kakali, Dissolution of aluminosilicate minerals and by-products in alkaline media, J Mater Sci, 42, (2007) 2967–2973.

[37] P. Duxson, A. Fernández-Jiménez, J. L. Provis, G. C. Lukey, A. Palomo, J. S. J. van Deventer, Geopolymer technology: the current state of the art, J Mater Sci, 42, (2007) 2917–2933.

[38] D. Khale, R. Chaudhary, Mechanism of geopolymerization and factors influencing its development: a review, J Mater Sci, 42, (2007) 729–746.

[39] D.M.J. Sumajouw, D. Hardjito, S.E. Wallah, B.V. Rangan, Green Processing The Australian Institute of Mining and Metallurgy, Fremantle, Western Australia, (2004) p 237.

[40] H. Rahier, J.F. Denayer, B. Van Mele, J Mater Sci, Low-temperature synthesized aluminosilicate glasses Part IV Modulated DSC study on the effect of particle size of metakaolinite on the production of inorganic polymer glasses, 38, (2003) 3131-3136-

[41] A. Fernández-Jiménez, A.G. de la Torre, A. Palomo, G. López-Olmo, M.M. Alonso, M.A.G. Aranda, Quantitative determination of phases in the alkali activation of fly ash. Part I. Potential ash reactivity, Fuel, 85, (2006) 625–634.

[42] A. Fernández-Jiménez, A. Palomo, Mid-infrared spectroscopic studies of alkali-activated fly ash structure, Microporous and Mesoporous Materials, 86, (2005) 207–214.

[43] L.M. Keyte, G.C. Lukey, J.S.J. Van Deventer In: Nzihou A (ed) Wasteeng. Albi, France. CD-ROM Proceedings (2005).

[44] A. Fernández-Jiménez, A. Palomo, Characterisation of fly ashes. Potential reactivity as alkaline cements, Fuel 82, (2003) 2259-2265.

[45] J. L Provis, J.S.J. Van Deventer, eds. Geopolymers: structures, processing, properties and industrial applications. Elsevier, (2009).

[46] N. Tsuyuki, K. Koizumi, Granularity and surface structure of ground granulated blast-furnace slags. Journal of the American Ceramic Society, 82, (1999) 2188–2192.

[47] C. Shi, P.V. Krivenko, D. M. Roy, Alkali-Activated Cements and Concretes, Abingdon, UK, Taylor and Francis, (2006).

[48] H. Wan, Z. Shui, Z. Lin, Analysis of geometric characteristics of GGBS particles and their influences on cement properties, Cement and Concrete Research, 34, (2004) 133–137.

[49] P. Z Wang, R. Trettin, V. Rudert, Effect of fineness and particle size distribution of granulated blast-furnace slag on the hydraulic reactivity in cement systems. Advances in Cement Research, 17, (2005) 161–166.

[50] D. Bondar, C.J. Lynsdale, , N.B. Milestone, , N. Hassani, , A.A. Ramezanianpour, Effect of adding mineral additives to alkali-activated natural pozzolan paste, Construction and Building Materials, 25, (2011) 2906–2910.

[51] A. Allahverdi, K. Mehrpour, E. Najafi Kani, Taftan Pozzolan-Based Geopolymer Cement, IUST International Journal of Engineering Science, 19(3), (2008) 1-5.

[52] J. H. Chen, J. S. Huang, Y. W. Chang, A preliminary study of reservoir sludge as a raw material of inorganic polymer, Constr. Build. Mater., 23, (2009) 3264–3269.

[53] R. M. F. Fonseca, F. J. A. S. Barriga, P. I. S. T. Conceição, Clay minerals in sediments of Portuguese reservoirs and their significance as weathering products from over-eroded soils: a comparative study of the Maranhão, Monte Novo and Divor Reservoirs (South Portugal)', Int. J. Earth Sci., 99, (8), (2010)1899-1916.

[54] A. Palomo, A. Macias, M. T. Blanco, F. Puertas, Physical, chemical and mechanical characterization of geopolymers, Proc. 9th Cong. on 'Chemistry of cement', New Delhi, India, Vol. 5, (1992) 505–511.

[55] M. Schmücker, K. J. D. MacKenzie: 'Microstructure of sodium polysialate siloxo geopolymer', Ceram. Int., 31, (2005) 433–437.

[56] T. Bakharev, Resistance of geopolymer materials to acid attack, Cem. Concr. Res., 35, (4), (2005) 658–670.

[57] W.K.W. Lee, J.S.J van Deventer, The effect of ionic contaminatson tje early-age properties of alkali-activated fly ash-based cements, Cem. Concr. Res., 32, (2002) 577-584.

[58] A. Palomo, M. Grutzeck, M. T. Blance, Alkali-Activated Fly Ashes: A Cement for the Future, Cement and Concrete Research, 8 (1999)1323-1329.

[59] P. Duxon, J.L. Provis, F. Lukey, Understanding the relationship between geopolymer composition, microstructure and mechanical properties, Colloid and surface, 269, (2005) 47-58.

[60] J. Bell, M. Gordon, W. M Kriven, Use of geopolymeric cements as a refractory adhesive for metal and ceramic joins, Ceramic Engineering and Science Proceedings, 26, (2005) 407-413.

[61] I. Garcia-Lodeiro, A. Palomo, A. Fernandez-Jimenez, Alkali-aggregate reaction in activated fly ash systems, Cem. Concr. Res., 37, (2007) 175-183.

[62] D. Hardjito, S.E. Wallah, D.M.J. Sumajouw, B.V. Rangan, In: 18th Australasian conference on the mechanics of structures and materials (ACMSM)1-3. Perth Australia (2004).

[63] B.Majidi, Geopolymer technology, from fundamentals to advanced applications: a review, Materials Technology, 24:2, (2009) 79-87.

[64] E. Hermann, C. Kunze, R. Gatzweiler, G. Kiebig, J. Davidovits, Solidification of various radioactive residues by geopolymer with special emphasis on long-term stability', Proc. Conf. Géopolymère '99, Saint-Quentin, France, Institut Géopolymère, (1999) 211–228.

[65] D. Majersy, S. Sekely, M. Breza, Verified possibilities of specific and historical waste solidification, IAEA RCM on Behaviour of cementitious materials in Long term storage and disposal of radioactive waste meeting, 10–14 September, Moscow, Russia, (2007).

[66] J. Davidovits, 30 years of successes and failures in geopolymer applications. Market trends and potential breakthroughs, Proc. Int. Conf. Geopolymer 2002, Melbourne, Australia, (2002).

[67] H. Xu: 'Geopolymerisation of aluminosilicate minerals', PhD thesis, Department of Chemical Engineering, University of Melbourne, Australia.

[68] J. Davidovits, Geopolymers: man-made rock geosynthesis and the resulting development of very early high strength cement, Journal of Materials education, 16, (1994) 91-139.

[69] H.A. Gasteiger, W.J. Frederik, R.C. Streisel, Solubility of aluminosilicates in alkaline solutions and a thermodynamic equilibrium model, Ind Eng Chem Res, 31, (1992) 1183-1190.

[70] F. Puertas, S. Martinez-Ramirez, S. Alonso, T. Vazquez, Alkali-activated fly ash/slag cements: Strength behaviour and hydration products, Cement Concrete Res, 30, (2000)1625-1632.

[71] M. Atkins, F. P. Glasser, J. J. Jack, Zeolite P in cements: its potential for immobilizing toxic and radioactive waste species, Waste management, 15(2), (1995) 127-135.

[72] D. Hardjito, S. E. Wallah, D. M. Sumajouw, B. V. Rangan, On the development of fly ash-based geopolymer concrete, ACI Materials Journal-American Concrete Institute, 101(6), (2004) 467-472.

[73] J. C Swanepoel, C. A. Strydom, Utilisation of fly ash in a geopolymeric material, Applied Geochemistry, 17(8), (2002) 1143-1148.

[74] T. W Cheng, J. P. Chiu, Fire-resistant geopolymer produced by granulated blast furnace slag, Minerals Engineering, 16(3), (2003) 205-210.

[75] J. W. Phair, J. S. J. Van Deventer, J. D. Smith, Effect of Al source and alkali activation on Pb and Cu immobilisation in fly-ash based “geopolymers”, Applied Geochemistry 19.3, (2004) 423-434.

[76] P. K. Mehta, Advanced cements in concrete technology, Concrete Int., 21, (1999) 67–76.

[77] J. Davidovits, Geopolymer chemistry and applications 505, Saint Quentin, Institut Géopolymère (2005).

[78] J. Davidovits, Environmentally driven geopolymer cement applications, Proc. Int. Conf. Geopolymer 2002, Melbourne, Australia, October (2002).

[79] X. J. Song, M. Marosszeky, M. Brungs, R. Munn: Proc. 10DBMC Int. Conf. on Durability of Building Materials and Components, Lyon, France, April 2005.

[80] Z. Li, Z. Ding, Y. Zhang, Development of sustainable cementitious materials, Proc. Int. Workshop on 'Sustainable development and concrete technology', Beijing, China, (2004) 55–76.

[81] E. Landi, V. Medri, E. Papa, J. Dedecek, P. Klein, P. Benito, A.Vaccari, Alkali-bonded ceramics with hierarchical tailored porosity. Applied Clay Science, 73, (2013) 56-64.

[82] D. M. Roy, New strong cement materials: chemically bonded ceramics. Science, 235, (1987) 651-659.

[83] A. S. Wagh, Chemically bonded phosphate ceramics: twenty-first century materials with diverse applications, Elsevier, (2016).

3. Design and synthesis of hybrid geopolymeric foams

Research in the field of geopolymers has historically been application-focused. The mechanisms and processes underlying geopolymer formation, which control the structures of the products of these reactions, have only relatively recently become the subject of detailed attention. However, more and more progress is being made in this area as widely described in the previous chapter.

The same surge of activities has been observed in the field of ceramic foams, because these innovative materials have started to be used as components in special and advanced engineering applications. Improvements in conventional processing methods and the development of innovative fabrication approaches are required because of the increasing specific demands on properties and morphology (cell size, size distribution and interconnection) for these materials, which strictly depend on the application considered [1].

So alkali-bonded ceramics and foams with tailored porosity have very interesting applications in particular as thermal and acoustic insulators. One of the most important and most compelling requirements for insulating materials suitable for building, transport sector, automotive or aerospace industry is the incombustibility. The materials used in these sectors, in fact, have to respect very strict standard regulations about the fire behavior because of safety issues involved in the transport and in reside of millions of people.

In order to satisfy the need of respecting the incombustibility requirement, a smart decision in the production of insulators could be the selection of inorganic and ceramic materials as main components of the foams. The presence in high percentages of this kind of materials, which are completely non-flammable, in fact should ensure the incombustibility of the final products. This should represent a huge innovation in the production of insulating materials, especially considering that the most of insulators offered and sold on the market are made of polymeric foams.

This is exactly the main idea at the base of this scientific work, which deals with the synthesis and characterization of organic–inorganic hybrid foams based on alkali alumino-silicate matrices with tailored porosity, obtained by synergistic effect of different kind of foaming, chemical and/or physical.

3.1 Foaming techniques

Pores can be incorporated into the structure of a ceramic through many processing techniques; in this scientific work, direct foaming has been selected as processing method for the production of geopolymeric foams. Direct foaming consists in the generation of air bubbles inside a liquid slurry containing ceramic powders to create a foam which then needs to be set in order to maintain its porous morphology and keep the structure of air bubbles created. This processing method allows the manufacturing of both closed and open-cell foams with walls containing interconnecting pores (cell windows), and leads to a wide range of cell dimensions and of relative densities (amount of porosity) that can be achieved [2]. Moreover, with direct foaming technique it is also easy to produce foams with a graded porosity along one direction and the process allows for a good versatility in terms of final part shapes [1]. It is a very versatile processing method and these are the main reasons of its selection as foaming process, in addition to the fact that in situ inorganic foaming approaches allow tailoring the cellular structure of the alkali-activated materials in the meso to macro range.

Recently, surfactants such as lipids and proteins have been often proposed to stabilize different kinds of foams and emulsions, since their active surface can lower the interfacial tension of fluid interfaces [3, 4]. In fact, protein molecules adsorb at the interface between air and water via hydrophobic areas, and a partial unfolding (i.e., surface denaturation) occurs which contributes to stabilize the air bubbles embedded in the matrix through a mixing operation [5-8].

The simultaneous use of ‘‘in situ’’ chemical foaming and protein-assisted foaming has never been proposed and it can be considered a completely innovative approach to tailor the chemical–physical properties and density of inorganic foaming.

Chemical foaming

Different foaming procedures based on gas evolution in the viscous matrix have been widely exploited. Some authors proposed the hydrogen peroxide (H_2O_2) as chemical blowing agent for the foaming of the geopolymeric pastes [9, 10]. In fact, H_2O_2 is thermodynamically unstable, and therefore it can be easily decomposed to water and oxygen gas with the latter playing the role of the blowing agent:

$$2H_2O_2 \rightarrow 2H_2O + O_2$$

Another chemical foaming process is based on the redox reaction of Al or Si, in alkaline solution, which induces porosity by H_2 evolution [11-13]. In particular, the redox reaction of metallic Si impurities in silica fume could also be used to prepare geopolymeric foams [13, 14]. The Pourbaix diagram of silicon indicates that, in alkaline conditions, H_2 is always favoured [15], according to the following reaction [14]:

$$4H_2O + Si^0 \rightarrow 2H_2 \uparrow + Si(OH)_4$$

So, considering the strong alkaline environment typical of geopolymeric materials, metallic silicon was selected as the foaming agent responsible for the in situ foaming process in the production of geopolymeric foams.

Mechanical foaming

This process, usually employed in porous ceramic materials production, consists in a strongly whipping, under vigorous stirring, of a water solution containing vegetal proteins as surfactants that, added to the inorganic mixture, can act as ‘‘meringue’’ type foam. This kind of approach allows the stabilization of the air bubbles already present in the liquid geopolymeric slurry, produced during the in situ foaming, through the protein addition, and, at the same time, the increasing of the amount of air bubbles embedded in the matrix through the whipping stage. Since the rate of whipping influences strongly the expansion grade, it has to be suitably selected, in order to obtain a stable foam network, able to maintain itself during the gelification and consolidation processes. In order to allow the entrapping of the bubbles in the geopolymeric matrix, the foaming step has to take place just before the gelification and consolidation of the system.

In Figure 3.1 a graphical summary of the combined use of the chemical and mechanical foaming techniques is reported.

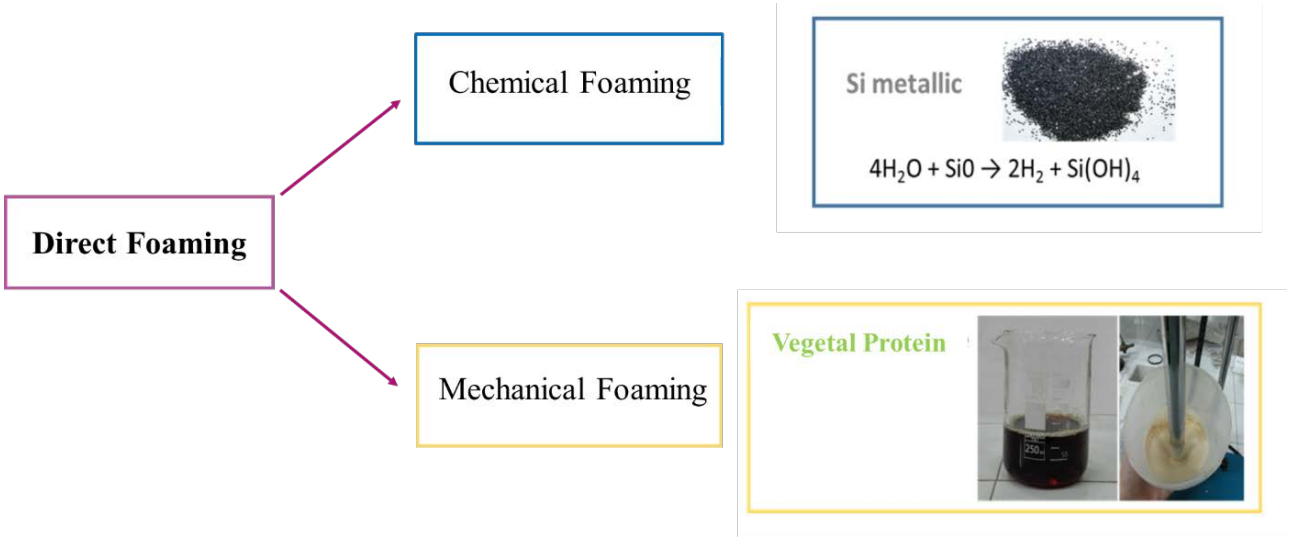

Figure 3.1 Schematic summary of the foaming processes used for the production of gepolymeric foams

Evaluation of foaming properties

In order to generate foams, large molecule surfactants, like proteins, need to approach the air/water interface, be denatured at the interface and then form a monolayer or film to trap air and form bubbles [16]. Good protein surfactants should be able to absorb to the interface rapidly, unfold and reorient quickly at the interface and form a strong, viscoelastic film around the air bubbles [17]. In addition, quick denaturation of proteins to expose their hydrophobic groups is favorable for forming a stable network at the interface during foaming [16]. During foaming, proteins form a monolayer or film at the interface through hydrophobic bonds, hydrogen bonds, etc., which presumably determines the stability of the foams. In fact, protein molecules act as hydrophilic and hydrophobic groups. The hydrophilic groups are arranged towards the water phase and the hydrophobic groups towards the air phase. During the whipping process air comes into the solution to form bubbles, the hydrophobic regions facilitate the adsorption at the interface, a process that is followed by partial unfolding (surface denaturation). This change in the molecular configuration results in the loss of solubility or precipitation of some proteins, which collect at the liquid-air interface. The attendant reduction in surface tension facilitates the forming of new interfaces and more bubbles. These partially unfolded molecules then associate to form a stabilizing film around the bubbles, which is essential for the stability of the foam. Excessive whipping of the protein solution produces a higher concentration of smaller bubbles resulting in more unstable foams. This

instability depends on the decrease in the bubble elasticity; it results from excessive insolubilisation of proteins at the air-albumen interface [18].

Foam collapses by three principal mechanisms. The first is the bubble disproportionation as a function of time, the bubbles reduce in size with time due to air diffusion from the interior which is a region of higher pressure. The second is the lamellae rupture – bubbles coalesce quickly due to pushing and pulling forces causing formation of holes between two bubbles. And the third is the drainage – water around the bubbles naturally drains down to the liquid layer removing proteins from the film around the bubble, which eventually becomes too thin to support the bubble.

Properties of foams vary with the methods and equipment used for their preparation. In this case, foam is formed sparging air through the protein solution using an Ultra-Turrax disperser. Then, foaming properties are evaluated by foaming capacity (FC) and foam stability (FS) [19].

In particular, the samples were whipped, in 600 mL glass beakers for 1 min. The volume of the foam generated was recorded and used to calculate foaming capacity. The foamed samples were held for 30 min to evaluate foam stability and then the liquid drainage. The different steps of this procedure are reported in Figure 3.2. Foaming capacity was studied by whipping the water solution containing vegetal surfactants as described above and calculating relative overrun [20]:

$$Relative\ overrun = V_0/V_i,$$

where V_i is the initial liquid volume, V_0 is the foam volume at 0 min.

Foam stability was studied comparing the volume of foam after 30 min with the initial foam volume at 0 min [20]:

$$FS = V_{30}/V_0,$$

where V_{30} is the foam volume at 30 min, V_0 is the foam volume at 0 min.

Liquid drainage was calculated from the liquid drained from the foam in a 30 min period [20]:

$$Liquid\ drainage = 1-(V_i-V_{L30})/(V_i-V_{L0}),$$

where V_i is the initial liquid volume, V_{L30}, volume of liquid at 30 min, V_{L0} is the volume of liquid at 0 min.

Figure 3.2 Experimental procedure for the evaluation of foaming properties of the selected foaming agent

The values obtained for the foaming agent used in the production of the ceramic foams are the following:

- Relative overrun = 3
- Foam stability = 0.53
- Liquid drainage = 0.9

The values of all these factors, used to investigate the foaming properties of our foaming agent, are definitely comparable with the values that ca be found in literature for other vegetal proteins, like egg albumen [21].

3.2 Materials

Metakaolin

As already mentioned above, the reaction of an aluminosilicate powder with a highly concentrated aqueous alkali hydroxide and/or silicate solution produces a synthetic amorphous-to-semicrystalline alkali aluminosilicate material which is the amorphous counterpart of crystalline zeolites. Among the aluminosilicate raw powders, metakaolin is the most reactive in alkaline conditions [22]. Metakaolin is essentially an anhydrous aluminosilicate that is produced by the thermal decomposition of kaolin, a naturally occurring clay basically containing kaolinite [$Al_2Si_2O_5(OH)_4$] and trace amounts of silica and other minerals. It is known [23, 24] that thermal activation in air (at 600–900°C) of many clay mineral leads, through dehydroxylation, to breakdown or partial breakdown of the crystal lattice structure forming a transition phase with high reactivity. In fact, a

typical example is the production of metakaolin ($Al_2O_3 \cdot 2SiO_2$) by calcining clay or lateritic soils [25] rich in kaolinite. The hydroxyl ions are strongly bonded to the aluminosilicate framework structure; thus only temperatures in excess of 550°C are capable of eliminating them [26] and that's exactly what happens during kaolinite calcination at 450–600°C, it loses the OH lattice water [27] and is transformed into metakaolin, a material with some degree of order. In metakaolin, the Si–O network remains largely intact and the Al–O network reorganizes itself. The final result is a partially ordered structure that cannot rehydrate in the presence of water (or does so very slowly). While kaolinite is crystalline, metakaolin has a highly disordered structure and offers good properties as mineral additive. Metakaolin reacts particularly well with lime and forms, in the presence of water, hydrate compounds of Ca and Al silicates. Therefore, it is considered a good synthetic pozzolana and, due to its disorder and X-ray amorphous nature, it possesses a huge reactive potential in the presence of an alkali/alkaline earth containing solution.

The metakaolin (MK) powder, used as starting raw material for the synthesis of geopolymeric foams, was provided by Neuchem (Mefisto L 05) and it is shown in Figure 3.3. The chemical composition of the metakaolin was reported in Table 3.1.

Figure 3.3 Metakaolin powder

Table 3.1 Chemical composition of metakaolin (wt%)

	SiO_2	Al_2O_3	TiO_2	Fe_2O_3	K_2O	MgO	CaO
Metakaolin	52.90%	41.90%	1.80%	1.60%	0.77%	0.19%	0.17%

In order to find out which minearogical phases are present in the metakaolin, XRD analysis was performed on a powder sample using a Panalytical X'Pert Pro diffractometer equipped with PixCel 1D detector (operative conditions: CuKα1/Kα2 radiation, 40 kV, 40 mA, 2Θ range from 5 to 80°, step size 0.0131° 2Θ, counting time 40s per step) and the resulting spectrum was reported in Figure 3.4. The spectrum shows that the main crystalline phases present are: quartz (ICCD 03-065-0466) and kaolinite (ICCD 00-029-1490), as it was predictable, with the presence of chlorite (ICCD 00-039-0381) and halloysite (ICCD 00-029-1489).

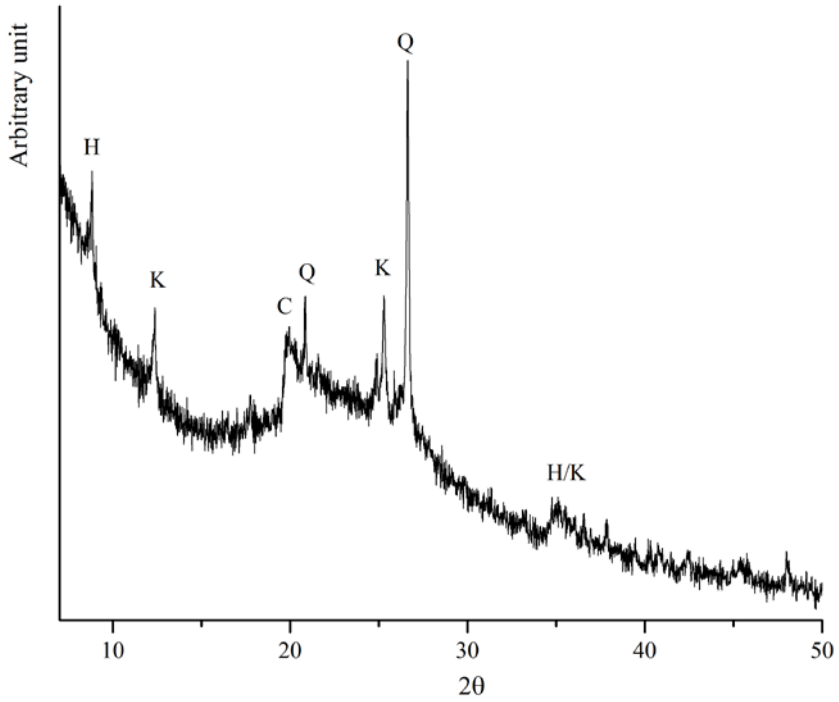

Figure 3.4 XRD spectrum of metakaolin (Q=quartz, K=kaolinite,C=chlorite, H=halloysite)

The microstructure of the metakaolin powder was analyzed using SEM analyses (SEM, LEO 1530, Zeiss). The microscopies are reported in Figure 3.5. From the images, it is possible to identify easily the layered microstructure associated with clay phases and, in particular, the typical plate structure of kaolinite [28, 29] that is one of the main component of metakaolin analysed.

Considering the fact that, as mentioned before, metakaolin is very reactive in alkaline environments, an important parameter to take in consideration is the specific surface area, because it can give precious information about the reactivity of powder. Surface area was

measured performing BET nitrogen adsorption analysis. The analysis was performed using a Nova 1000 machine (Quantachrome, USA).

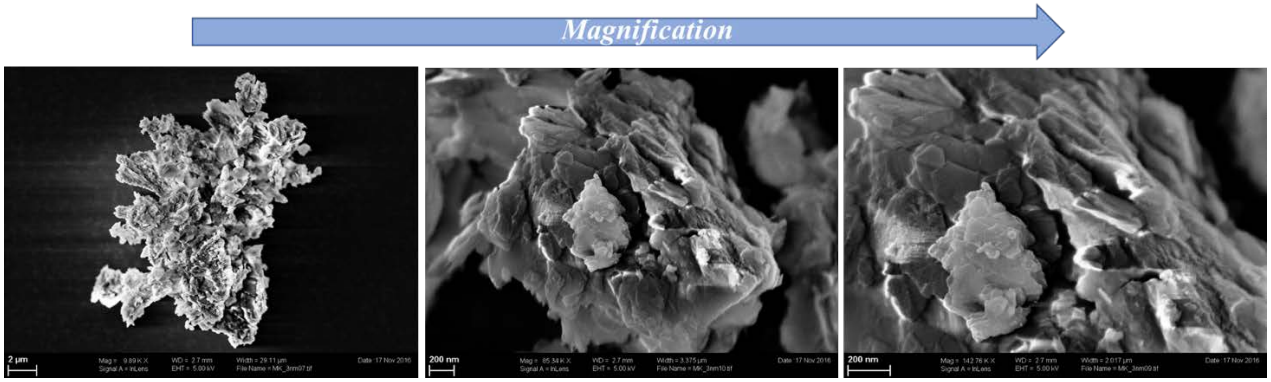

Figure 3.5 SEM micrographs of metakaolin

In Figure 3.6 is reported the adsorption isotherm of metakaolin.and the BET surface value obtained. According to the Brunauer classification of the adsorption isotherms, the one of metakaolin can be clearly classified as III type isotherm; it shows a convex regular shape, without any knee or plateau, this is representative of weak adsorbent-adsorbate interactions. The BET value obtained for the measure of specific surface is quite high and it can be related to the highly layered microstructure of metakaolin.

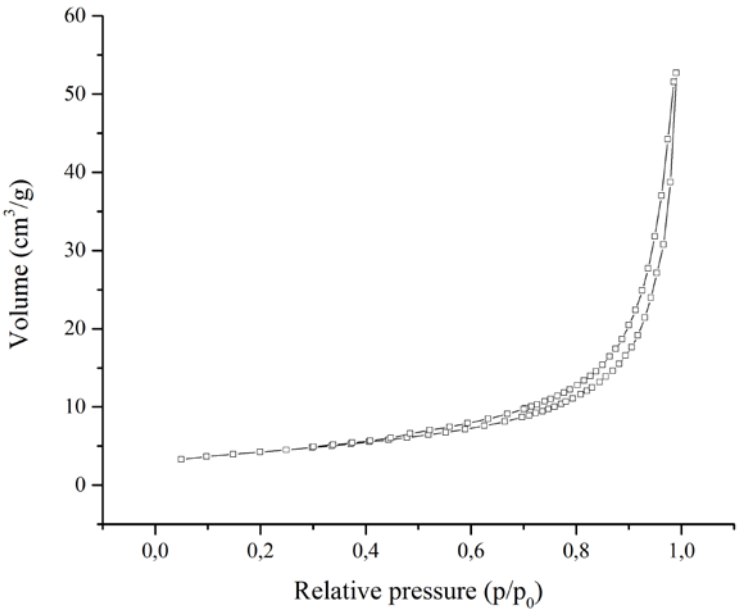

BET Surface Area = 14.867 m²/g

Figure 3.6 N_2 gas sorption isotherm of the metakaolin

Sodium silicate solution

Sodium silicate is the common name for compounds with the formula $(Na_2SiO_2)_nO$; in particular, a well-known member of this series is the sodium metasilicate, Na_2SiO_3. These materials, also known as waterglass or liquid glass, are available in aqueous solution and in solid form. The pure compositions are colorless or white, but commercial samples are often greenish or blue owing to the presence of iron-containing impurities. They are used in cements, passive fire protection, textile and lumber processing, refractories, and automobiles. Sodium silicate is a white powder that is readily soluble in water, producing an alkaline solution.

The Sodium Silicate water solution (SS), utilized as alkali activator for the production of geopolymeric foams, was provided by Prochin Italia Srl (Figure 3.7) and has the following chemical composition: Na_2O 8.15%, SiO_2 27.40 %. The weight ratio $R=SiO_2/Na_2O$ is a specific ratio typical of each different kind of silicate solutions, the SS used in this case has R = 3,3.

Figure 3.7 Sodium Silicate Solution (SS)

Sodium hexafluorosilicate

In order to promote the gelification of the sodium silicate and consequently of the entire geopolymeric system, sodium hexafluorosilicate (Na_2SiF_6) was added as catalyst. Sodium fluorosilicate is made by neutralizing fluosilicic acid with sodium chloride or sodium

carbonate [30]. It is used in some countries as additives for water fluoridation, opal glass raw material, ore refining, or other fluoride chemical (like sodium fluoride, magnesium silicofluoride, cryolite, aluminum fluoride) production.

The amount of catalyst and its typology have a key role on both setting time and mechanical characteristics of the final glassy material.

The sodium hexafluorosilicate was purchased by Carlo Erba Reagents srl (Figure 3.8).

Figure 3.8 Sodium hexafluorosilicate

Metal Silicon

Silicon is a chemical element with symbol Si and atomic number 14. It is a hard and brittle crystalline solid with a blue-gray metallic luster, and a tetravalent metalloid. It is rather unreactive, and has great chemical affinity for oxygen. It was first prepared and characterized in pure form only in 1823 by Jöns Jakob Berzelius. Silicon is the eighth most common element in the universe by mass, but very rarely occurs as the pure element in the Earth's crust. It is most widely distributed in dusts, sands, planetoids, and planets as various forms of silicon dioxide (silica) or silicates. Over 90% of the Earth's crust is composed of silicate minerals, making silicon the second most abundant element in the Earth's crust (about 28% by mass) after oxygen [31]. In its crystalline form, pure silicon has a gray color and a metallic luster (Figure 3.9). Silicon is widely used commercially without being separated, and often with little processing of the natural minerals. Such use includes industrial construction with clays, silica sand, and stone. Silicate is used in Portland cement for mortar and stucco, and mixed with silica sand and gravel to make

concrete for walkways, foundations, and roads. Silicates are used in white ware ceramics such as porcelain, and in traditional quartz-based soda-lime glass and many other specialty glasses. Silicon compounds such as silicon carbide are used as abrasives and components of high-strength ceramics.

Silicon powder, used as foaming agent for the production of hybrid geopolymeric foams, was purchased by Merck.

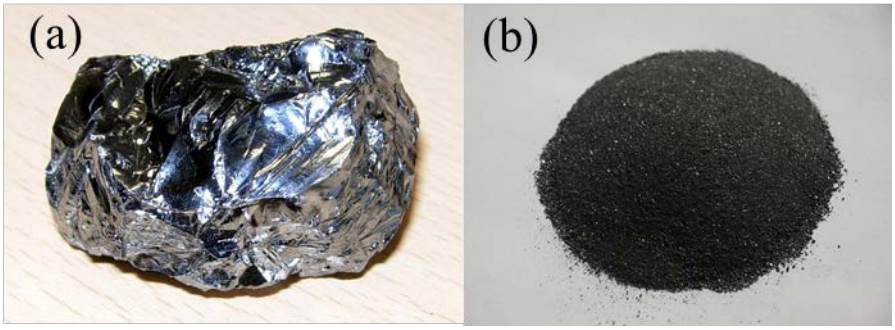

Figure 3.9 Silicon metal in solid state (a) and as powder (b)

Vegetable surfactant

The vegetable surfactant in water solution (pH 7) is called ISOCEM S/L and it was supplied by Isoltech s.r.l. Italia. It is a foaming agent for cellular cement developed by Isoltech and made mainly of natural surfactants deriving from vegetal proteins and fatty acids. A sample of ISOCEM S/L is reported in Figure 3.10, while in Table 3.2 the most important physical properties of this natural foaming agent are reported.

Table 3.2 Physical properties of the vegetable protein used as foaming agent

Physical Properties	**ISOCEM S/L**
State	Liquid
Color	Light brown
Specific weight	1025 g/l
pH	7
Freezing point	-2° C

Figure 3.10 Vegetable protein ISOCEM S/L in water solution

3.3 Design of geopolymeric foams

In order to control the morphology and porosity of the geopolymeric foams, the kinetic of the chemical–physical reactions that occur during the process of geopolymerization and following foaming was evaluated. It is useful to remember thar geopolymerization is a complex process that involves the dissolution of silicoaluminate amorphous phases in contact with high pH alkaline solutions (i.e., sodium silicate). In particular, both SiO_4 and AlO_4 units, released from the amorphous phase, reorient and polycondense leading to a strong network, which provides interparticle bonding and physical strength of geopolymer [32]. The schematic formation of a geopolymer can be illustrated by the following reactions [33]:

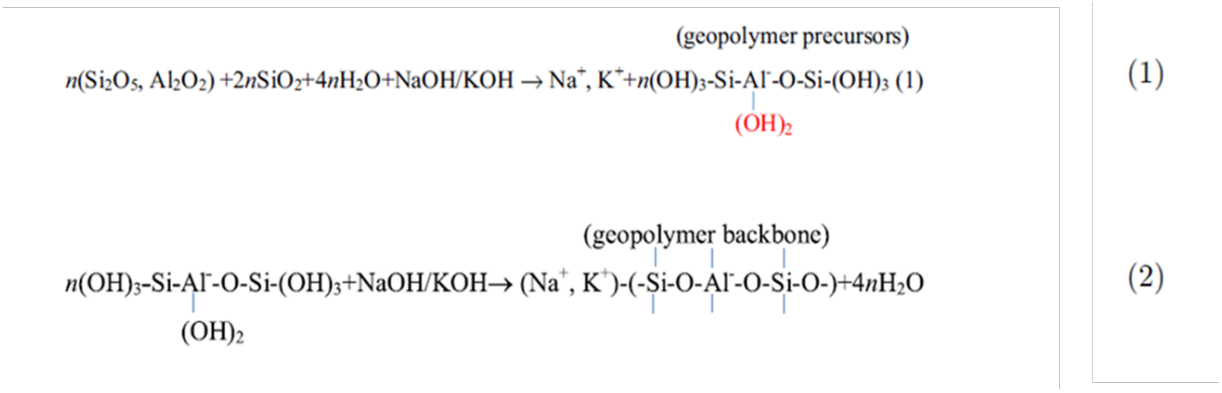

Simultaneously to the dissolution, the sodium silicate solution condenses to form a silica gel $[(SiO_2)_n 2n(H_2O)]$, which evolves in a glassy material $[(SiO_2)n]$. This mechanism is based on the following reactions. The SS solution consists of a water solution of alkaline silica made of silicic acid:

$$SiO_2/Na_2O + 3H_2O \Leftrightarrow 2NaOH + Si(OH)_4. \qquad (3)$$

The addition of a specific catalytic acid additive, Na_2SiF_6, allows to control the gel's formation of the SS solution. In fact, Na_2SiF_6, in alkaline solution at 40°C gives SiF_6^{2-} ions, which have an acid hydrolysis as follow [34]:

$$SiF_6^{2-} + (n+2)\,H_2O \Leftrightarrow SiO_2 * nH_2O + 6F^- + 4H^+ \qquad (4)$$

The catalyst affects the equilibrium reaction (Eq. 3) promoting the formation of silicic acid ($Si(OH)_4$) and consequently the gelification of the system. Even though either the content of silicic acid or the condensation reactions allow the formation of a network with high crosslinking degree (Eq. 5):

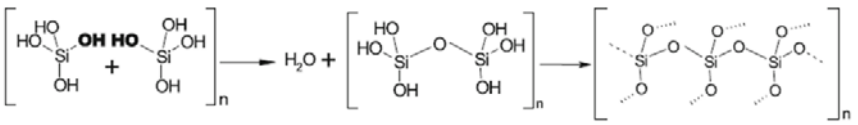

(5)

3.4 Preparation of geopolymeric foams

Three different ceramic foams were prepared. All of the three ceramic foams are based on the starting mixture of 70 % wt. SS, 8.7 % wt. Na_2SiF_6, and 21.3 % wt. metakaolin (MK).

In particular, the first foam, named SCF, was prepared by mixing 8 wt% of Si powder to the other solid raw materials, MK and Na_2SiF_6; they were homogeneously dry mixed (Figure 3.11a) and then the SS solution was added (Figure 3.11b). The so obtained paste was mixed for about two minutes and cast in appropriate molds.

Figure 3.11 Preparation of SCF geopolymeric foam

The second foam (PCF) was prepared by adding to the starting mixture 12 wt% of a ‘‘meringue’’ type foam, obtained from the whipping of the vegetable protein ISOCEM S/L. The ‘‘meringue’’ was prepared using an Ultra-Turrax disperser at 12000 rpm up to obtain a volume 8 times the initial one. The disperser and the procedure to whip the protein are reported in Figure 3.12. The third foam, named HCF, was prepared using simultaneously the Si powder and the whipped protein, adding both of them to the starting mixture. All the slurries were cast in plastic prismatic (40x40x160 mm) open molds (Figure 3.13) and cured at 40°C for 24 hours at room humidity.

Figure 3.12 Ultra-Turrax disperser and whipping of vegetable protein

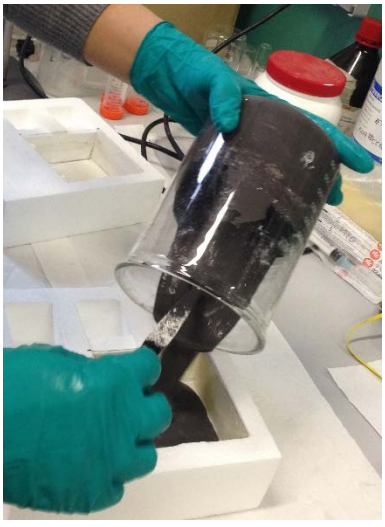

Figure 3.13 Casting of SCF foam in the plastic prismatic mold

The three different typologies of ceramic foams produced, reported in Figure 3.14, have been characterized from mechanical, morphological and chemical point of view in order to find out the final properties of the products obtained and the influence of the different foaming methods and foaming agents used.

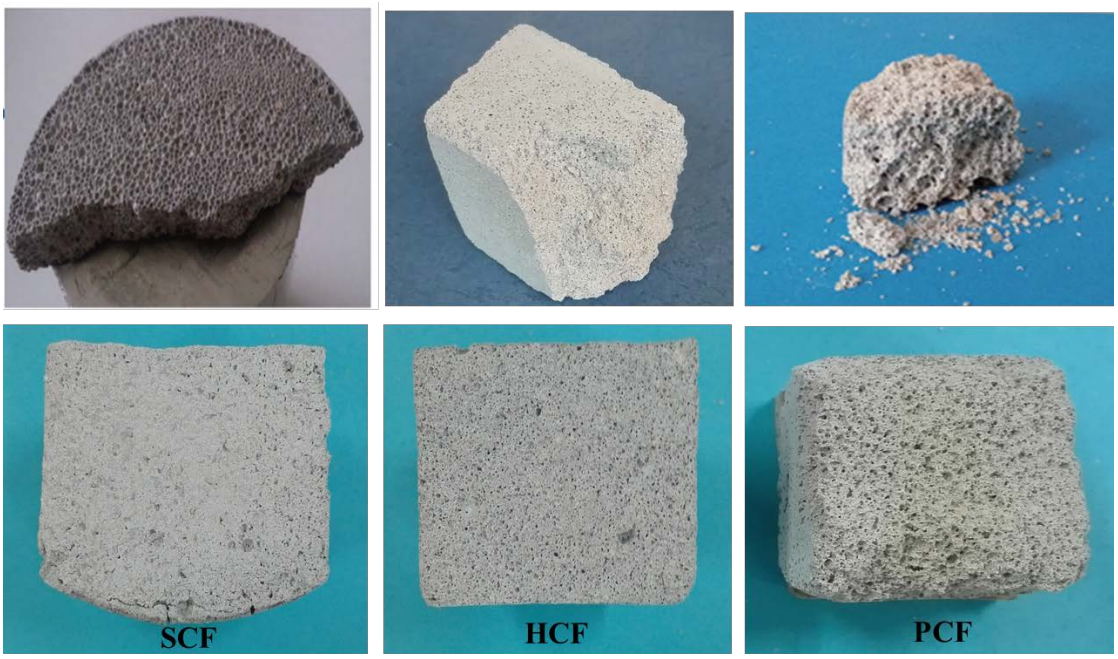

Figure 3.14 Samples of the three different types of ceramic foams produced

3.5 Optimization of process parameters affecting final foam properties

There are different parameters that can affect the foaming process and, consequently, the final features of the ceramic foams produced. For this reason, in order to optimize the properties of the final products obtained, the influence of some of these process parameters on the final porosity of the foams has been investigated.

In particular, the attention has been focused on three main factors:

a) Alkalinity of the activating solution
b) Amount of pore forming agent used
c) Curing temperature

All the ceramic foams produced are based on a starting mixture with the following composition: 70 % wt. SS solution, 8.7 % wt. Na_2SiF_6, 21.3 % wt. metakaolin (MK). All

the powder components were previously homogeneously dry mixed and then the SS solution was added [35].

The parameter that gives important information about the alkalinity of the activating solution is the ratio R = SiO_2/Na_2O, that is a characteristic ratio for sodium silicate solutions; it is quite clear that the increasing of this ratio leads to a reduction of the alkalinity of the solution considered. Two different SS solutions, one with R=3 and another one with R=2, have been tested in producing two different geopolymeric foams. The foams were produced adding each activating solution to the raw powder materials (MK, Na_2SiF_6 and metal silicon) previously homogenized and dry mixed. Then, the pastes obtained were cast in cylindrical open molds and cured at 40°C for 24 hours. In Figure 3.15 are reported respectively the sample obtained using SS solution with R=3 (3.14a) and the one obtained using SS solution with R=2 (3.14b). As it is possible to see from Figure 3.15, the sample produced starting from a more alkaline SS solution looks like a more "expanded" foam, with a higher and irregular open porosity, while the foam obtained with the SS solution with R=3, appears much more dense and characterized by a more regular and smaller porosity.

(a) (b)

Figure 3.15 Geopolymeric foam samples produced using SS solution with R=3 (a) and R=2 (b)

Regarding the amount of pore forming agent used, two different foams have been produced with two different percentages of metal silicon, one with 10% wt of silicon (Figure 3.16a) and the other one reducing the amount of silicon to the 8% wt (Figure 3.16b).

(a) (b)

Figure 3.16 Geopolymeric foam samples produced using 10% (a) and 8% (b) of metal silicon

It is evident from Figure 3.16 that the reduction of the percentage of metal silicon used to create porosity inside the ceramic matrix, did not lead to significant changes or differences in the final structure of the two foams produced. This means that the difference between the two percentages is maybe too slow to influence the effective capacity of the silicon to produce bubbles inside the matrix. So, it is clearly preferable using, considering the same final properties, a lower amount of metal silicon, especially because the presence of eventual unreacted silicon could represent a source of defect and can contribute to increase weight and density of the samples while, for these kinds of materials, low density and lightness are critical points.

It is well known that curing temperature represents an important parameter in the geopolymer production. In particular, it has been proved that prolonging the curing time and increasing the curing temperature (up to 60°C) can speed up the harden process and improve the physical properties of a geopolymer sample. However, curing at too high temperatures (80° and 100°C) or for longer time (more than 72 hours) do not provide any significant improvement in chemical and mechanical properties [36]. For this reason, the two different curing temperatures selected to study their influence on the final properties of the produced foams are 40°C and 70°C. Figure 3.17 shows how the foam samples cured respectively at 40°C (Figure 3.17a) and 70°C (Figure 3.17b) looked like; the two samples are extremely similar in appearance, size and type of porosity. This underlines that the curing temperature does not influence in a significant way the finished products obtained, for what concerns the porosity of samples. This could be also a consequence of the addition of the sodium hexafluorosilicate, which, acting as catalyst, chemically promotes the gelification of the sodium silicate and of the entire geopolymeric matrix, affecting in this way the consolidation of the system especially during the first moments of the process. In particular, the catalyst, accelerates the reactions that lead to the

hardening of geopolymeric matrix and, for this reason, in this specific case, the effect of curing temperature is not so much significant as it would have been expected from literature [36].

So, it is possible to conclude that the best curing temperature to use for the production of geopolymeric foams is the lower one, 40°C.

(a) (b)

Figure 3.17 Geopolymeric foams cured at the temperature of 40°C (a) and of 70°C (b)

Bibliography

[1] P. Colombo, Conventional and novel processing methods for cellular ceramics, Philosophical Transactions of the Royal Society of London A: Mathematical, Physical and Engineering Sciences, 364.1838, (2006) 109-124.

[2] M. D. M. Innocentini, P. Sepulveda, V.R. Salvini, V.C. Pandolfelli, Permeability and structure of cellular ceramics: a comparison between two preparation techniques. J. Am. Ceram. Soc. 81, (1998) 3349–3352.

[3] O. Lyckfeldt, J. Brandt, S. Lesca, Protein forming—a novel shaping technique for ceramics, J Eur Ceram Soc 20(14), (2000) 2551–2559.

[4] I. Garrn, C. Reetz, N. Brandes, L.W. Kroh, H. Schubert, Clotforming: the use of proteins as binders for producing ceramic foams, J Eur Ceram Soc 24(3), (2004) 579–587.

[5] B.S. Murray, R. Ettelaie, Foam stability: proteins and nanoparticles, Curr Opin Colloid In, 9(5), (2004) 314–320

[6] Bos MA, Van Vliet T (2001) Interfacial rheological properties of adsorbed protein layers and surfactants: a review. Adv Colloid Interfac 91(3):437–471

[7] Damodaran S (2005) Protein stabilization of emulsions and foams. J Food Sci 70(3): 54 66

[8] Chen J, Dickinson E (1998) Viscoelastic properties of proteinstabilized emulsions: effect of protein-surfactant interactions. J Agr Food Chem 46(1):91–97

[9] W. Van Bonin, U. Nehen, U. Von Gizycki, Hydrogen peroxides blowing agent for silicate foams. US Patent 3,864,137, (1975).

[10] V. Vaou, D. Panias , Thermal insulating foamy geopolymers from perlite, Miner Eng 23, (2010) 1146–1151.

[11] E. Prud'Homme, P. Michaud, E. Joussein, C. Peyratout, A. Smith, S. Rossignol, In situ inorganic foams prepared from various clays at low temperature, Appl Clay Sci, 51(1), (2011) 15–22.

[12] A.R. Studart, U.T. Gonzenbach, E. Tervoort, L.J. Gauckler, Processing routes to macroporous ceramics: a review, J. Am. Ceram. Soc.89 (2006) 1771–1789.

[13] P. Colombo, C. Vakifahmetoglu, S. Costacurta, Fabrication of ceramic with hierarchical porosity, J Mater Sci, 45, (2010) 5424–5455.

[14] E. Prud'homme, P. Michaud, E. Joussein, C. Peyratout, A. Smith, S. Arrii-Clacens, J.M. Clacens, S. Rossignol, Silica fume as porogent agent in geo-materials at low temperature, Journal of the European Ceramic Society 30, (2010) 1641–1648.

[15] X.G. Zhang, Electrochemistry of Silicon and its Oxide, Kluver Academic/Plenum Publishers, New York, (2001).

[16] R. Nakamura, E. Doi, Egg processing. In S. Nakai & H. W. Modler (Eds.), Food proteins. Processing applications (2000) 171–207. New York: Wiley.

[17] S. Damodaran, K. B. Song, Kinetics of adsorption of proteins at interfaces: role of protein conformation in diffusional adsorption, Biochimica et Biophysica Acta, 954, (1988) 253–264.

[18] T.M. Johnson, M.E. Zabik, Ultrastructural examination of egg albumen protein foams. Journal of Food Science, 46, (1981) 1237–1240.

[19] M. Ferreira, R. Benringer, R. Jost, Instrumental method for characterizing protein foams, Journal of Food Science, 60, (1995) 90–93.

[20] M. Hammershøj, K.B. Qvist, Importance of hen age and egg storage time for egg albumen foaming, Lebensmittel-Wissenschaft & Technologie, 34, (2001) 118–120.

[21] Y. Liang, H. G. Kristinsson, Structural and foaming properties of egg albumen subjected to different pH-treatments in the presence of calcium ions, Food research international, 40(6), (2007) 668-678.

[22] C. Panagiotopoulou, E. Kontori, T. Perraki, G. Kakali, Dissolution of aluminosilicate minerals and by-products in alkaline media, J Mater Sci, 42, (2007) 2967–2973.

[23] R.A. Sayanam, A.K. Kalsotra, S.K. Mehta, R.S. Sing, G. Mandal, Studies on thermal transformations and pozzolanic activities of clay from Jammu region (India), J. Thermal Analysis, 35, (1989) 9–106.

[24] J. Ambroise, M. Murat, J. Pera, Investigations on synthetic binders obtained by middle-temperature thermal dissociation of clay minerals Silicates Industries, 7(8), (1986) 99–107.

[25] J. Pera, J. Ambroise, A. Messi, Pozzolanic activity of calcined laterite Silicates Industries, Ceram. Sci. Technol., 63(7-8), (1998) 107–111.

[26] A. Palomo, M. T. Blanco-Varela, M. L.Granizo, F.Puertas, T. Vazquez, M.W. Grutzeck, Chemical stability of cementitious materials based on metakaolin, Cement and Concrete Research, 29(7), (1999) 997-1004.

[27] R. Grim, Clay Mineralogy, McGraw-Hill, New York, (1968).

[28] A. Namdar, Kaolinite chemical composite and morphology in geotechnical engineering, Advances in Natural and Applied Sciences, 5(2), (2011) 93-100.

[29] J. A. González, A. C. Carreras, M. del C. Ruiz, Phase transformations in clays and kaolins produced by thermal treatment in chlorine and air atmospheres, Latin American applied research, 37(2), (2007) 133-139.

[30] Lewis, R.J., Sr (Ed.). Hawley's Condensed Chemical Dictionary. 12th ed. New York, NY: Van Nostrand Rheinhold Co., 1993, p. 1057.

[31] R. Nave, Abundances of the Elements in the Earth's Crust, Georgia State University (2012).

[32] L. Verdolotti, E. Di Maio, G. Forte, M. Lavorgna, S. Iannace, Hydration-induced reinforcement of polyurethane–cement foams: solvent resistance and mechanical properties, J Mater Sci, 45(12), (2010) 3388–3391.

[33] H. Xu, J.S.J. Van Deventer, The geopolymerisation of alumino- silicate minerals, Int J Miner Process, 59(3), (2000) 247–266.

[34] L. Wang, S. Tomura, M. Suzuki, F. Ohashi, K. Inukai, M. Maeda, Synthesis of mesoporous silica material with sodium hexafluorosilicate as silicon source under ultra-low surfactant concentration, J Mater Sci Lett, 20 (2001) 277–280.

[35] J. S. Luckanuck, Method of insulating with inorganic non-combustible foam. U.S. Patent No. 4,960,621. 2 Oct. 1990.

[36] B.H. Mo, H. Zhu, X.M. Cui, Y. He, S.Y. Gong, Effect of curing temperature on geopolymerization of metakaolin-based geopolymers, Appl Clay Sci 99, (2014) 144–148.

4. Characterization of hybrid ceramic foams

The geopolymeric hybrid foams produced were widely characterized from multiple point of view.

4.1 Mechanical characterization

Mechanical properties are really important in structural and building materials. They include all the properties used to describe the strength of materials such as: elasticity / plasticity, tensile strength, compressive strength, shear strength, fracture toughness, ductility (low in brittle materials), and hardness. In particular, in modern materials science, fracture mechanics is an important tool in improving the mechanical performance of materials and components. Ceramic materials are usually ionic or covalent bonded materials; it is well known that this kind of material, held together by either type of bonds, will tend to fracture before that any plastic deformation could take place, which results consequently in poor toughness for these materials. Additionally, because these materials tend to be porous, the pores and other microscopic imperfections act as stress concentrators, decreasing the toughness further, and reducing the tensile strength. These combine to give catastrophic failures, as opposed to the normally much more gentle failure modes typical of metals. Considering that the materials produced in this scientific work are ceramic foams, and that the porosity can be considered as one of their main features, it is really important to investigate their mechanical behavior and to find out the values of their mechanical strengths.

Flexural tests were carried out on the prismatic samples (40x40x160 mm), on three specimens for each mixture, using a SANS testing machine (mod. CMT4304, Shenzhen SANS Testing Machine Co., China) with a 30 kN load cell, according to ASTM D1621 [1] and with a loading rate of 4 mm/min. Figure 4.1 shows one of the samples during the three points bending test. In the Figure it is already evident the presence of a crack on the same direction of the load application.

The compressive tests were performed on cubic samples (40x40x40 mm) with the same testing machine and process parameters (Figure 4.2).

Figure 4.1 Sample of ceramic foam during three points bending test

In Figure 4.3 the stress-strain curves, obtained for all the three kinds of foam after that flexural test have been performed, were reported. It is possible to deduce from the reported curves that the values of flexural strengths obtained for all the foams are very low. The numeric values of these strengths can be found summarized in Table 4.1. In any case, it is important to underline that the ceramic foams showed a really poor mechanical behavior in terms of flexural strength as expected for this kind of materials and it is possible to assess that there is essentially no difference for all the tested samples. This means that, independently from the foaming agent used to obtain the porosity, the foams showed a brittle mechanical behavior, without any presence of plastic deformation, typical of ceramic materials.

Figure 4.2 Sample of ceramic foam during compressive test

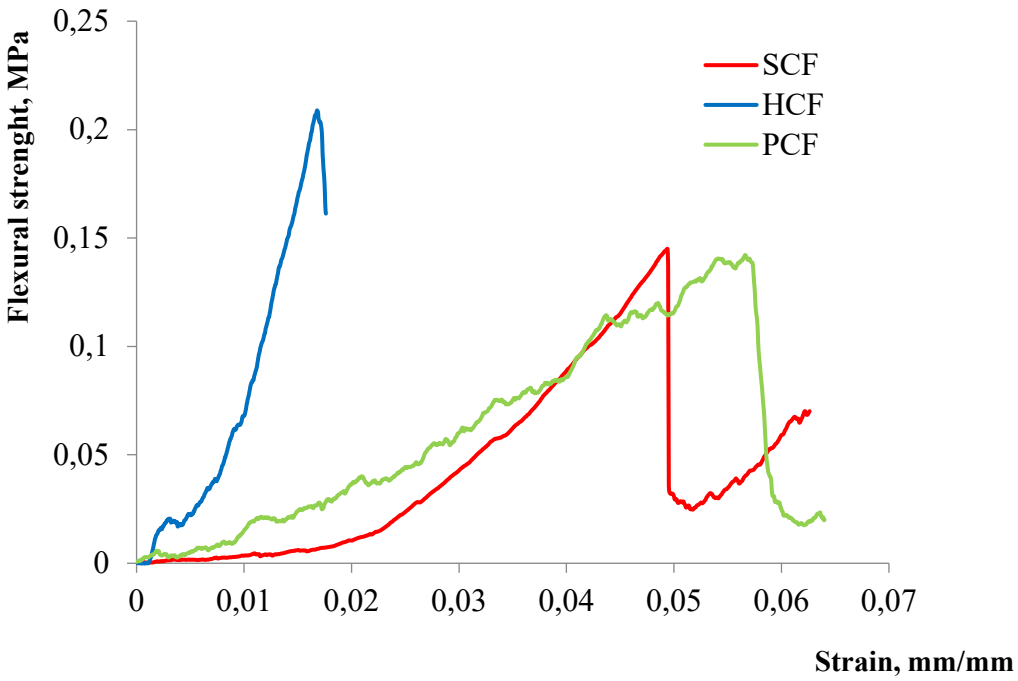

Figure 4.3 Flexural strengths of geopolymeric foams

On the contrary, the compressive strength data, reported in Figure 4.4 and in Table 4.1, highlighted that, for the SCF and HCF foams, the presence of the Si component strongly contributed to the consolidation of the inorganic structure providing higher mechanical performances [2]. In particular, the SCF foam showed a definitely higher compressive strength compared to that of the other ones. In addition, for HCF system, a toughness effect was also observed, because the presence of ‘‘meringue’’ foam acted not only as simple templating agent, but it contributed actively to stabilize the hybrid foam through the formation of a cross-linked organic network [3] chemically bonded to inorganic phase. In particular, the HCF system can be classified as a hybrid material belonging to the I class type of hybrid materials because the functional groups, present in the organic surfactants used as blowing agents in the production of this kind of foam, form secondary bonds (i.e. hydrogen bonds) with the silanol groups present in the geopolymeric inorganic network. In the meantime, PCF foam showed very poor mechanical properties (see Table 4.1) due to a low extent of geopolymeric reactions. In fact, it is believed that, in this case, the amount of un-reacted material acts as defect site and affects negatively the mechanical behavior [4].

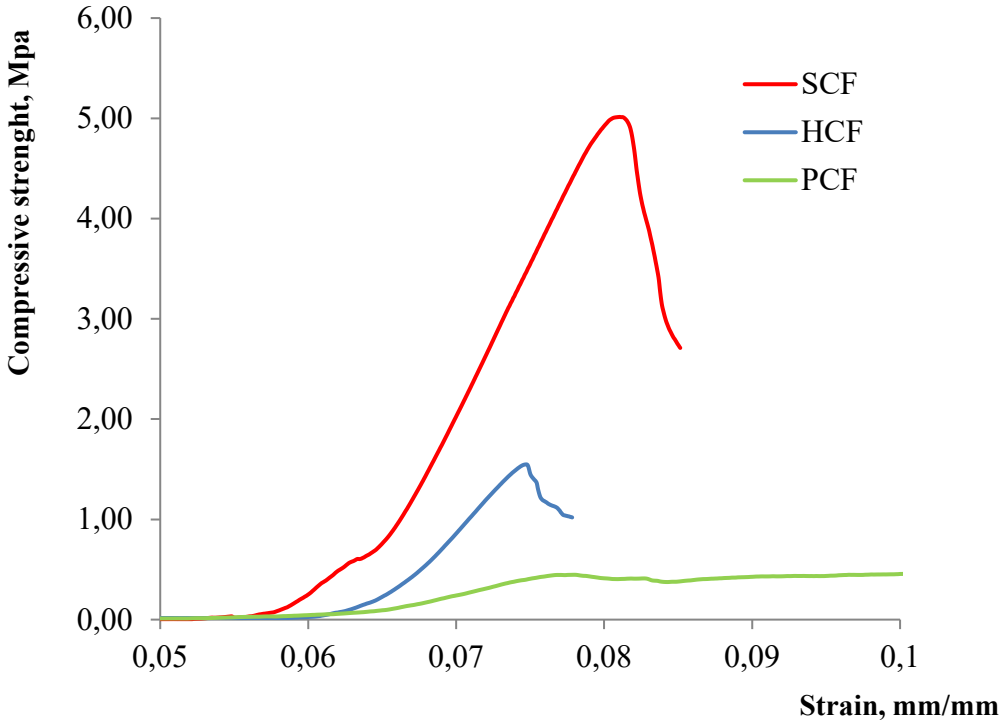

Figure 4.4 Compressive strengths of geopolymeric foams

Table 4.1 Mechanical characterization of the ceramic foams produced

Sample	Density (g/cm^3)	R_c (Mpa)	R_f (Mpa)
SCF	1.000	4.62 ± 0.07	0.15 ± 0.01
HCF	0.450	1.41 ± 0.07	0.21± 0.01
PCF	0.290	0.49 ± 0.03	0.14 ± 0.01

In Table 4.1 also the values of foam densities are reported. Density is one of the most important parameter to consider and to know when the topic of the discussion are porous and cellular materials, exactly like in this case. In fact, as proposed by Gibson-Ashby [5], the relative strength of a cellular material is related to its relative density by the following equation:

$$\frac{\sigma_F^*}{\sigma_C} = C\left(\frac{\rho_F^*}{\rho_C}\right)^n$$

where ρ_F^* and σ_F^* are the relative density and compressive strength of the ceramic foam, respectively. ρ_c and σ_C are referred to the compact solid. C is a dimensionless constant and the exponent n depending on the cell morphology. The values obtained for a compact solid are the following: ρ_c =1100 kg/m^3, σ_C =5.92 ± 0.07 MPa. Figure 4.5 reports strength data as a function of the relative density and compares the foam behavior either with a completely open-cell or closed-cell foams. The lack of a perfect fit to Ashby's theory can be due to the presence of mixed closed and open cells. In fact, the hybrid ceramic foams are characterized by an interconnected porosity, where some pores are present in most of the cell walls [6, 7].

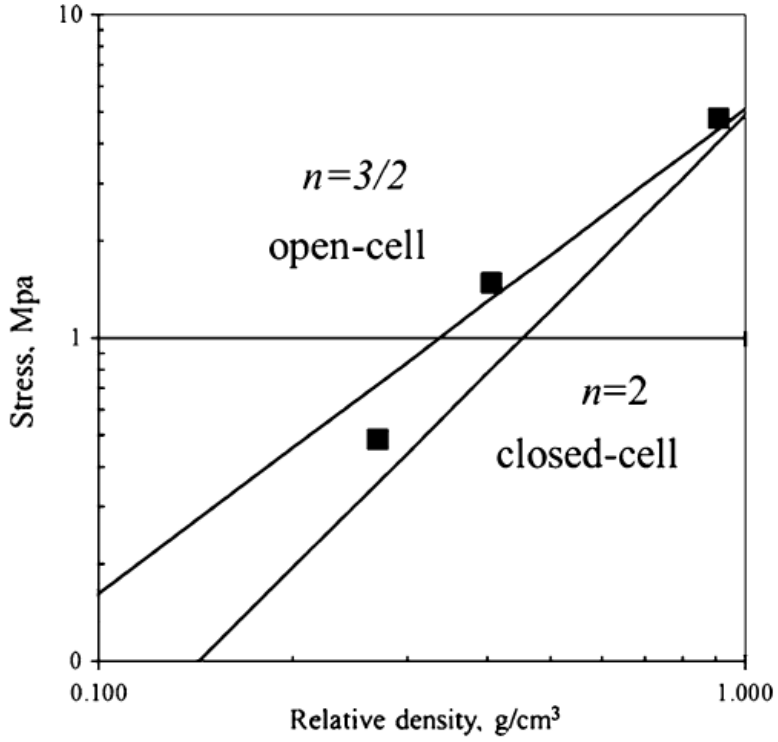

Figure 4.5 Compression strength as a function of relative density

4.2 Morphological characterization

The scanning electron microscope (SEM) is a type of electron microscope that produces images of a sample by scanning it with a focused beam of electrons. The electrons interact with atoms in the sample, producing various signals that contain information about the sample's surface topography and composition. The electron beam is generally scanned in a raster scan pattern, and the beam's position is combined with the detected signal to produce an image. SEM can achieve resolution better than 1 nanometer. Specimens can

be observed in high vacuum, in low vacuum, in wet conditions (in environmental SEM), and at a wide range of cryogenic or elevated temperatures. The most common SEM mode is detection of secondary electrons emitted by atoms excited by the electron beam. The number of secondary electrons that can be detected depends, among other things, on specimen topography. By scanning the sample and collecting the secondary electrons that are emitted using a special detector, an image displaying the topography of the surface is created. Nonconductive specimens tend to charge when scanned by the electron beam, and especially in secondary electron imaging mode, this causes scanning faults and other image artifacts; for this reason, non-conducting materials are usually coated with an ultrathin coating of electrically conducting material, deposited on the sample either by low-vacuum sputter coating or by high-vacuum evaporation. Conductive materials in current use for specimen coating include gold, gold/palladium alloy, platinum, osmium, iridium, tungsten, chromium, and graphite.

The cellular morphology of the hybrid foams was examined by Scanning electron microscopy SEM (SEM, LEO 1530, Zeiss, Figure 4.6) and then image (Image J) analysis was performed in order to assess the pore structure of all foamed systems. The foam samples were cross-sectioned and, because they are nonconductive materials, they were gold sputtered, and then analyzed at an accelerating voltage of 20 kV.

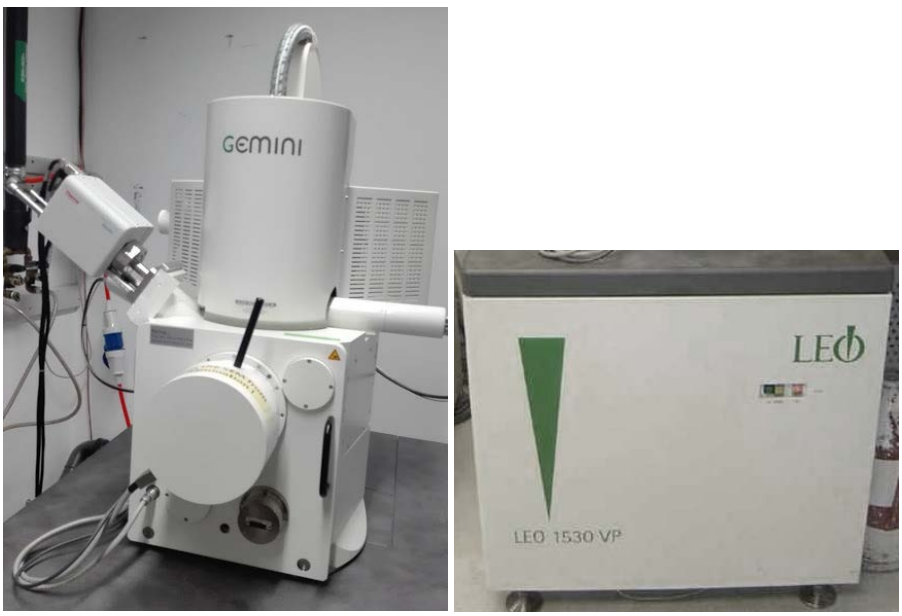

Figure 4.6 Scanning Electron Microscope LEO 1530, Zeiss

The morphological properties of each foam are shown in Figure 4.7. In Figure 4.7(a), a cellular structure with a large number of closed cells for SCF system was observed.

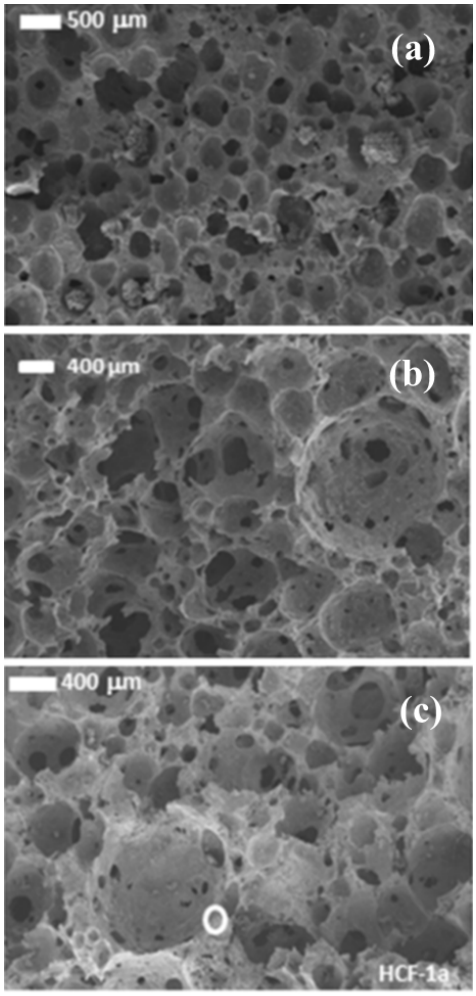

Figure 4.7 SEM micrographs of SCF (a), PCF (b) and HCF (c) samples produced

This morphology confirms that the hydrogen produced during the redox reaction of the Si powder generates a cellular structure within the inorganic matrix. A different morphology was observed in PCF foams (Figure 4.7(b)). Here the foamed structured was characterized by a non-homogeneous microstructure with the presence of a large number of open cells. Figure 4.7(c) shows the morphology of HCF foam. The cellular morphology of the foam is characterized by an open-cell structure with an interconnected porosity.

At higher magnification (Figure 4.8), the presence of different inorganic structures located in the cell walls of HCF was shown (enlargement of the white circle in Figure 4.7(c)). In particular, it is possible to distinguish the geopolymeric nano-precipitates

(Figure 4.8(b)) resulting from the reaction of silico-aluminate source in silicate solution media, and some un-reacted silico-aluminate particles (Figure 4.8(c)) [8, 9].

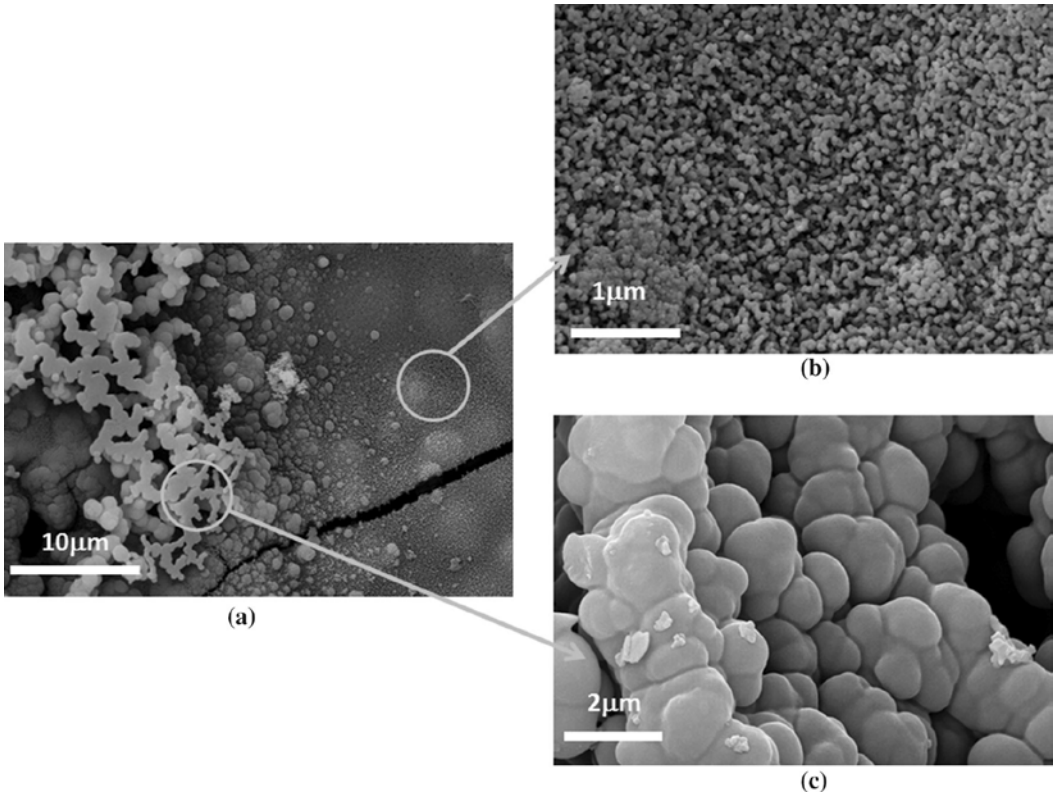

Figure 4.8 SEM images of HCF foam at different magnifications 7000X (a), 64000X (b) and 29000X (c)

A further confirmation of the presence of two different kinds of porosity in the SCF and HCF samples appears evident in Figure 4.9. In this figure in fact, two SEM images, taken at similar conditions, of the two foam samples are reported. It is possible to see a clearly closed structure for the SCF sample (Figure 4.9(a)) with the complete absence of capillary and passing porosity, while Figure 4.9(b) shows the interconnections between the pores and a typical open cell structure for the HCF sample.

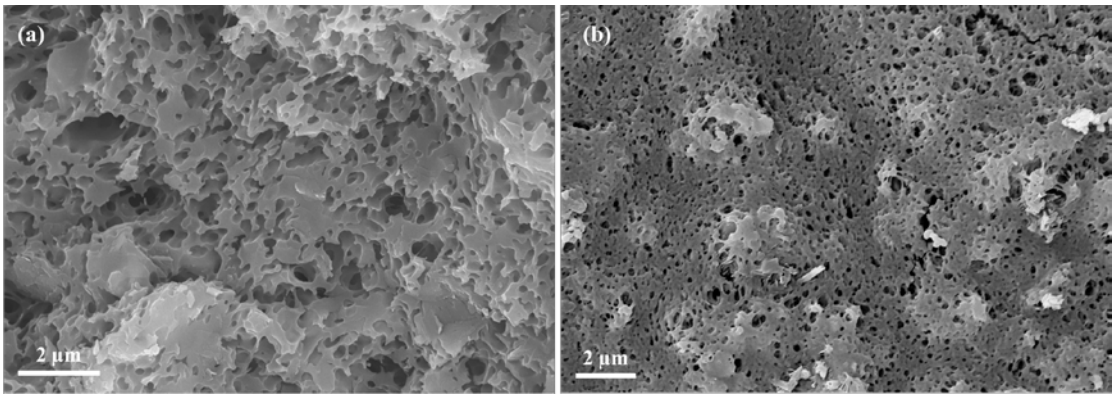

Figure 4.9 SEM images of SCF (a) and HCF (b) foams

4.3 Porosimetric characterization

In order to evaluate the pore size distributions and the mean pore size (ASTM D3576) of the ceramic foams produced, the SEM micrographs of Figure 4.7 were converted to 8-bit digital images prior to be analyzed by the Image J software for the image analysis. The results obtained for the pore size distribution of all the samples produced are reported in Figure 4.10.

As it results quite evident from Figure 4.10, SCF sample showed a pore size distribution ranging from 70 µm to 350 µm, while for HCF sample the pore size distribution increased up to 200–700 µm. PCF sample resulted to be characterized by a more heterogeneous pore size distribution, ranging from 100 µm to 750 µm. It is possible to conclude that the chemical foaming, obtained with Si addition in the geopolymeric matrix, leads to a smaller pore size distribution compared to the porosity obtained only with the addition of the “meringue” type foam. In the HCF sample it is possible to see again the combined effect of the two foaming methods, in fact it showed a homogeneous pore size distribution, like SCF sample, but with wider pore size range, like PCF sample.

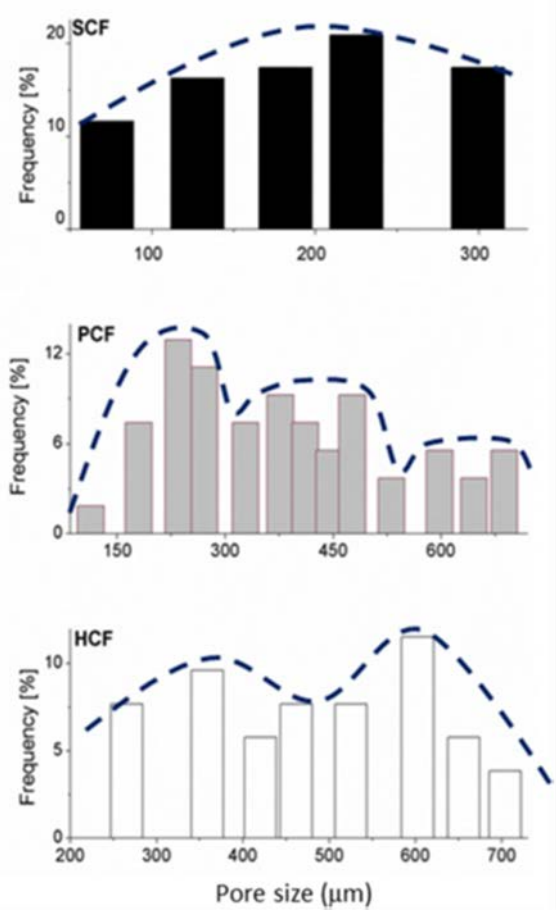

Figure 4.10 Pore size distribution of the three ceramic foams produced

4.4 Chemical characterization (FTIR spectroscopy)

Infrared spectroscopy is an important technique used especially in organic chemistry but that can be widely used also on inorganic samples in order to characterize them from a chemical point of view. In fact, it is an easy way to identify the presence of certain functional groups in a molecule. Moreover, it is possible to use the unique collection of absorption bands to confirm the identity of a pure compound or to detect the presence of specific impurities. In fact, the IR spectroscopy is based on the principle of the interaction of electromagnetic waves, in this case the ones of the infrared range, with matter. In particular, the IR radiation, interfere with the internal bonds of the molecules present in samples inducing bending and / or stretching of chemical bonds. Each type of chemical bond is characterized by an absorption at a specific wavelength in the infrared field, then, from these absorptions it is possible to obtain information about the molecules present. For this reason the infrared spectra are often considered as real typical "fingerprint" unique for each material.

Figure 4.11 shows schematically how a FTIR spectrometer works. There is a source of IR radiation, a sample and a detector. All the source energy is sent through an interferometer and then onto the sample. In every scan, all source radiation gets to the sample. The light passes through a beamsplitter, which sends the light in two directions at right angles, one beam goes to a stationary mirror then back to the beamsplitter, while the other goes to a moving mirror. The motion of the mirror makes the total path length variable versus that taken by the stationary-mirror beam. When the two beams meet up again at the beamsplitter, they recombine, but the difference in path lengths creates constructive and destructive interference: the result of this kind of interactions is an interferogram. The recombined beam passes through the sample. The sample absorbs all the different wavelengths characteristic of its spectrum, and this subtracts specific wavelengths from the interferogram. The detector reports then variation in energy versus time for all wavelengths simultaneously. Energy versus time is an odd way to record a spectrum, so a mathematical function called a Fourier transform is used to convert an intensity-vs.-time spectrum into an intensity-vs.-frequency spectrum.

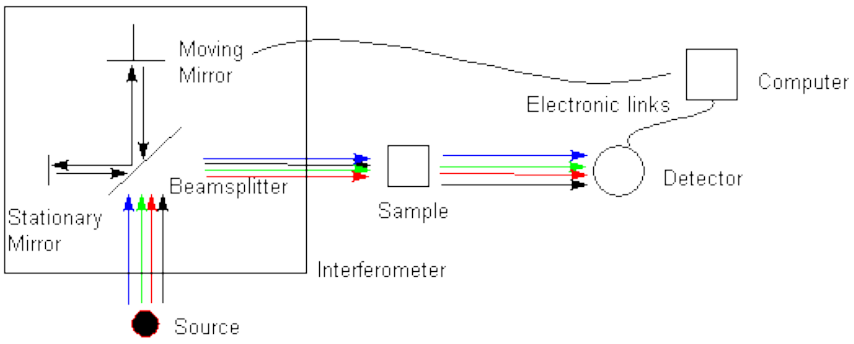

Figure 4.11 Schematic representation of FTIR spectroscopy technique

In order to chemically characterize the hybrid geopolymeric foams produced , FTIR analyses were performed. FTIR spectra were collected at room temperature using a Nicolet apparatus 8700 (Thermo Scientific, Italy) from 4000 to 400 cm^{-1} with a wavenumber resolution of 4 cm^{-1} for 64 scans. The FTIR spectra were collected in absorbance mode on transparent pellets obtained by dispersing the sample in the form of powder in KBr (~2 wt%). The FTIR spectrometer used is reported in Figure 4.12.

Figure 4.12 FT-IR Spectrometer Apparatus Nicolet 8700

Figure 4.13 shows the FTIR spectra of MK, SCF, HCF and PCF samples. All spectra contain broad absorption bands at about 3450 and 1650 cm^{-1} associated to the hydration water present in the structures. Those peaks are much more evident in the spectra of foam samples than in the MK spectrum because of the water formation as product of geopolymerization process. Moreover it is possible to underline the presence in the HCF and PCF spectra of two small peaks at respectively 2940 and 2850 cm^{-1} that can be associated to the C–H stretching vibrations deriving from fatty acids [10] of the vegetal surfactant used as foaming agent in the production of the considered samples.

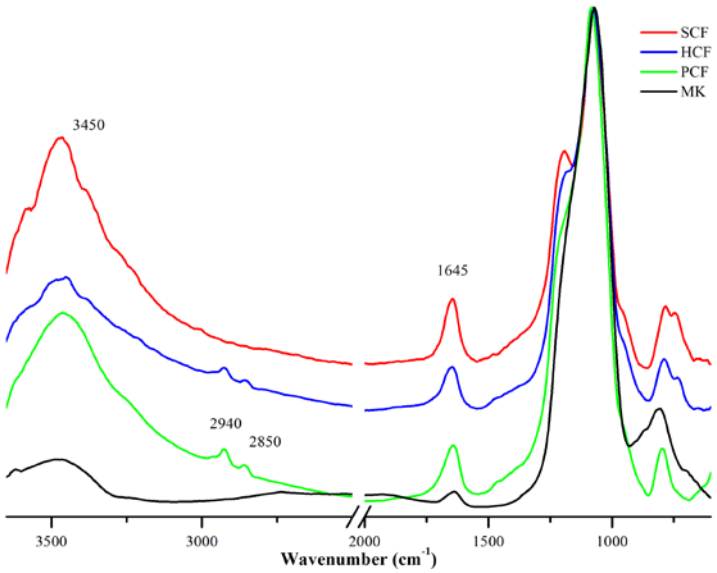

Figure 4.13 FTIR spectra of metakaolin (MK) and of all the geopolymeric foams produced

Figure 4.14 shows the same spectra of Figure 4.13, but reporting only a specific range on wavenumbers in order to focus attention on the main absorbance peaks. In particular, it is possible to see that the MK shows a broad absorption band centered at 1069 cm^{-1} frequency assigned to the overlapping of T–O–Si (T = Si or Al) asymmetric stretching peaks typical of alumino-silicate species [11, 12]. The SCF, HCF, and PCF samples evidenced a shift of this band towards higher wavenumber, 1079, 1080, and 1085 cm^{-1} respectively. This shift may be ascribed to the change in the relative amounts of T–O–Si species [11], which takes place in alkaline solution. In details, the SiO_4 and AlO_4 units of the amorphous phases of silico-aluminate structure, in alkaline conditions, break and re-combine in species with a higher covalent connectivity inducing a shift of the T–O–Si bond toward higher wavenumber. In addition, the SCF and HCF spectra displayed an absorbance peak around 735 cm^{-1} ascribed to intrinsic stretching vibrations of Al at the octahedral site (Al(6)), according to the geometrical configuration of nearest neighbors [11, 12].

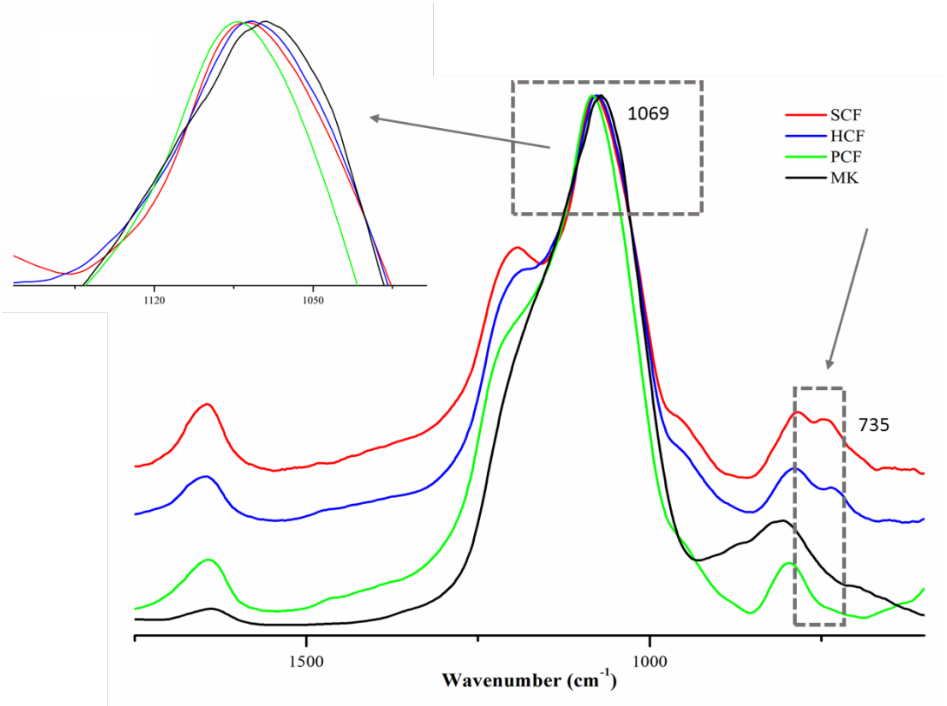

Figure 4.14 Zoomed FTIR spectra of metakaolin (MK) and of all the geopolymeric foams produced

Some foam samples, after curing, were let at 60°C in hydrothermal conditions (100 % Relative Humidity) for 72 h (namely h-SCF, h-HCF, and h-PCF). Then, FTIR analysis

was performed on them and the resulting spectra are reported in Figure 4.15. The peak at around 735 cm^{-1} that was evident in SCF and HCF spectra (Figure 4.14), disappears after hydrothermal curing (see Figure 4.15) due to depolymerization of silico-aluminate species, Al(6), and structural amorphous reorganization of the same species, Al(4)) tetrahedral coordinated [12]. This behavior is not observed for the h-PCF.

These findings, confirmed by previous SEM results, suggest that the presence of metal silicon in the SCF and HCF system enhances the formation of a geopolymeric network. The generation of hydrogen from the redox reaction between the Si powder and the alkaline solution was followed by the gelification of silicate and then by dissolution and formation of new silico-aluminate phases, which contributed to the hardening of the inorganic continuous phase.

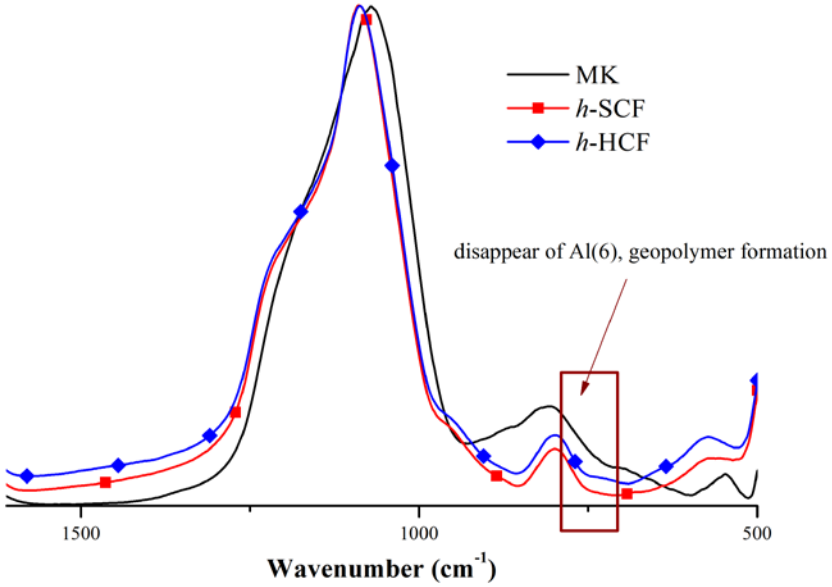

Figure 4.15 FTIR spectra of metakaolin (MK), SCF and HCF samples at hydrothermal conditions (h-SCF, h-HCF)

Bibliography

[1] ASTM D1621-16, Standard Test Method for Compressive Properties of Rigid Cellular Plastics

[2] V. Medri, E. Papa, J. Dedecek, H. Jirglova, P. Benito, A. Vaccari, E. Landi, Effect of metallic Si addition on polymerization degree of in situ foamed alkali-aluminosilicates, Ceram Int 39(7), (2013) 7657–7668.

[3] O. Lyckfeldt, J. Brandt, S. Lesca, Protein forming—a novel shaping technique for ceramics. J Eur Ceram Soc 20(14), (2000) 2551–2559.

[4] K. Komnitsas, D. Zaharaki, Geopolymerisation: a review and prospects for the minerals industry, Miner Eng 20(14), (2007) 1261–1277.

[5] L.J. Gibson, M.F. Ashby, Cellular solids: structure and properties, Cambridge University Press, Cambridge, MA (1999).

[6] P. Colombo, J.R. Hellmann, D.L. Shelleman, Mechanical properties of silicon oxycarbide ceramic foams, J Am Ceram Soc 84(10), (2001) 2245–2251.

[7] T.C. Hung, J.S. Huang, Y.W. Wang, Y.C. Fan, Microstructure and properties of metakaolin-based inorganic polymer foams, J Mater Sci 48(21), (2013) 7446–7455.

[8] H. Xu, J.S. van Deventer, The effect of alkali metals on the formation of geopolymeric gels from alkali-feldspars, Colloid Surface A 216(1), (2003) 27–44.

[9] K. Komnitsas, D. Zaharaki, Geopolymerisation: a review and prospects for the minerals industry, Miner Eng 20(14), (2007) 1261–1277.

[10] H. Schulz, B. Malgorzata, Identification and quantification of valuable plant substances by IR and Raman spectroscopy, Vibrational Spectroscopy 43(1), (2007) 13-25.

[11] L. Verdolotti, E. Di Maio, G. Forte, M. Lavorgna, S. Iannace, Hydration-induced reinforcement of polyurethane–cement foams: solvent resistance and mechanical properties, J Mater Sci 45(12), (2010) 3388–3391.

[12] J. Davidovits, Geopolymers, J Therm Anal Calorim, 37(8), (1991) 1633–1656.

[13] A. W. Coats, J. P. Redfern, Thermogravimetric Analysis: A Review, Analyst. 88 (1053), (1963) 906–924.

5. Hybrid ceramic foams with hierarchical porosity: addition of different levels of porosities

As widely discussed in the previous chapters, low-density and highly porous ceramics are increasingly relevant for a number of applications such as catalysis, filtration, heat exchange, biomedical scaffolds, and energy storage due to their tunable thermal properties and high relative mechanical strength [1]. These properties are intrinsically related to their structure, in fact, while closed pore structures tend to show high resistance to thermal transport, open pore structures have high accessible surface area and high permeability [2]. The characteristic size of the pores and their hierarchical organization, namely the presence of porosities at multiple length scales, are important factors in determining the structure–property relationship in these materials [3, 4]. It is known that hierarchical porous structures outperform their nonhierarchical counterparts in regards to relative compressive strength as well as accessibility of the active surface of the material [3, 5]. Although a vast range of technologies, including the use of replica, sacrificial templates, and 3D printing of ceramic scaffolds, have been developed for the production of highly porous ceramics, the synthesis of hierarchical porous ceramics still represents a challenging scientific and technological task [1, 2, 6, 7].

For this reason, the following step, after the complete characterization of the produced foams, has been the addition of two other levels of hierarchical porosity. Considering that, the ceramic foams, obtained with the combined use of chemical and mechanical foaming, as described in the previous chapters, had already shown porosity in a dimensional range of 70-700 μm, the idea was to add porosity on both nanometric and macrometric scale to the expanded systems. The nano-porosity has been included into the system using diatomite as partial or total replacement of the metakaolin in the starting geopolymeric matrix, while the macropores have been added to the hybrid ceramic foams by a 3D printed polymeric template (3D printing inverse replica method). In fact, processing methods that rely on the template-free direct deposition of materials, such as three-dimensional (3D) printing, extrusion, and spinning processes belong to the most important set of techniques available for the creation of macroporous materials. The macroporous structures obtained via these approaches can be further modified to incorporate additional pores at smaller length scales, leading to truly hierarchical porous architectures.

5.1 Use of diatomite as nanometric porosity source

Diatomite and its characterization

Diatomite is a sedimentary rock primarily composed mainly of amorphous silica (silicon dioxide, SiO_2) and some other minerals such as clay minerals and feldspar. Diatomite is a kind of mineral assemblage in natural sediments and it is available in large quantities and at low cost [8]. Diatoms belong to the diploid eukaryotic unicellular algae (Bacillariophyta) with wide ranges of structures and shapes. Each of these has its own distinct shape and size [9]. The outstanding feature of diatoms is their siliceous "shell" or frustule, which can be preserved for millions of years. In this manner, fossil deposits of microscopic diatom shells were built up as thick layers of "diatomaceous earth" or diatomite, which could be extending over several miles [9].

Diatoms skeletons and shells are highly porous (at nanometric scale), lightweight, chemically stable and inert [10]. Moreover, diatomite easily dissolves in basic solutions. Thanks to all these properties, combined with strong absorbability and excellent thermal resistance, diatomite has been used in variety of applications, mainly as filtration agent, as source to produce carbon- mineral adsorbents of low molecular substance [11-13], functional fillers for paints and plastics [13] and pozzolanic additives. Moreover, because of its resistant to high temperatures and chemical action, it is also used in fireproof cement, insulation materials as an absorbent in explosives manufacture [13]. Similar to synthetic amorphous silicas, the reactivity of diatomite intrinsically links to the presence of reactive sites on their surface. Reactive sites not only condition the charge, acidity, solubility, and hydrophilicity of the surface, but they are also the sites of grafting and ligand-exchange reactions [14], so that they govern the properties of related diatomite products to great extent. To better understand and control the properties of diatomite, it is important to have detailed information of the reactive sites. Generally, the hydroxyl groups are primary reactive sites on the surface of amorphous silica. According to previous studies on synthetic amorphous silica by MAS NMR and IR [14-17] surface hydroxyl groups have been classified based on their coordination and their hydrogen bonding (isolated and H-bonded hydroxyl groups). To the best of our knowledge, however, the surface hydroxyl species of diatomaceous silica have not yet been systematically investigated. Besides hydroxyl groups, acid sites have been also thought as important surface sites of diatomite.

As is well known, silica surface consists of siloxane bridges and different types of hydroxyl groups (i.e. silanols), which are key reactive sites for various surface reactions: wetting, dispersion in solutions, adsorption and surface modification (e.g. silylation) etc. [17, 18]. The distribution and evolution of different types of silanols and siloxanes largely depend on thermal treatment condition, as well as on ambient humidity and storage time [19]. At room temperature, both of the isolated and H-bonded silanols associate with the physically adsorbed water by hydrogen bond. After calcinations treatment, physically adsorbed water will be desorbed from the silanols, and the silanols will condense with the increase of temperature. Generally, the H-bonded silanols condense more easily than the isolated ones [8]. A schematic model is reported in Figure 5.1 in order to elucidate the hydroxyl structure and the dehydration process of diatomite. At room temperature, both the isolated and H-bonded hydroxyl groups on the diatomite surface are H-bonded with physically adsorbed water. With the increase of temperature of 200 - 1000ºC, five dehydration processes are assumed, shown as scheme I to IV in Figure 5.1 [8]. So, when diatomite is heated at high temperature, the active groups on its surface (–OH groups) are removed and the surface acquires stronger hydrophobic properties [8].

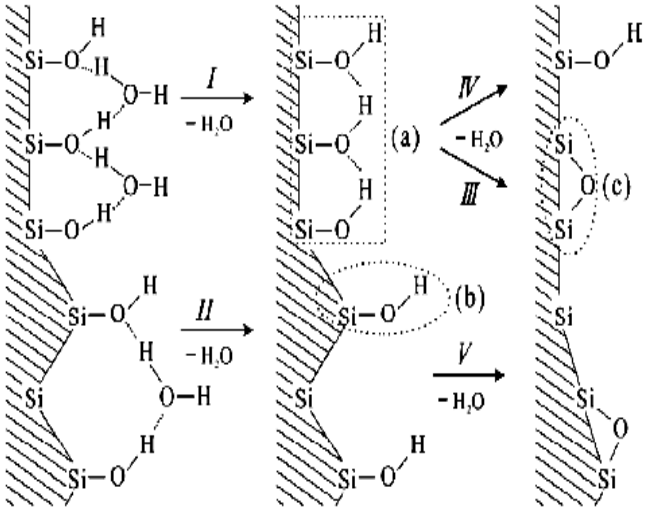

Figure 5.1 The hydroxyl structure and the dehydration process of diatomaceous silica (a) H-bonded silanols, (b) isolated silanols, (c) siloxane [8]

In this work, diatomite was used as a partial (or total) replacement of metakaolin in the production on hybrid geopolymeric foams in order to obtain, as final products, foams characterized by the presence of nanopores in addition to their intrinsic porosity. In

particular, the effects of the addition of different amounts (5, 10, 50, 70 and 100% by weight) of diatomite were investigated.

The diatomite used (Celite® 545), flux calcined diatomaceous earth, was provided by Celite France. Flux-calcined products are obtained by calcining at high temperatures (about 900°C) in presence of a fluxing agent such as soda ash (sodium carbonate). During flux calcination, the fluxing agent helps to fuse the diatoms together, which considerably increases the particle size of the product. Flux-calcined diatomite may contain up to 70% of crystalline silica. The chemical composition reported in the technical sheet can be read in Table 5.1

Table 5.1 Chemical composition of Celite® 545 (wt%)

	SiO_2	Al_2O_3	Fe_2O_3	Na_2O+K_2O	MgO	CaO	P_2O_5
Diatomite	91.5%	1.00%	1.5%	2.5%	0.30%	0.30%	0.004

The particle size distribution is characterized by a retained on 106 and 45 µm mesh of 25 and 62 (wt%) respectively, with a median particle size of 53.1 µm. The mineralogical composition was evaluated by XRD analysis using a Panalytical X'Pert Pro diffractometer equipped with PixCel 1D detector (operative conditions: $CuK\alpha_1/K\alpha_2$ radiation, 40 kV, 40 mA, 2Θ range from 5 to 80°, step size 0.0131° 2Θ, counting time 40s per step). Cristobalite (ICCD #77-1317) and wollastonite ($CaSiO_3$) resulted as the main crystalline phases as it is possible to see in Figure 5.2.

The thermal treatment did not destroy the nanometric porosity of the diatomite, as can be seen in Figure 5.3 in which SEM micrographs of diatomite, at different magnification, are reported. From the SEM images, it is possible to see clearly the presence of pores of dimensions around 100 nm and even smaller (Figures 5.3(b) and 5.3(d)) present in the microstructure of diatomite.

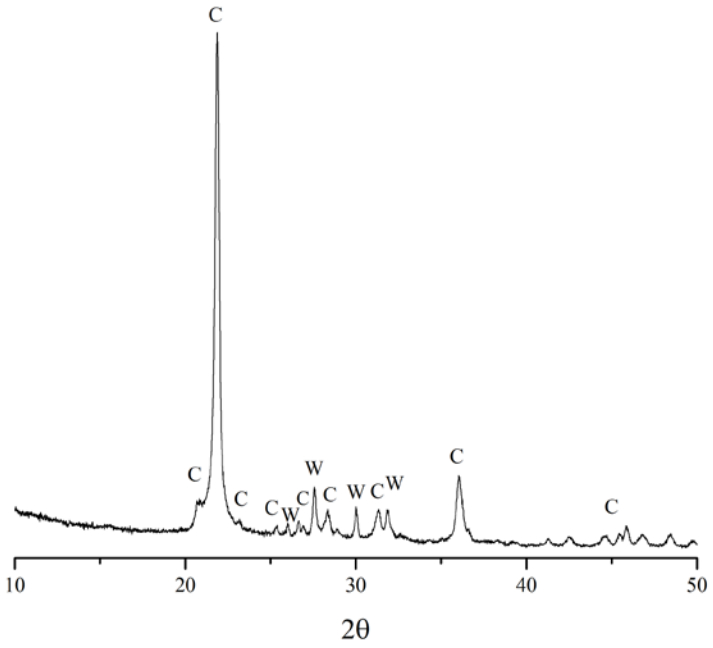

Figure 5.2 XRD spectrum of diatomite (Celite 545 C) C=Cristobalite, W=Wollastonite

In order to characterize more precisely the porosity and the specific surface of the diatomite, nitrogen adsorption analysis have been performed and the results are reported in Figure 5.4. The analysis was performed using a Nova 1000 machine (Quantachrome, USA). Figure 5.4 shows both the BET surface numeric value and the N_2 sorption isotherm of diatomite. According to the Brunauer classification of the adsorption isotherms, the isotherm belongs to the III type of isotherms and shows a convex regular shape, without any knee or plateau with a low-pressure hysteresis. This kind of isotherm is associated with weak adsorbent-adsorbate interactions. The shoulder of the hysteresis loop of the desorption branch runs parallel to the adsorption curve as shown in Figure 5.4. This could be explained in terms of the swelling of the particles, which accompanies adsorption. The swelling distorts the structure, for example by prising apart weak junctions between primary particles and opens up cavities, which were previously inaccessible to adsorbate molecules. Since the distortion is not perfectly elastic, some molecules become trapped and can escape only very slowly, or possibly not at all, during the desorption run [20]. The BET value obtained for the measure of specific surface is 1.072 m^2/g, which can be explained considering that the diatomite analyzed is a commercial product calcined at about 900 °C and consequently the surface area of the raw diatomite was remarkably decreased. In fact, in the case of calcined diatomite, raising the temperature leads to loss in the total surface area that indicates that a significant structure changes took place [21].

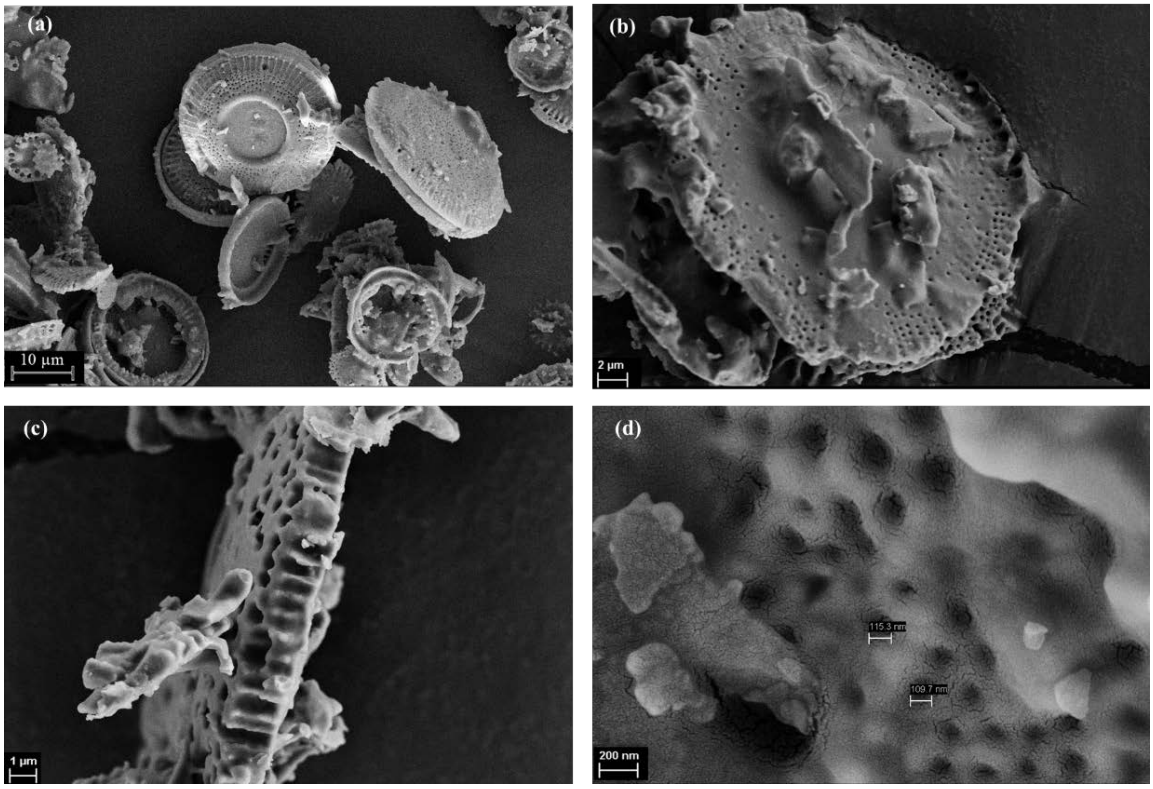

Figure 5.3 SEM images at different magnifications of diatomite

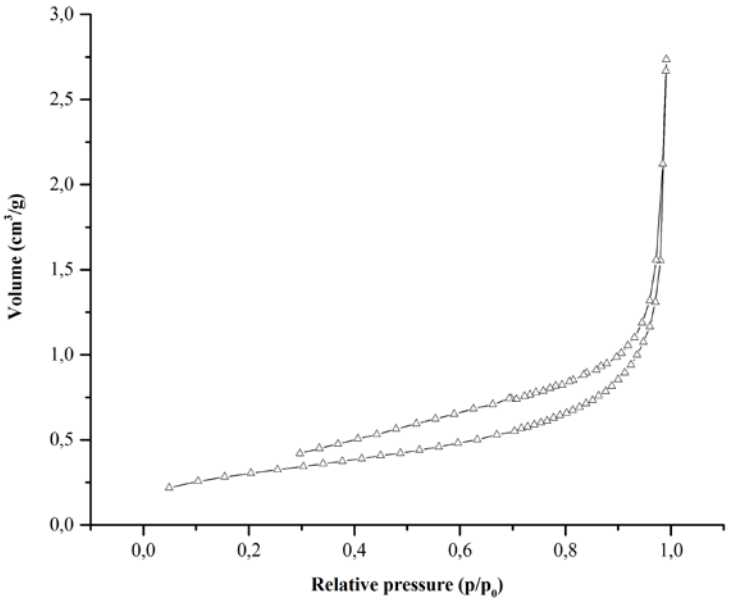

BET surface area = 1.072 m²/g

Figure 5.4 N_2 gas sorption isotherm for diatomite

Moreover, in Figure 5.5 the pore size distribution of diatomite (DFT method pore size distribution) is reported. From the curve, it is possible to see a very narrow peak between the values of about 2 and 5 nanometers; this is a further confirmation, after the SEM images, of the presence of nanoporosity of very small dimensions in the diatomite used as metakaolin substitute in the production of foams.

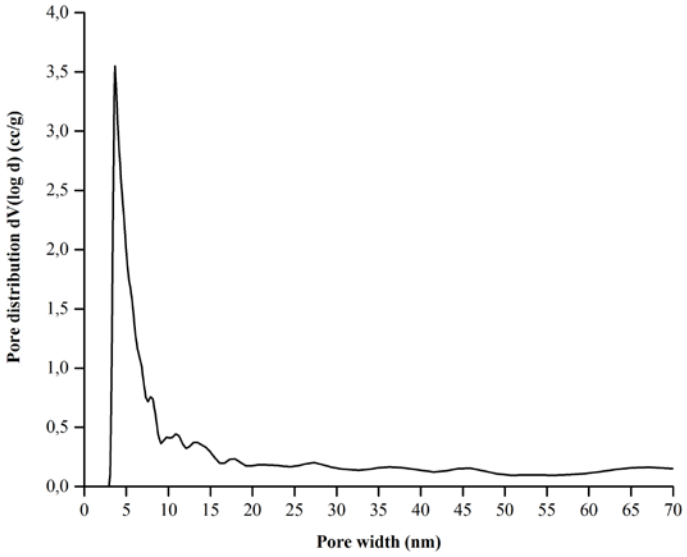

Figure 5.5 DFT pore size distribution of diatomite

Production of foams with diatomite addition

The procedure followed for the preparation of the samples is exactly the same of all the foam samples produced before. The hybrid ceramic foam (HCF) used as reference sample, has been produced using the following mixture (wt%): 70% of SS, 8.65% of Na_2SiF_6, 21.3% of wt. silico-aluminate source (MK), 0.05% of Si powder. Based on 100 parts of the above mixture 12 part of a "meringue" type foam was added. In particular, the amount of metal silicon has been significantly reduced, from 8% wt of the previous HCF samples produced, to 0.05% wt. This choice was a consequence of a process of optimization of the metal silicon amount performed on the SCF sample. In fact, it was found out that the reduction of the Silicon percentage added as pore forming agent, led to an increase in the mechanical properties of the final products. This can be explained considering that the amount of metal silicon which effectively reacts, producing gaseous hydrogen, is really low, while the silicon remained unreacted, does not contribute to the mechanical properties and on the contrary acts as a source of defectiveness. Other

different expanded hybrid ceramic systems were prepared by replacing metakaolin (MK) in the starting mixture with several percentages of diatomite, in particular 5, 10, 50, 70 and 100 wt % (namely D-HCF/5, D-HCF/10, D-HCF/50, D-HCF/70, and D-HCF/100). The so obtained foams (reported in Figure 5.6) were widely characterized in order to verify the eventual influence of the metakaolin replacement with diatomite on the final properties of products.

It is worth to notice that, even looking at the pictures of the samples reported in Figure 5.6, it is possible to see significant differences in the microstructure and in the porosity of the different kind of foams produced. These differences have been widely discussed in the following paragraphs.

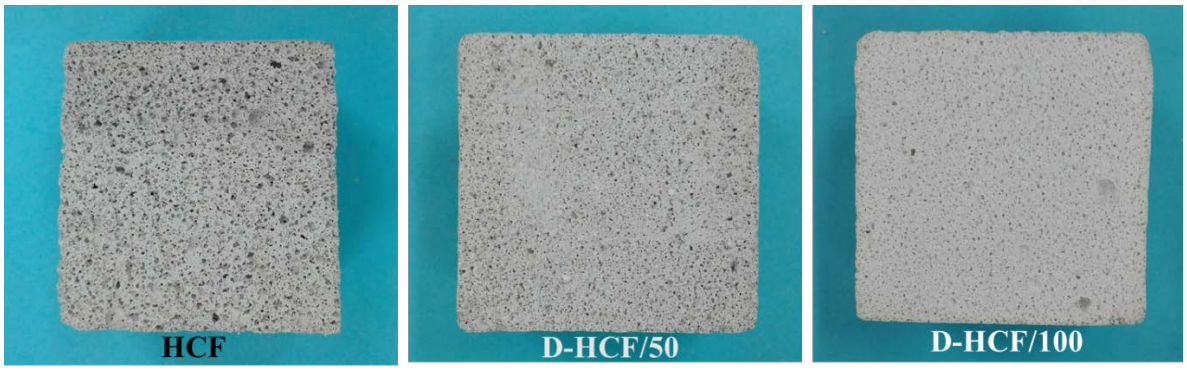

Figure 5.6 HCF, D-HCF/50 and D-HCF/100 samples

5.2 Properties of the produced ceramic foams

Mechanical characterization

Flexural tests were carried out on prismatic samples (40x40x160 mm) on three specimens for each mixture, using a SANS testing machine (mod. CMT4304, Shenzhen SANS Testing Machine Co., China) with a 30 kN load cell and with a loading rate of 4 mm/min. Three points bending setup was used and the support span was equal to 80 mm. The compressive tests were performed on cubic samples (40x40x40 mm) with the same testing machine and process parameters. The results of the flexural and compressive strength tests of all the different samples are reported respectively in Figures 5.7 and 5.8.

In Figure 5.7 it is possible to see that all the samples, regardless of the percentage of diatomite addition, show a mechanical behavior typical of ceramic materials,

characterized by brittle fracture without any presence of plastic deformation. Moreover, as it is possible to see also from Table 5.2, in which the numeric values of mechanical properties are reported, all the specimens tested show poor values of flexural strengths. In fact, according to the ceramic nature, they do not exhibit good mechanical performances when they are exposed to flexural loads.

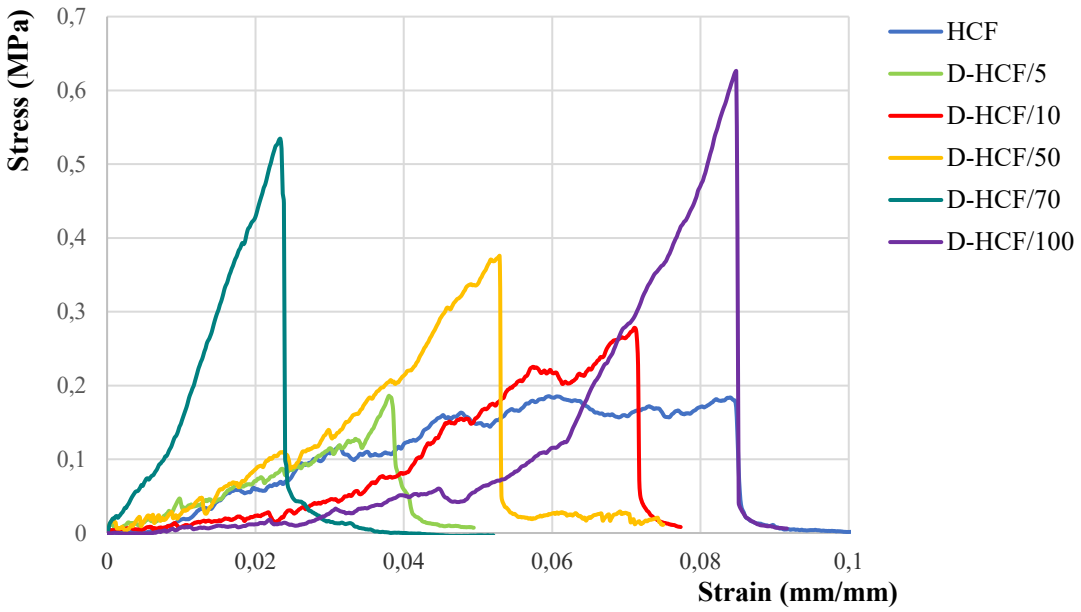

Figure 5.7 Flexural strengths of all the foam samples produced

Table 5.2 Density and mechanical properties of the ceramic foams

Sample	Density (g/cm^3)	Rc (MPa)	Rf (MPa)
HCF	0.401 ± 0.050	0.50 ± 0.07	0.18 ± 0.11
D-HCF/5	0.343 ± 0.017	0.74 ± 0.03	0.19 ± 0.01
D-HCF/10	0.345 ± 0.019	0.83 ± 0.07	0.23 ± 0.03
D-HCF/50	0.340 ± 0.024	1.04 ± 0.07	0.33 ± 0.05
D-HCF/70	0.455 ± 0.009	1.25 ± 0.01	0.53 ± 0.09
D-HCF/100	0.423 ± 0.002	1.49 ± 0.06	0.63 ± 0.01
CS*	1.100 ± 0.013	5.92 ± 0.07	1.30 ± 0.07

* = *compact solid*

The compressive strength data for all the samples are reported in Figure 5.8 and in Table 5.2. As it is possible to see, the presence of diatomite improved effectively the compressive strength for D-HCF samples. In fact, the stress-strain curves reported in Figure 5.8 show an increase of the compressive strengths with the increase of diatomite amount in the samples. Moreover, for HCF system, a toughness effect was also observed, as previously discussed. This effect disappears with the addition of diatomite, as it is clearly visible also from Figure 5.8, in which are reported HCF and D-HCF/100 samples after the compression test.

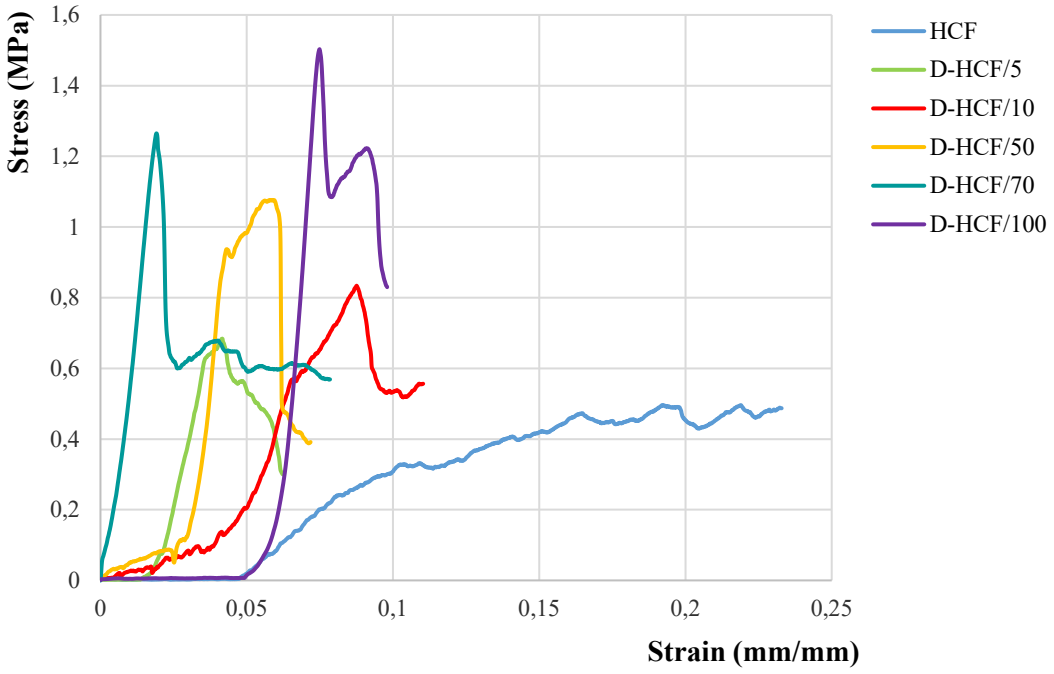

Figure 5.8 Compressive strengths of all the foam samples produced

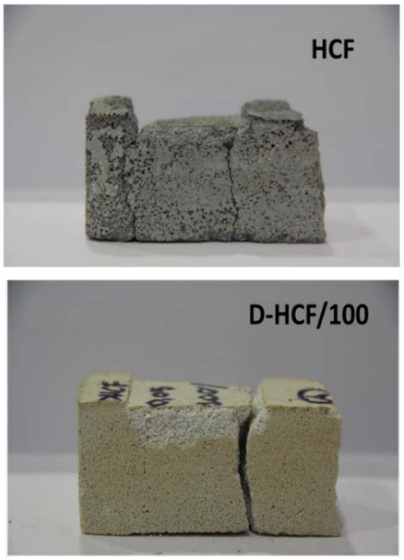

Figure 5.9 HCF and D-HCF/100 samples after the compression test

Density and strength data, reported in Table 5.2, were modelled following the equation suggested by Gibson-Ashby [5]. The results of the modeling are reported in Figure 5.10 that shows the strength data as a function of the relative density and compares the foam behavior either with a completely open-cell or closed-cell foams. The hybrid ceramic foams showed an intermediate behavior owing to a mix of closed and open cells. In fact, they are characterized by an interconnected porosity, where some pores are present in most of the cell walls [23]. It is interesting to notice that the increase of diatomite amount leads to a better fitting of the behavior of the ceramic foams to Ashby's theory for open-cell foams due the presence of open nano-porosity. The HCF foam moved away from a perfect fit to Ashby's theory because of the presence of macrostructural inhomogeneity [5, 23]. Moreover, the simultaneous presence of diatomite and metakaolin in the mixture reduced the density of the hybrid foams regardless of its amount. Nevertheless, the samples obtained with only diatomite (D-HCF/100) and with the highest percentage of metakaolin replacement (70%) showed density higher than HCF.

The different physical and mechanical properties of the hybrid foams can be considered consequence of two different consolidation mechanisms. In particular, metakaolin based foams hardened by geopolymerization joint with the templating effect of the whipped protein, which contributes actively to stabilize the hybrid foam through the formation of a cross-linked organic network chemically bonded to inorganic phase [2]. On the other hand, the replacement of diatomite leads to a consolidation process due to the formation of a polysilicate on the surface of diatomite, coupled to the templating effect. In particular,

the polycondensation of sodium silicate as glassy materials produced bridges between grains and, ensuring higher cohesion, resulted in better mechanical properties [24].

In Figure 5.11 the correlation between the diatomite percentages and the mechanical properties are reported. The fitting of the experimental data shows a good linear correlation (R2 = 0.97 and 0.96 respectively) between the values of flexural and compressive strengths and the amount of diatomite added in the hybrid foams.

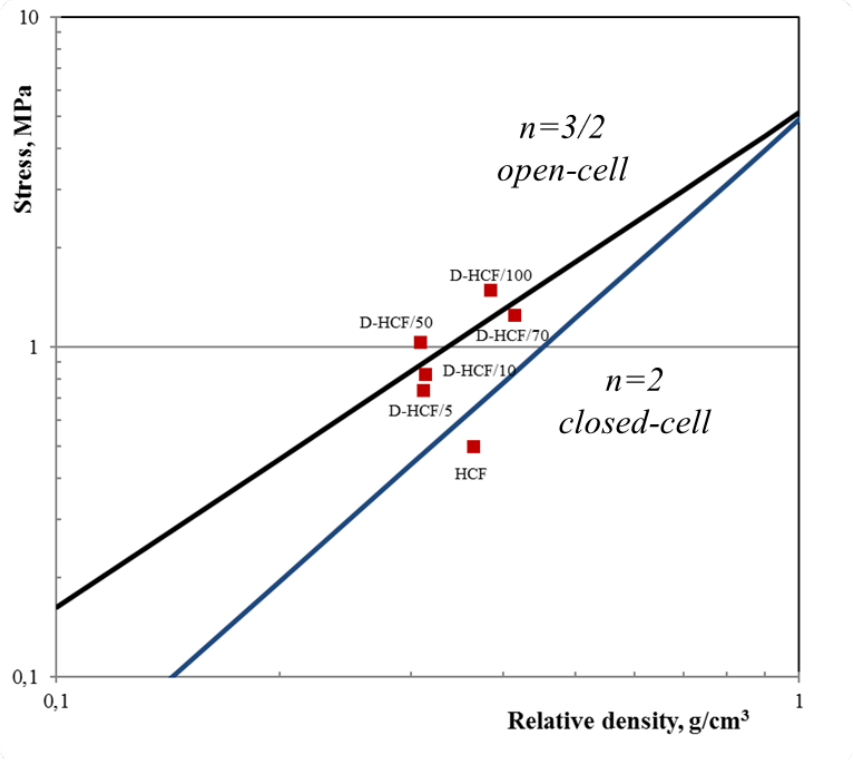

Figure 5.10 Modeling of compression strength as a function of relative density following Gibson-Ashby theory

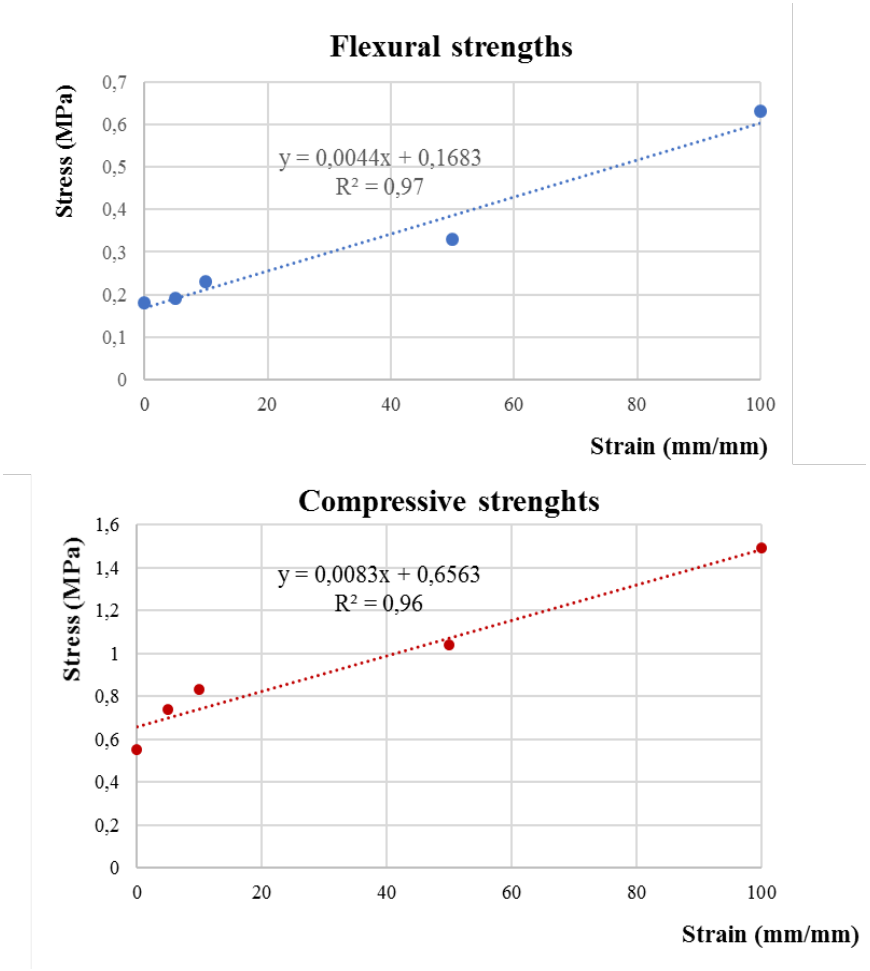

Figure 5.11 Correlation between diatomite percentages and mechanical properties

Morphology of hybrid foams

The cellular morphology of the samples obtained with diatomite replacement, was examined by SEM (SEM, LEO 1530, Zeiss), in order to assess the pore structure of all the systems produced and to verify the presence of eventual microstructural changes depending on the different amounts of diatomite added. In Figure 5.12 SEM images of some of the different kinds of foam produced (HCF, D-HCF/50, D-HCF/70, D-HCF/100) are reported. The micrographs clearly show the presence of a changing microstructure in relation to the percentage of diatomite present in the ceramic matrix. In fact, it is quite evident that the D-HCF/100 sample, in which the metakaolin is completely replaced by the diatomite, showed a more homogenous microstructure characterized by a considerable compactness of the ceramic matrix and by a very fine and small porosity (Figure 5.12(d)), well distributed within the matrix. On the contrary, the HCF sample (Figure 5.12(a)), used as a reference sample, resulted to be characterized by a porosity of larger dimensions that leads to a less compact matrix. It is important to underline that the

dimensions of pores seem to decrease with the increasing of diatomite content, while their finesse and homogeneous distribution seem to increase with the increasing of diatomite.

The difference in the microstructures can be ascribed to the different chemical mechanism of consolidation of the foams. For the samples with lower percentages of diatomite, in fact, the consolidation and hardening processes are consequences of a typical geopolymeric reaction, while for the foams produced with higher amounts of diatomite, in particular in the case of D-HCF/100 sample, it is not possible to say the same. The consolidation process, in this case, changed from geopolymerization to a silicate polycondensation mechanism. The replacement of diatomite, in fact, leads to a consolidation process due to the formation of a polysilicate on the surface of diatomite. In particular, the polycondensation of sodium silicate as glassy materials produced bridges between grains and, ensuring higher cohesion, resulted in a more homogeneous microstructure and, as a consequence, in better mechanical properties (Figures 5.7, 5.8).

A further confirmation of the higher compactness of the matrices with higher percentages of diatomite can be found in the SEM micrographs of Figure 5.13. In that Figure, in fact, are reported SEM images of HCF, D-HCF/50, D-HCF/70, D-HCF/100 samples at nanometric scale. It is possible to repeat the same considerations made for the previous SEM images, it is evident, in fact, the higher compactness and homogeneity of the system in the D-HCF/100 sample. This is a further explanation of the increment of the mechanical strengths showed in Figures 5.7 and 5.8.

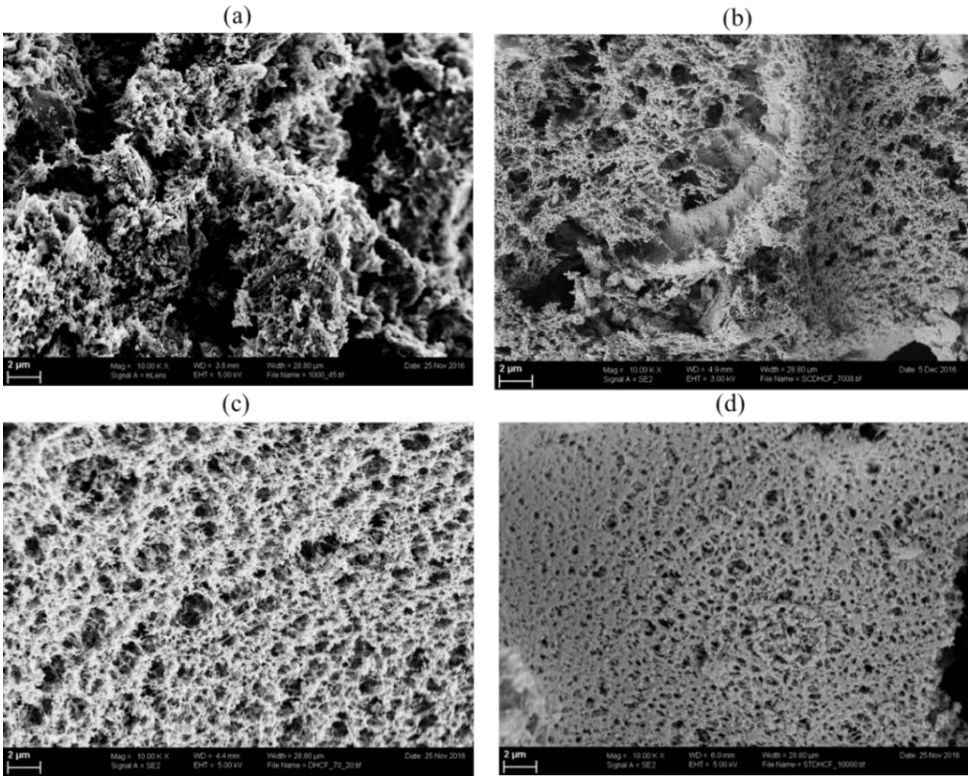

Figure 5.12 SEM images of HCF (a), D-HCF/50 (b), D-HCF/70 (c), D-HCF/100 (d) samples

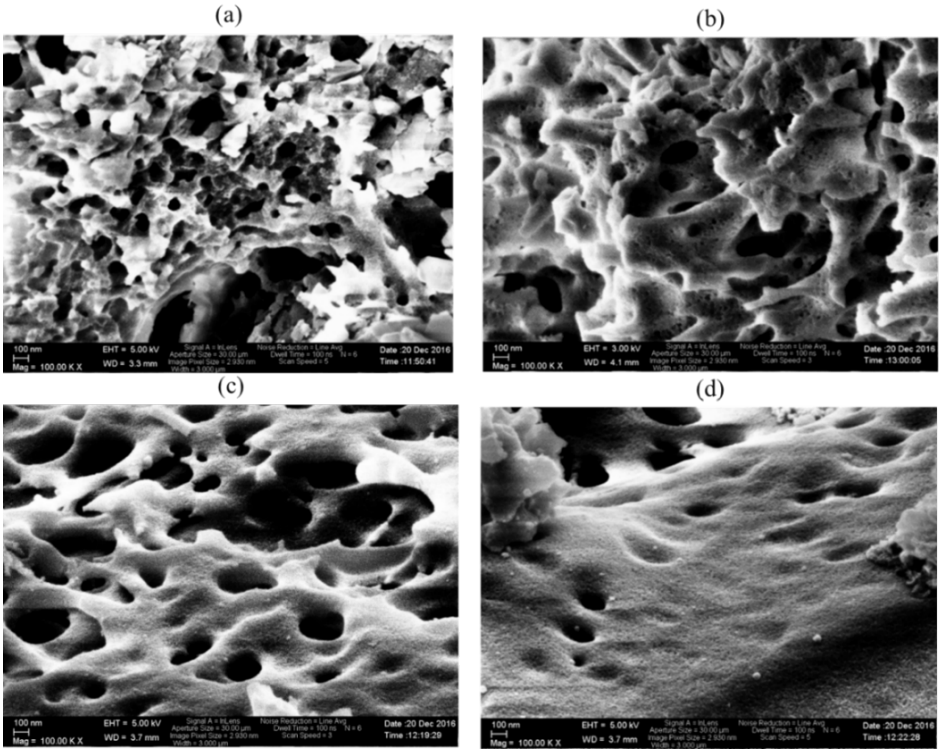

Figure 5.13 SEM images at nanometric scale (100 nm) of HCF (a), D-HCF/50 (b), D-HCF/70 (c), D-HCF/100 (d) samples

In figure 5.14 SEM images at higher magnification (compared to those of Figures 5.12 and 5.13) of HCF, D-HCF/50 and D-HCF/100 samples are reported. The cellular morphology of the HCF is characterized by a partially open cell structure with an interconnected porosity.

Figure 5.15 shows the morphology of D-HCF/50 and D-HCF/100 samples at different magnifications. The D-HCF/50 showed cellular structure similar to HCF, but characterized by microporous struts. As already discussed the consolidation mechanisms seems to be very different when all the MK was replaced by diatomite, as evidenced by the glassy material present in the D-HCF/100.

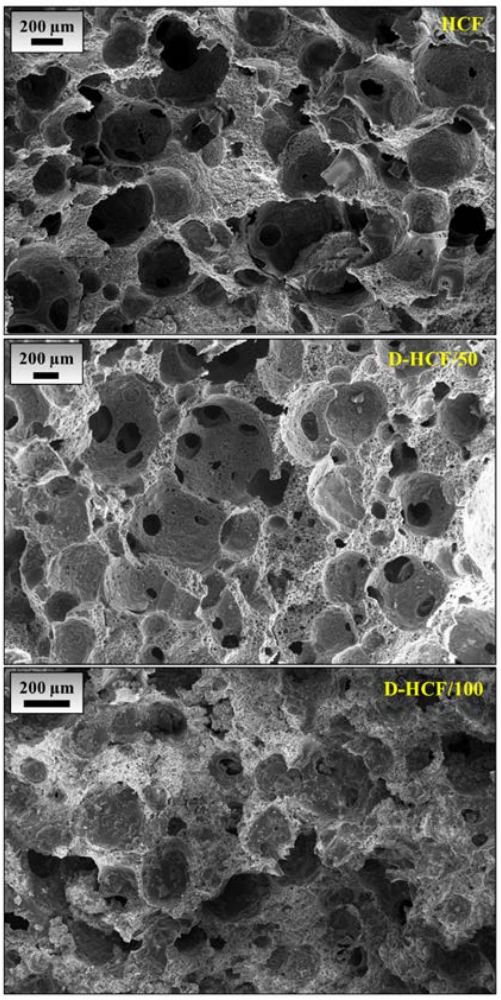

Figure 5.14 SEM images at high magnification of HCF, D-HCF/50 and D-HCF/100 samples

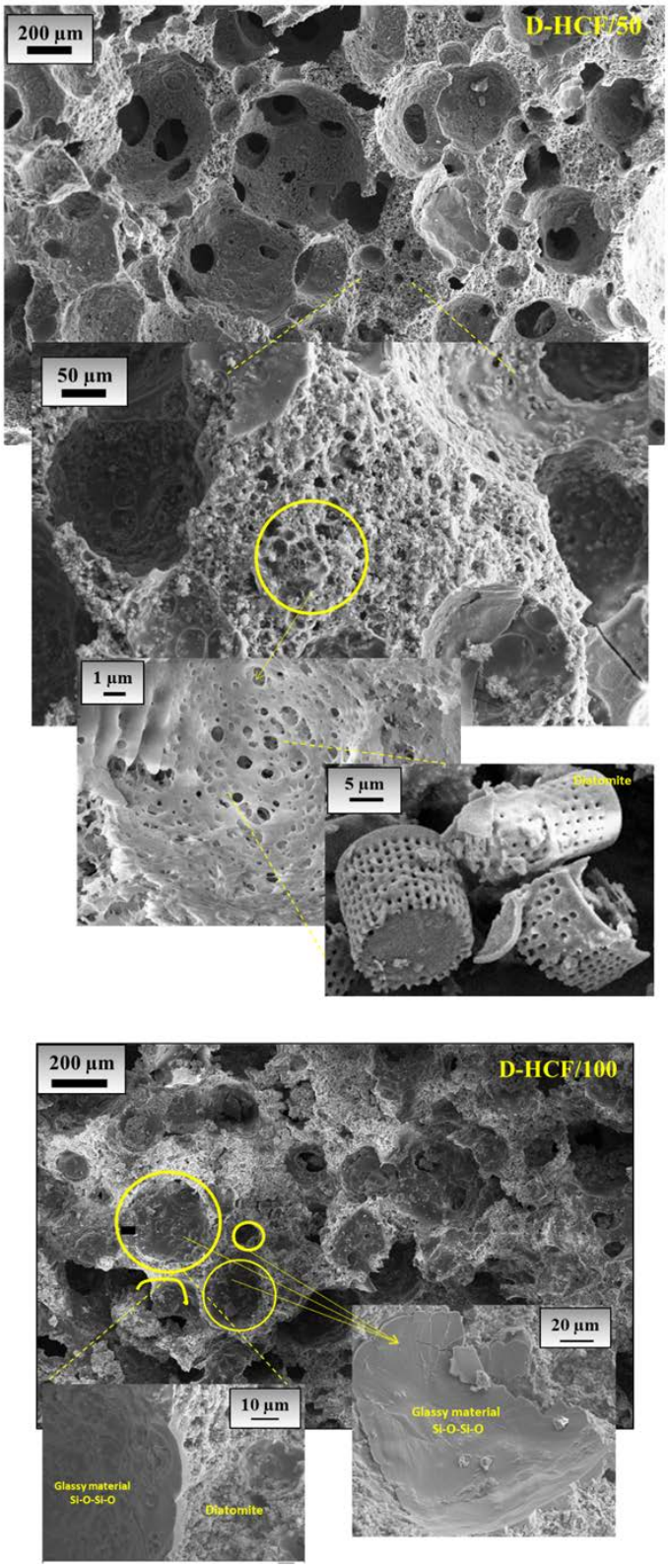

Figure 5.15 SEM images of D-HCF/50 and 100 at different magnifications

Porosity characterization

In Figure 5.16, the pore size distributions of HCF, D-HCF/50 and D-HCF/100 samples are reported. The HCF sample showed a pore size distribution that ranged between 100-400 µm. The substitution of 50% of MK with diatomite retained the cellular morphology of HCF (see D-HCF/50 in figure 5.13), but the pore size dimension shifted towards values smaller than 100 µm. On the contrary, the D-HCF/100, showed a wide dispersion in the pore dimension distribution, ranging from 80 to 400 µm.

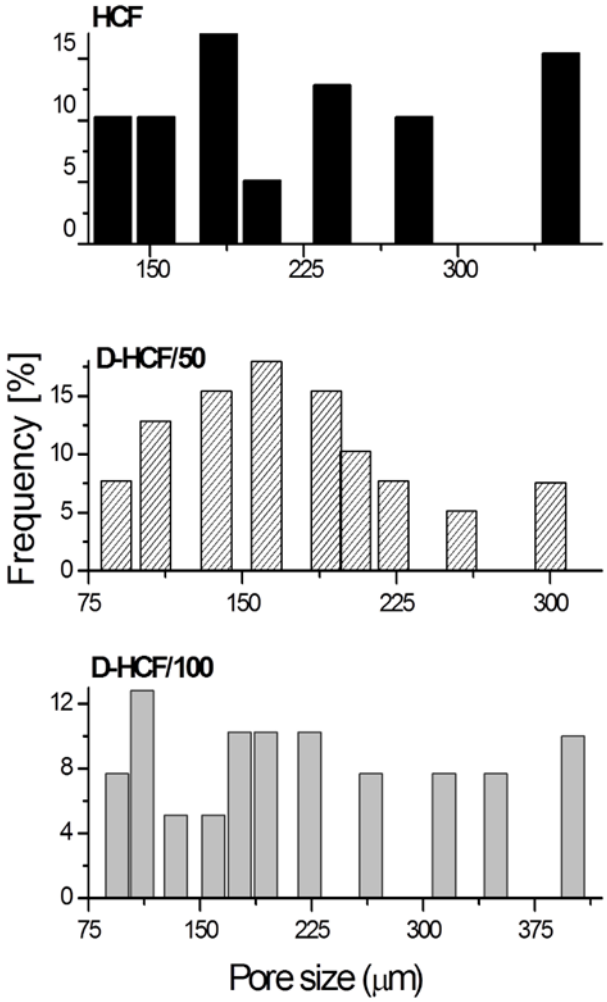

Figure 5.16 Pore size distribution of HCF, D-HCF/50 and D-HCF/100 samples

In order to characterize more precisely the porosity and the specific surface of the hybrid ceramic foams, nitrogen adsorption analysis have been performed and the results are reported respectively in Figure 5.17 and in Table 5.3. The analyses were performed using a Nova 1000 machine (Quantachrome, USA).

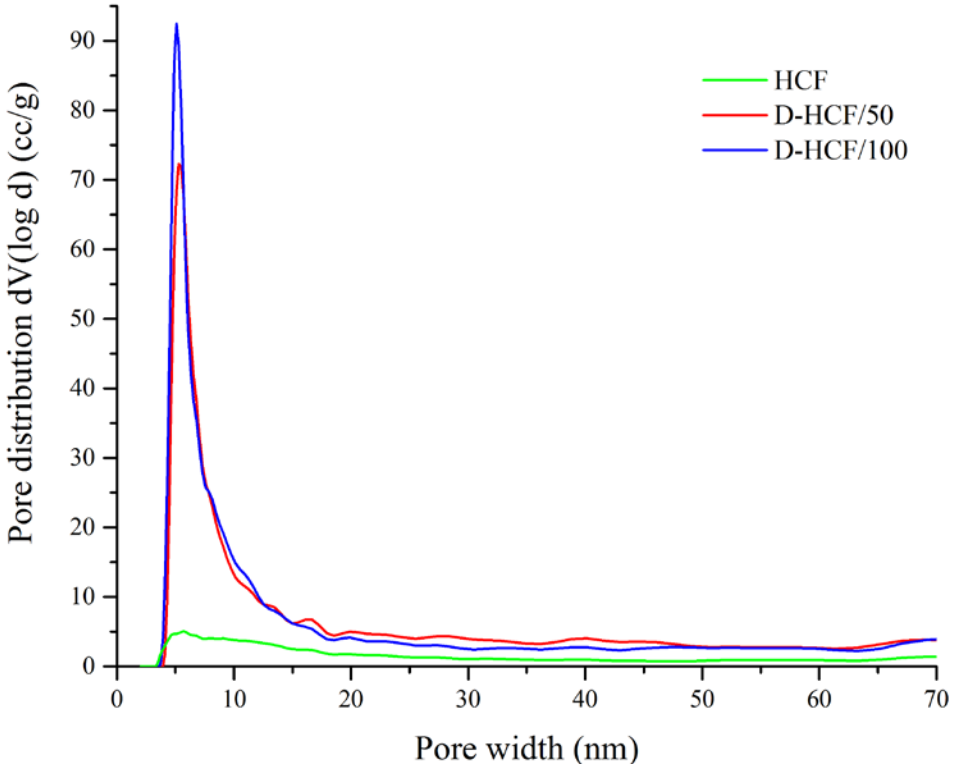

Figure 5.17 DFT pore size distributions of HCF, D-HCF/50 and D-HCF/100 samples

In particular, in Figure 5.17 the DFT (density functional theory) pore size distributions of HCF, D-HCF/50 and D-HCF/100 samples are reported. From the curves results clearly evident the significant change in the porosity that takes place after the replacement of metakaolin with the diatomite. The D-HCF/50 and D-HCF/100 samples, in fact, showed a very narrow and high peak between the values of about 5 and 7 nanometers. This means that the most of the pores present in those foams, has dimensions included in that dimensional range. It is a confirmation of the presence of nanoporosity of very small dimensions that derives from the nanopores originally present in the diatomite; the HCF sample does not present this kind of peak, on the contrary, its pore size distribution is characterized by a quite completely flat curve, without the presence of significant peaks. This means that in the HCF sample, porosity on nanometric scale is completely absent.

In Table 5.3 BET surface values of metakaolin, diatomite and hybrid ceramic foams are summarized. It is important to notice that the foaming process leads to a significant increment in the BET surface value for all the kinds of foams considered. In particular, this tendency is more evident for the hybrid foams produced with diatomite addition, because, as already discussed previously, the starting value of diatomite BET surface, is quite low, so in this case the increase of specific surface is really high, from 1.072 m^2/g

to 23.202 m^2/g for D-HCF/100 sample. Anyway, considering the specific surfaces of all the samples, it is possible to assess that there is not much difference between the values of BET surface obtained. The small variations that can be noticed for the different kinds of foams produced could be due to the heterogeneity that characterize these kinds of materials.

Table 5.3 BET surface values of metakaolin, diatomite and hybrid ceramic foams

Sample	BET surface area (m^2/g)
MK	14.87
Diatomite	1.07
HCF	21.62
D-HCF/50	19.61
D-HCF/70	16.83
D-HCF/100	23.20

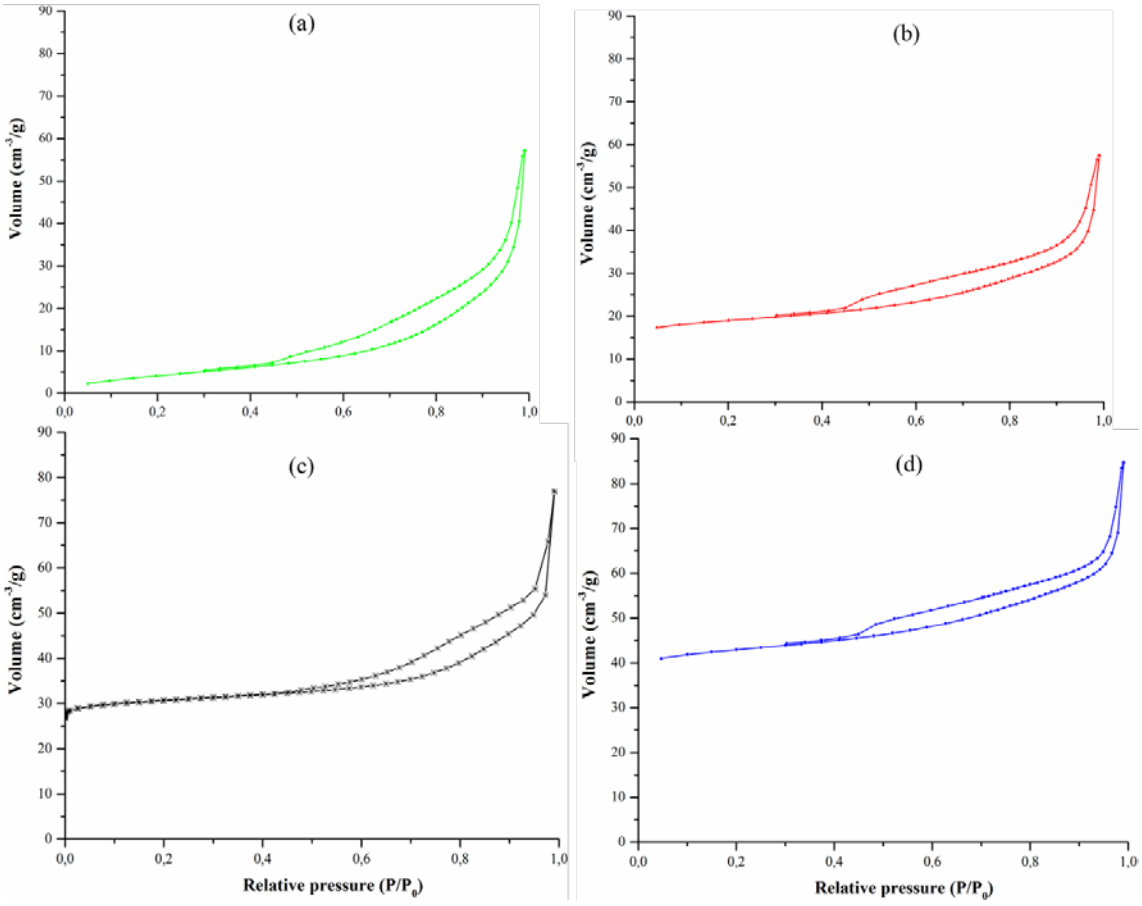

Figure 5.18 N_2 adsorption isotherms of HCF (a), D-HCF/50 (b), D-HCF/70 (c) and D-HCF/100 (d) samples

In Figure 5.18 the N_2 adsorption isotherms of HCF, D-HCF/50, D-HCF/70 and D-HCF/100 samples are reported. According to the Brunauer classification of the adsorption isotherms, all the samples considered, showed isotherms belonging to the type II. Moreover, all the isotherms resulted to be characterized by the appearance of hysteresis that can be explained as a consequence of the presence of mesoporosity in the microstructure of ceramic foams. In particular, in this case, the shape of the hysteresis seems to suggest the existence of mesoporosity with slit-like morphology, typical of pores deriving from the aggregation of flat particles. This effect results to be more evident in the isotherms of the samples in which metakaolin has been partially or totally replaced with diatomite (D-HCF/50 and D-HCF/100).

The evaluation of pores total volume fraction (x_p) was determined as follows:

$$x_P = 100\times(1 - \frac{\rho}{\rho_0})$$

in which ρ_0 is the real density and ρ was the bulk density of the foam, calculated as the mass of the foam divided by its apparent volume. The apparent volume was geometrically calculated using a caliper (accuracy ± 0.05 mm). The real density was obtained performing a He picnometry (Accupyc II 1340, Micromeritics; accuracy 0.03%). Gas pycnometry, in fact, is recognized as one of the most reliable techniques for obtaining true, absolute, skeletal, and apparent volume and density. This technique is non-destructive as it uses the gas displacement method to measure volume. Inert gases, in this case helium, are used as the displacement medium. Density calculations using the gas displacement method are much more accurate and reproducible than the traditional Archimedes water displacement method. volume of a solid is calculated from the measured drop in pressure when a known amount of gas is allowed to expand into a chamber containing the sample. Thus, the true volume obtained by pycnometry excludes any pore volume accessible to the gas. Helium is the preferred gas, because it exhibits ideal gas behavior. The values of pores total volume fractions obtained for the hybrid ceramic foams produced are reported in Table 5.4. These values fit perfectly the values of density obtained and reported in Table 5.2. In fact, it is possible to confirm that the simultaneous presence of diatomite and metakaolin in the mixture reduced the density and, consequently, increased the pore total volume fraction of the hybrid foams regardless of its amount. Nevertheless, the D-HCF/100 sample, obtained with only diatomite, showed a lower value of total porosity than the sample obtained with only metakaolin

(HCF). This behavior can be explained with the different consolidation mechanism, previously widely described, that takes place in the systems with the simultaneous presence of diatomite and metakaolin and in that with only diatomite.

Table 5.4 Pores total volume fractions of the hybrid ceramic foams produced

Sample	x_p **(%)**
HCF	83.18
D-HCF/5	85.61
D-HCF/10	85.32
D-HCF/50	85.26
D-HCF/100	82.05

Mercury intrusion porosimetry

Mercury intrusion porosimetry (MIP) is a widely used technique for characterizing the distribution of pore sizes in porous materials. It is a simple and quick indirect technique, but it has limitations when applied to materials that have irregular pore geometry. It is based on the intrusion of a nonwetting fluid, mercury, into porous structures under increasing pressure. Mercury intrusion porosimetry is one of only a few analytical techniques that permits an analyst to acquire data over such a broad dynamic range using a single theoretical model. Mercury porosimetry routinely is applied over a capillary diameter range from 0.003 μm to 360 μm. It is applicable over a wide range of pore sizes and the data it produces (the volume of mercury intruded into the sample as a function of applied pressure) are indicative of various characteristics of the pore space, so this technique can be used to reveal a variety of physical properties of the solid material itself. Mercury intrusion porosimetry has been performed (Micromeritics, Autopore III) on the hybrid ceramic foams produced in order to characterize the porosity of larger dimensions compared to that previously investigated through the nitrogen adsorption analyses. The pore size distributions resulted from the Hg intrusion are reported in Figure 5.19. The Figure shows that for the D-HCF/100 sample the pore distribution is monomodal and located at around 60 μm, while for the other two foam samples, the pore distribution

becomes bimodal, with main peaks detected at around 0.2 and 60 µm and 0.6 and 60 µm respectively for D-HCF/50 and HCF sample. The HCF sample showed another small peak located at around 8 µm that is indicative of the presence of a dimensional class of pores completely absent in the other two samples.

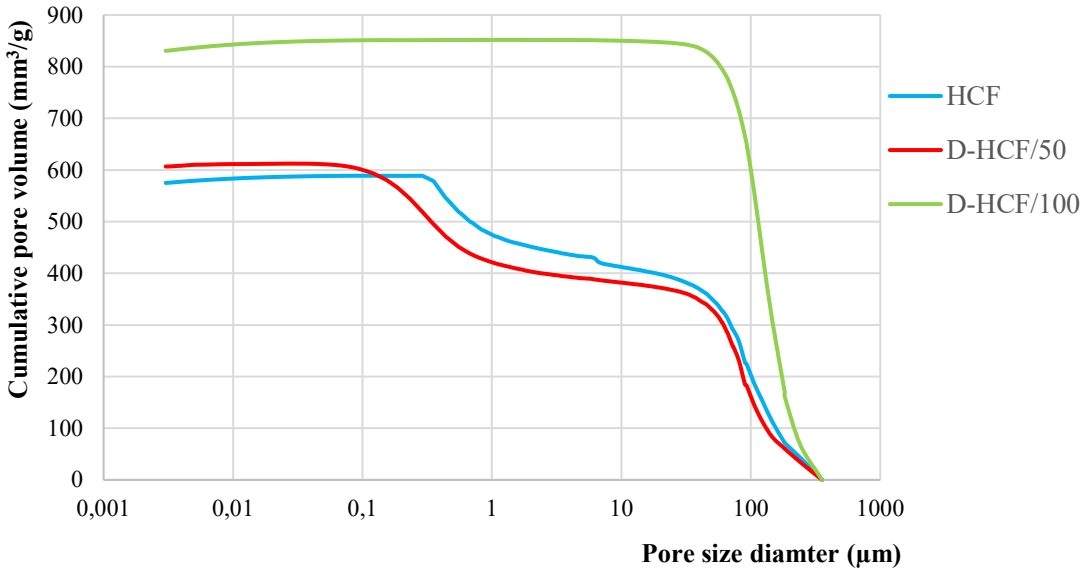

Figure 5.19 Pore size distributions measured by Hg intrusion porosimetry of HCF, D-HCF/50 and D-HCF/100 samples

Chemical and mineralogical characterization

The chemical modifications, which occur in the system during the formation of geopolymeric foam, were evaluated by FTIR spectroscopy. FTIR spectra were collected at room temperature by using a Nicolet iS10 (Thermo Scientific, Italy) from 4000 to 400 cm^{-1} with a wavenumber resolution of 4 cm^{-1} for 64 scans, and in absorbance mode on transparent pellets obtained by dispersing the sample in the form of powder in KBr (2% wt). FT-IR results for all the samples, reported in Figure 5.20, showed, in the region 1300-700 cm^{-1}, several absorbance peaks related to the asymmetric and symmetric stretching of Si-O-Si and Si-O-Al bonds. The MK spectrum highlighted a broad vibration bands located around of 1069 cm^{-1} and 800 cm^{-1}, attributed to the overlapping of the average of the contributions of T-O-Si units (T= Si or Al(IV) present in the amorphous aluminosilicate structure, where the Al is tetrahedral coordinated [22]. However, when the MK (in the several hybrid mixture HCF and D-HCF/x) is activated by an alkaline

solution (SS solution) a geopolymerization process occurs [25] and the peak at 1069cm^{-1} shifts to higher wavenumber (~1090 cm^{-1}), due to the change in the relative amounts of T-O-Si [25]. In the same region, it is possible to observe also the absorbance peaks of D-HCF/100 (in which the MK is completely absent), which are related to the contribution of the set of Q^4, Q^3 and Q^2 (ν_{as} Si-O-Si) units, obtained by condensation reactions of the silicate solution (SS) on the surface of diatomite. In fact, the amorphous silica present in the diatomite, reacting with SS solution, dissolves and precipitates, producing polysilicate system Si-O-Si-O anchored on the surface of diatomite grains.

In addition, a new peak around 730 cm^{-1} appeared: this peak is the major fingerprint of a geopolymeric structure, because it is attributed to the symmetric vibration bond of Si-O-Al (VI), where the Al is in octahedral co-ordination. For instance, the presence of this peak is connected to the well-known process of dissolution of amorphous aluminosilicate phase of MK (in which the Al is tetra-coordinated) and subsequently structural re-organisation of the new aluminosilicate phases (Si-O-Al), in which the Al is octahedral coordinated [25]. However, the presence of this peak deals with the aluminum incorporation in polysialation and it is due to the reaction of both Al-O and Si-O units because of the geopolymerization mechanisms [22, 26]. This peak was more evident for the samples (HCF and DHCF/5, where the amount of silico-aluminate powder (MK) is higher, whereas decreased, until disappearing, with the decreasing of MK (from 100 to 0%wt.) in the matrix. This outcome is related to the reduction of Al amount in the final system.

The XRD patterns (Figure 5.21) presented a “featureless hump” centered at approximately at 2θ equal to 27–29°. In the D-HCF foams, the width of this hump decreases with the increase of metakaolin replacement, whereas crystalline peaks of cristobalite persist.

This result confirmed that, when the MK is replaced by diatomite, the consolidation mechanism in the hybrid foams changed from geopolymerization, associated to a dissolution-precipitation of silico-aluminate phases in alkaline media [26], to a silicate polycondensation, due to the dissolution of the amorphous silica phase (present in the diatomite) and its precipitation into the grain boundary of diatomite [27], as already described in the FTIR analysis.

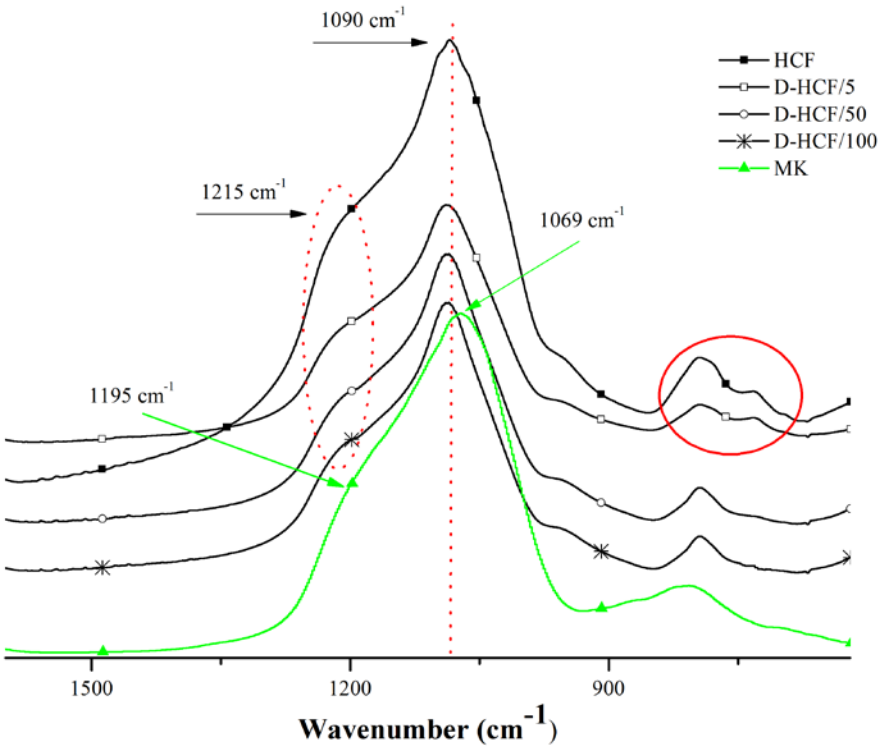

Figure 5.20 FTIR spectra of metakaolin (MK) and of hybrid foams produced

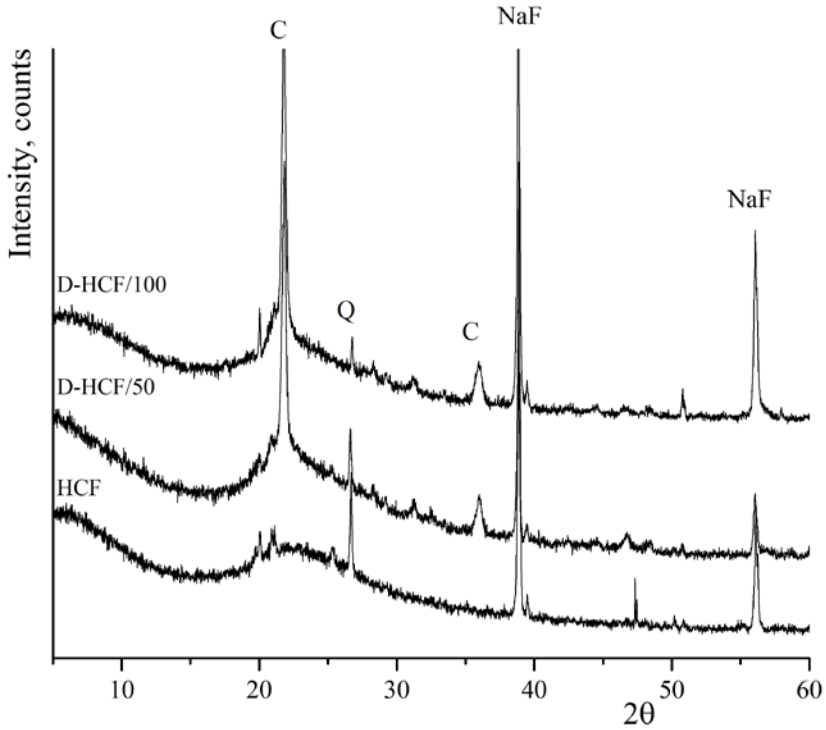

Figure 5.21 XRD spectra of HCF, D-HCF/50 and D-HCF/100 samples

C = Cristobalite, Q = quartz, NaF= Sodium fluoride

Acoustic characterization

Due to the presence of a partially open-cells (micro- and nano-scale) structure, that permits to the air particles to move through the pores of the material, the acoustic properties, in terms of sound absorption coefficient (α), were also measured according to the standard UNI EN 10534. For these measurements, an impedance Kundt tube, 100 mm in diameter, 570 mm in length was used. The distance between first microphone and samples was 200 mm, while the distance between first and second microphone was fixed at 50 mm. The frequency ranged from 200 to 2,000 Hz. A loudspeaker placed at one end of the tube generated the signal (white noise), while the samples are placed on a rigid surface at the opposite end. The thicknesses of samples where equal to 33 mm.

In figure 5.22 the acoustic absorption curves for selected samples (HCF and D-HCF/50) are reported. Commonly the parameters affecting the acoustic absorption behavior of a porous material are related to the porosity, the tortuosity, the flow resistivity and the thickness of the layer. When the sound propagates in a porous media (with interconnected pores) energy is lost, this behavior is due to the complex heterogeneous microstructure and to the viscous boundary layer effects [28]. In our samples, the results showed a broader "hopscotch" curve with a maximum value of α around 0.47 at 300 Hz for both systems. This behavior is related to the presence of "cavities" that amplify, at specific frequency, the capability to absorb the sound [29]. At higher frequency, the two systems, HCF and D-HCF, showed two distinct peaks at 1248 and 1527 Hz respectively with a value of α equal to 0.2 and 0.33. The presence of diatomite induced a shift to lower frequency value with an increasing of α value (related to the second peak), probably due to an increasing in tortuosity of porous media. This peculiarity could be enhanced in those applications in which a specific absorption, in a defined range of frequencies, is required.

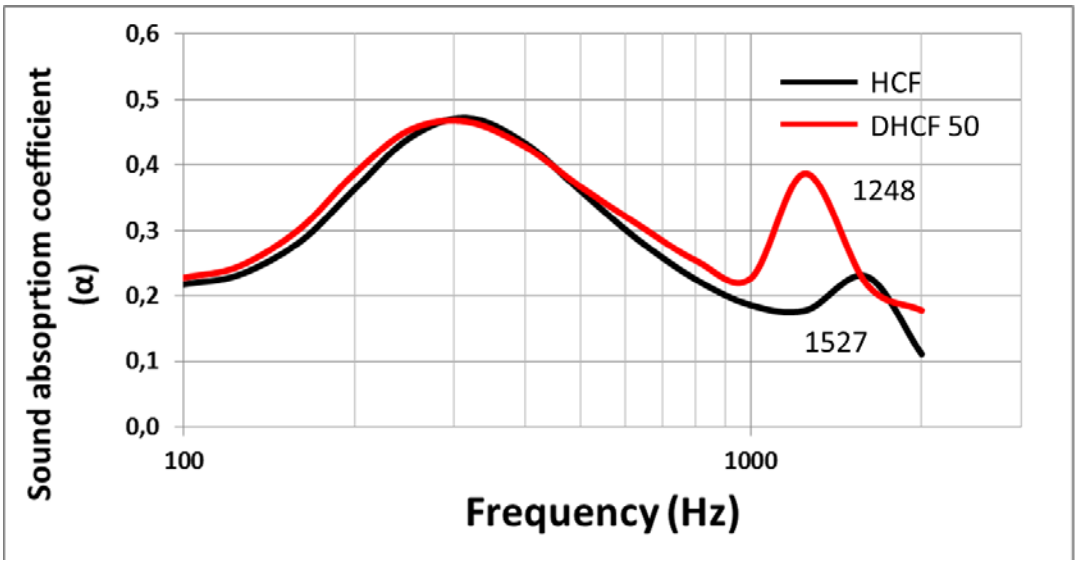

Figure 5.22 Sound absorption coefficient as function of frequency for HCF and D-HCF/50 samples

Thermal stability

In order to evaluate the behavior of the hybrid ceramic foams in isothermal condition, each specimen was thermally treated at 200, 400 and 600°C, using a Nabertherm HTC 03/15 oven. The thermal cycles used consisted in a heating ramp with heating rate of 10°C/min followed by an isothermal step at the fixed temperature for 2 hours. Before and after every thermal treatment, the foams were accurately weighted, using a Mettler Toledo XS105 Dual Range microbalance with an accuracy of ± 0.1 mg, and measured using a caliper (accuracy ± 0.05 mm). These temperatures were chosen to have an idea of the thermal behaviour of foams in a quite wide range of temperatures. The HCF, D-HCF/50 and D-HCF/100 samples after the treatments are shown in Figure 5.23 and it is evident the absence of significant cracks, fractures or other defects due to the exposure to high temperatures. In Figures 5.24 and 5.25 are reported respectively the weight losses and the volume variations of the samples exposed to thermal cycles. Figure 5.24 shows that mass losses increased with temperature for all the foam samples considered, because weight losses are due to dehydration processes that are facilitated at higher temperatures. This is confirmed from the fact that, at 600°C, HCF, D-HCF/50 and D-HCF/100 samples exhibit a very similar value of weight loss (~5-6%). For the lower temperatures, the sample obtained with total diatomite replacement of metakaolin, showed the best performance also compared to the sample with the 50% of diatomite. From Figure 5.25 it is possible to see that the addition of diatomite to the starting hybrid ceramic foam, leads to an

increase in the thermal stability of the material in terms of volume variation. In fact, for all the temperatures considered, the D-HCF/50 and D-HCF/100 samples showed lower values of ΔV%. This trend results to be particularly evident at 600°C considering that the HCF sample showed a volume reduction of quite 12%, while D-HCF/50 and D-HCF/100 samples showed volume reductions of respectively 5.3% and 3.0%. The positive effect of the diatomite addition on thermal stability of foams is much more significant considering the volume restriction of samples than considering the weight loss. This is probably because all the samples, independently from the diatomite content, contain some unreacted or chemically bonded water that evaporates as consequence of the thermal treatments. Regarding the volume variations, it is possible to consider that diatomite is really stable at high temperature and probably causes a lower shrinkage compared to metakaolin.

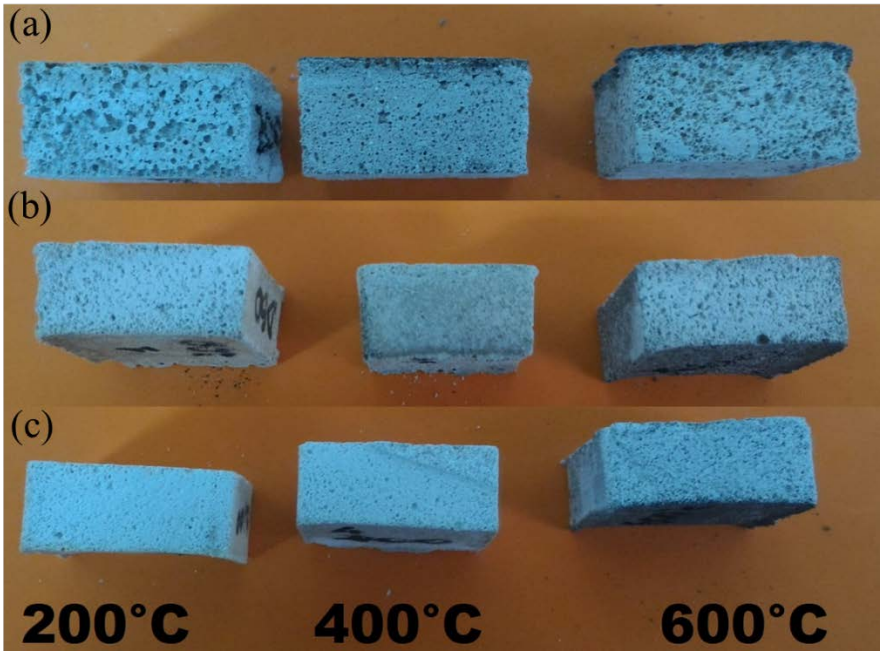

Figure 5.23 HCF (a), D-HCF/50 (b) and D-HCF/100 (c) samples after thermal treatments

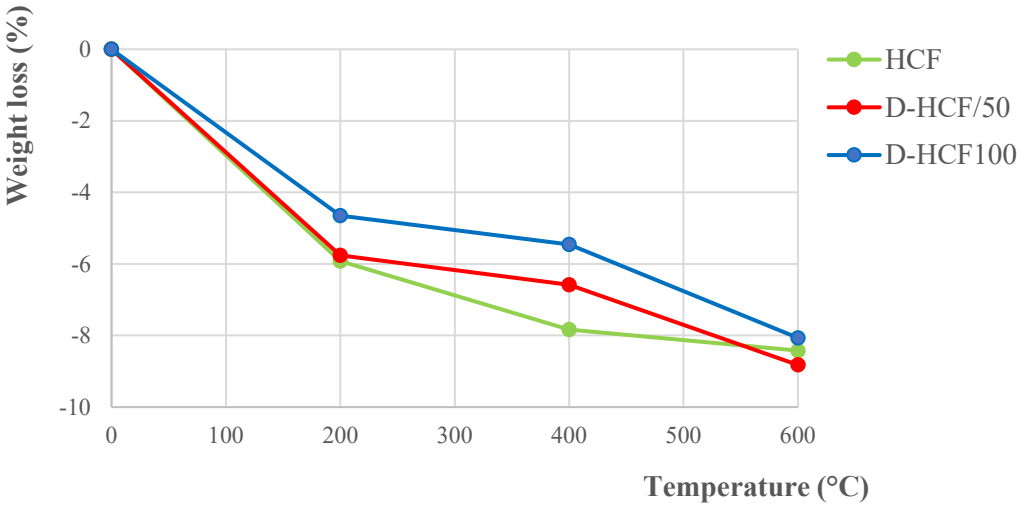

Figure 5.24 Weight losses of HCF, D-HCF/50 and D-HCF/100 samples after thermal treatments

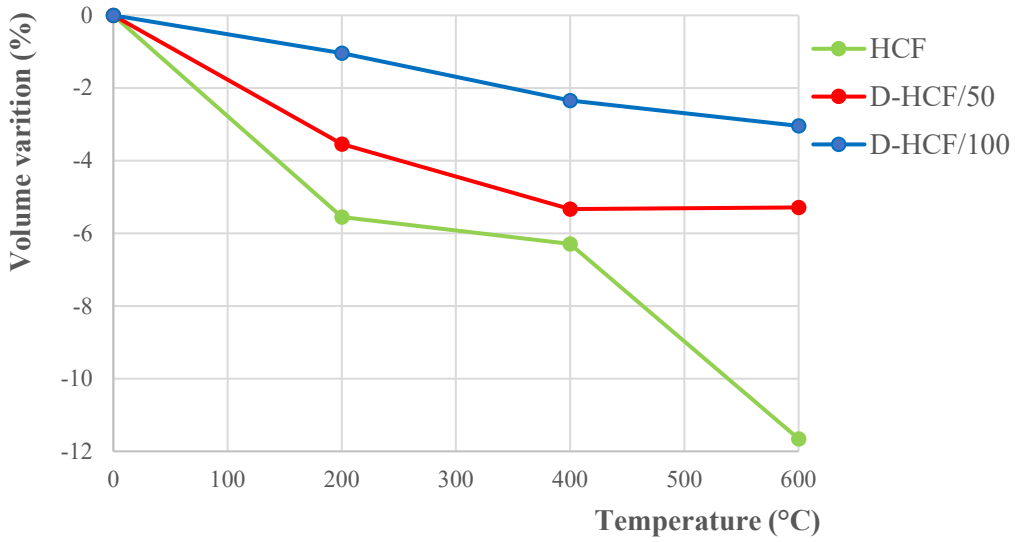

Figure 5.25 Volume variations of HCF, D-HCF/50 and D-HCF/100 samples after thermal treatments

The thermal degradation of the produced foams was investigated by thermogravimetric (TGA) and derivative TGA (dTGA) analyses with a TGA 2950 apparatus (T.A. Instruments, USA) under air atmosphere. The samples were heated on platinum pans from 30 to 1000 °C with heating rate of 20 °C/min.

Table 5.5 shows the main weight percent losses observed in three specific temperature ranges, after thermogravimetric analyses have been performed on all the samples produced. All the hybrid ceramic foams show comparable weight losses gathered in the same temperature ranges and that the total amount of these weight losses is always lower than 10%.

Table 5.5 Main weight losses of the ceramic foams produced

Sample	T_{max} (°C)	Weight loss1 (%) (≈ 50°- 200°)	T_{max} (°C)	Weight loss2 (%) (≈ 550°- 600°)	T_{max} (°C)	Weight loss3 (%) (≈ 700°- 850°)
HCF	106	4,08	574	0,45	838	2,00
D-HCF/5	96	4,48	560	0,31	840	0,55
D-HCF/10	102	4,52	555	0,60	830	2,06
D-HCF/50	109	4,27	556	0,65	803	2,44
D-HCF/70	103	4,23	555	0,67	810	2,35
D-HCF/100	99	3,56	554	0,50	796	3,88

Three main temperature ranges have been identified. the first range, from about 50°C to 200°C, is related to the condensation reactions of the sodium silicate solution. In fact, usually, using inorganic silicate precursors, siloxane domains are generated and a sort of sol-gel process takes place [30]. The several steps involved in the sol-gel process can be summarized in three steps (1) hydrolysis of the silicate precursors of the constituent oxides, (2) condensation reactions between the resulting monomers ($Si(OH)_4$) to produce highly branched oligomers that evolve into “sol” particles, and (3) self-assembling and aggregation of the “sol” particles to form an irreversible “gel” [30]. The three steps of the process can be schematized as follow:

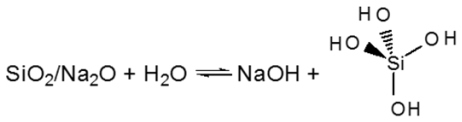

(1)

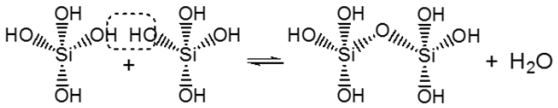

(2)

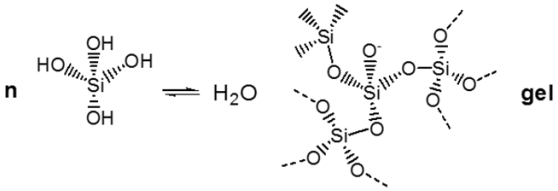

(3)

So, the weight loss detected between 50°C and 200°C for the hybrid ceramic foams, can be identified as a consequence of the removal of the water deriving from the condensation of the silicate phases. The other two main weight losses identified, can be both connected to the thermal degradation of the sodium hexafluorosilicate, one of the raw components present in all the different kinds of ceramic foams prepared. In particular, between 550° and 600°C, there is a very small weight loss (0.31÷0.67%, see Table 5.5) that can be attributed to the decomposition of the unreacted sodium hexafluorosilicate [31]. In the temperature range 700°- 850°C, a higher weight loss, equal to about 2%, can be identified and attributed to the vaporization of melted NaF [31], which has been obtained as product of the reaction deriving from the interactions between sodium hexafluorosilicate and sodium silicate solution (see eq. 4 of chapter 3).

Fire behavior

When a hybrid organic-inorganic material is proposed in a civil and/or transport application it is essential to assess its fire behavior. There are several methods for determining the fire performance of materials in building applications, specified in many international standards [32-34]. The cone calorimeter has emerged in recent years as the most widely used apparatus for this purpose. In fact, it has been demonstrated that the cone calorimeter is suitable for measuring heat release rate (HRR) from materials and products with low heat content [35]. The heat release rate represents the most important variable to characterize the ‘‘flammability’’ of a product and its consequent fire hazard [36].

Fire resistance was studied by means of cone calorimetry. The fire behavior exhibited by each foam in realistic fire conditions was evaluated by cone calorimetry, using an oxygen consumption cone calorimeter (Fire Testing Technology, FFT dual cone calorimeter model). The standard procedure [37] used in this analysis involves tiles shape specimens (100 mm ×100 mm × 20 mm) in horizontal orientation to an external radiant flux of 50 kW/m^2, representing a generalized fire [38]. Three samples for each mixture were investigated. Samples were previously conditioned to constant mass at 23 ± 2 °C with a relative humidity of 50 ± 5% in accordance with ISO 554 [39]. The conventional data are: time to ignition (TTI, s), heat release rate (HRR, kW/m2), peak of heat release rate (PHRR, kW/m2), i.e. maximum of HRR, fire performance index (FPI which corresponds to the ratio of TTI to pHRR, $s*m^2/kW$), Total Heat Release (THR, kJ/m2) [35]. The time to ignition (TTI) is the period that a combustible material can withstand exposure to a constant radiant heat flux before igniting and undergoing sustained flaming combustion. This value can be used as a qualitative measure of flammability resistance of a material. Heat release rate is considered the most important fire reaction property, because it is the best indicator of the fire hazard of a combustible material. Specifically, the HRR represents the thermal energy released by a material per unit area, when exposed to a fire radiating at constant heat flux. The HRR values were calculated on the basis of oxygen depletion due to combustion [37, 40]. The pHRR represents the peak value of the HRR and dictates the flashover potential in a real fire scenario.

Cone calorimeter results (Figure 5.26) showed that samples in the condition of external heat flux selected (50 kW/m^2) do not burn. A very low contribution considering the heat released (HRR), that is the contribution in terms of heat of the material in a possible fire scenario, seems to be clear (Figure 5.26(a)). Also, the CO and CO_2 produced are of a negligible quantity. A little percentage of smoke, which does not reach the concentration necessary to ensure the ignition, was developed (Figure 5.26(b)).

In table 5.6 the results of non-combustibility tests in terms of temperature rise of surface and center of sample, temperature rise in furnace, mass loss during the test and development of flame for HCF, D-HCF/50 and D-HCF/100 samples have been reported. Samples exhibit a very good fire behavior regardless of content of diatomite; the mass lost during the tests is <15%, flames are not developed, the temperature rise of the surface and center of the sample and in the furnace, is less than 10°C.

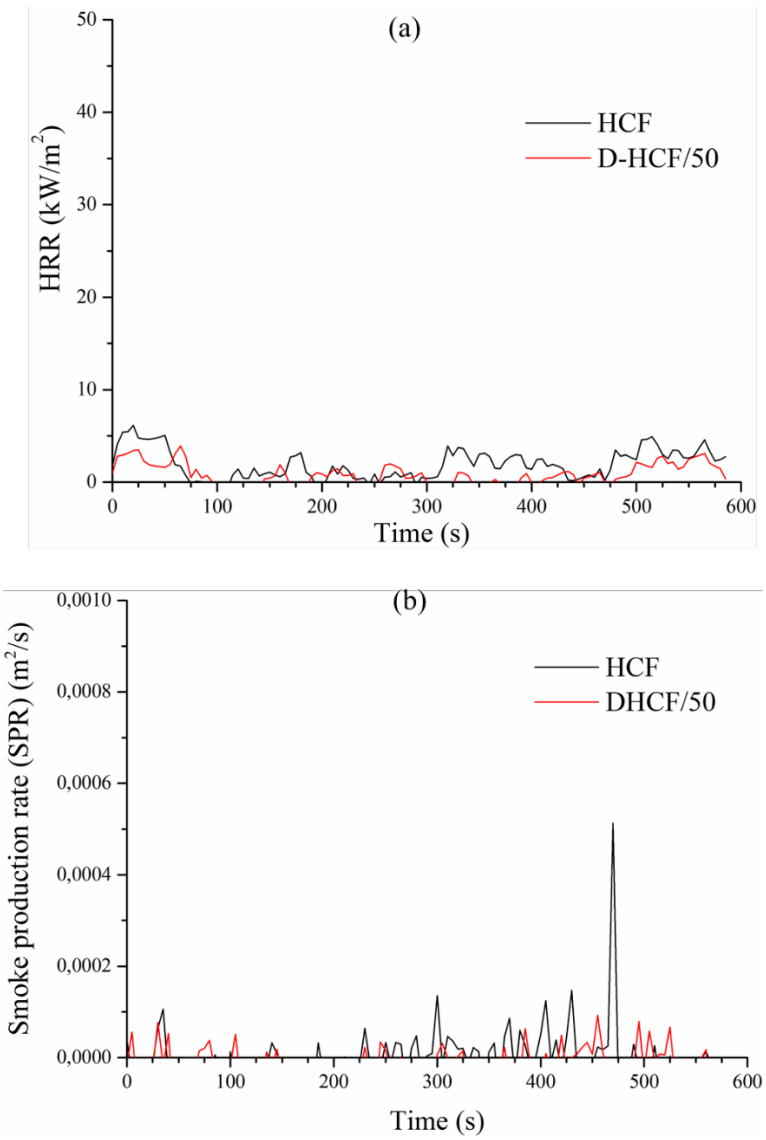

Figure 5.26 Cone calorimeter results for HCF and D-HCF/50 samples: Heat release rate (a) and smoke production (b)

Table 5.6 Parameters obtained by combustibility tests on HCF, DHCF/50 and DHCF/100 samples

Parameters	**HCF**	**D-HCF/50**	**D-HCF/100**
$\Delta T_{(surface)}$ (°C)	1,0 ± 0,4	2,0 ± 0,2	4,0 ± 0,2
$\Delta T_{(center)}$ (°C)	1,1 ± 0,5	1,8 ± 0,3	3,5 ± 0,3
$\Delta T_{(furnace)}$ (°C)	2,1 ± 0,4	1,5 ± 0,1	5,2 ± 0,4
Δwt (%)	10 ± 1	9 ± 1	8 ± 1
Sustained flame (s)	0	0	0

The behavior exhibited certifies the non-combustibility of these materials with the best features for application as insulators in the buildings and transport fields (i.e marine). The temperature trends for all the samples tested are reported in Figure 5.27.

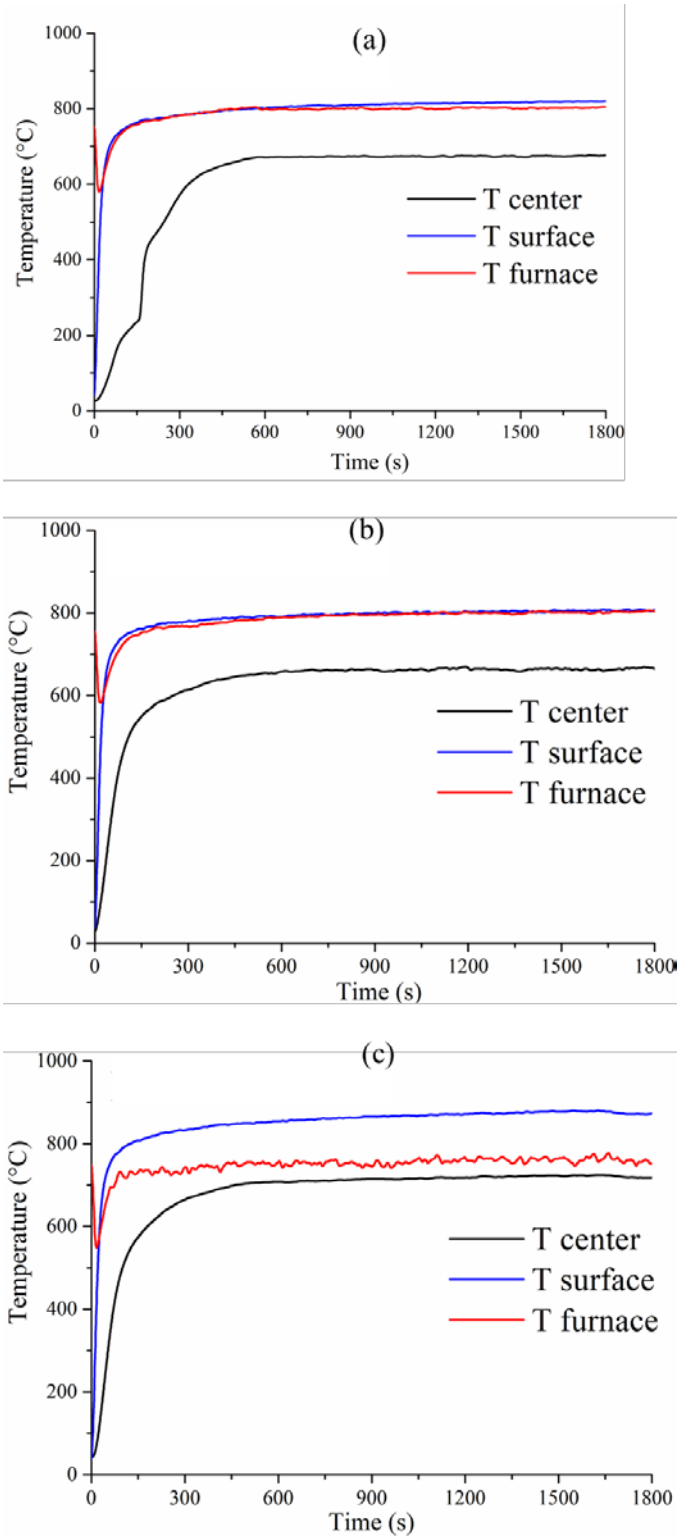

Figure 5.27 Temperature trend during the non-combustibility test for HCF (a), D-HCF/50 (b) and D-HCF/100 (c) samples

Thermal conductivity

The thermal conductivity was measured with a thermal conductivity analyzer (TCi Thermal Conductivity Analyzer, C-Therm Technologies) utilizing the modified transient plane source technique. The equipment used for the analyses is reported in Figure 5.28

Figure 5.28 Thermal conductivity analyzer used for thermal conductivity measurements

The thermal conductivity of the hybrid foams is given in Table 5.7. Thermal conductivity of the foamed samples decreases with increase in the diatomite content. Foam HCF shows a thermal conductivity value of 0.128 W/m·K whereas DHCF/50 shows 0.088 W/m·K. The thermal conductivity decreases substantially to 0.074 W/m·K with the total replacement of metakaolin by diatomite. The results confirm that the thermal conductivity of foamy material is not correlated to the bulk density (see Figure 5.29) and a substantial decrease of the thermal conductivity value can be achieved by incorporating an appropriate amount of diatomite, that is characterized by very low thermal conductivity (~ 0.05-0.06 W/m·K).

Table 5.7 Thermal conductivity of the hybrid foams

Sample	**Thermal conductivity (W/m·K.)**
HCF	0.128
D-HCF/50	0.088
D-HCF/100	0.074

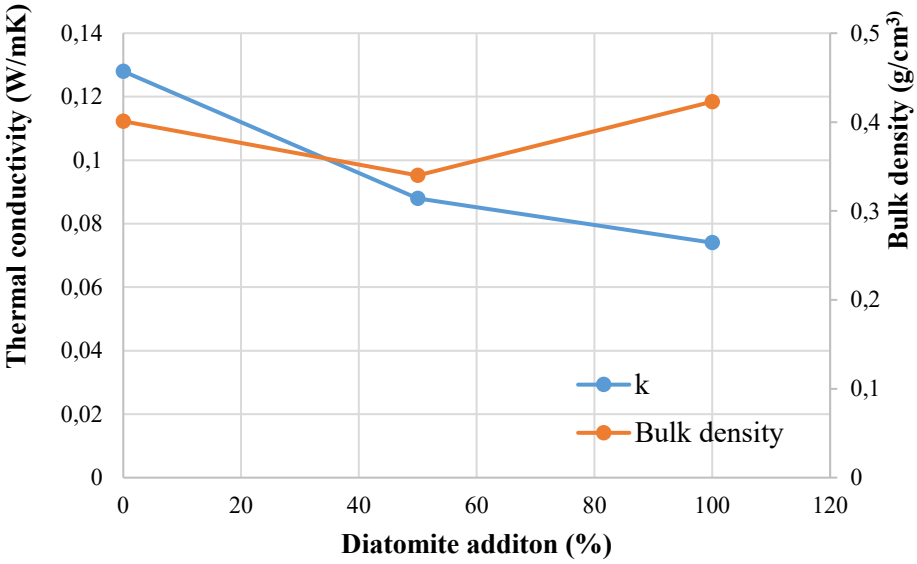

Figure 5.29 Correlation between thermal conductivity, bulk density and diatomite addition

5.3 Use of 3D printing inverse replica method to create macroporosity

Additive manufacturing and 3D printing process

Three-dimensional printing technology has emerged as a promising tool to fabricate scaffolds with high precision and accuracy, creating intricately detailed biomimetic 3D structures [41]. The techniques currently being used to achieve 3D printing of scaffolds involve a layer-by-layer process, which includes, but is not limited to, direct 3D printing, fused deposition modeling, stereolithography, and selective laser sintering. These techniques have been used to produce scaffolds ranging from millimeter to nanometer sized scaffolds. It is also important to note that solid free-form fabrication, additive manufacturing and 3D printing have become synonymous over the past decade and are now used interchangeably.

Additive manufacturing is defined as layer by layer process of joining materials by selectively depositing, curing, or consolidating to make objects from 3D model data. In comparison to traditional production processes where the shape of the object is given by removing material by machining, forming and casting, additive manufacturing builds the final object by adding material. Minimal waste is produced while reaching high geometric accuracy [42, 43]. Thus, AM techniques allow a cost-effective production of on-demand

customized products. The big advantage of AM, besides rapid prototyping, is the design flexibility of components. There are no restrictions on the complexity of a part [42, 44].

One disadvantage of these kinds of techniques is the production time that it takes to fabricate scaffolds, which dramatically increases as the scaffold design becomes more precise and intricate [45]. This is especially the case for conventional methods which involve a lot of manual labor compared to an automated process [46].

Stereolithography Process

A wide variety of AM technologies exist that enable printing of polymers, metals and ceramics. Stereolithography is one of the oldest AM technologies and has first been developed for rapid prototyping. Nowadays, it is also used for industrial production of components like hearing devices and dental braces. The concept of stereolithography is to use photopolymerization by which monomers are linked into a polymer chain using visible or UV light. Originally, the part was printed bottom to top, on a vertically actuated platform that was lowered after every layer so that new resin was allowed to settle and spread across the surface (Figure 5.30) [43].

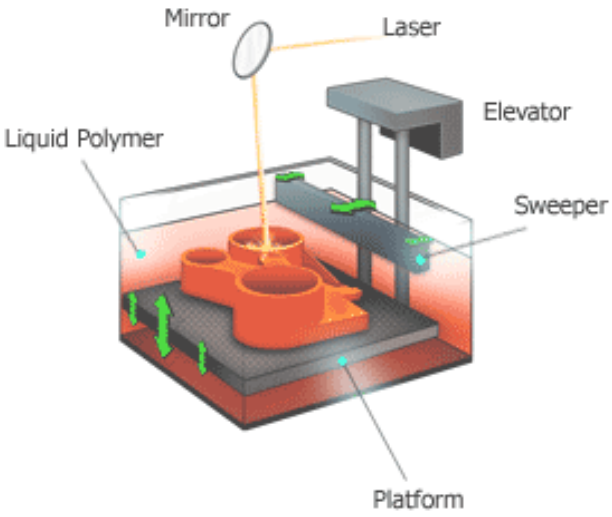

Figure 5.30 Schematic representation of the working principle of Stereolithography Process

Newer machines use a bottom-up approach (Figure 5.31) that prints top to bottom. Instead of a platform the machines use a build head that is moved up a step after every printed layer, similar to direct digital light projection technology (DLP). The technique has one of the highest fabrication accuracy in additive manufacturing and increasing amounts of

materials are developed for it. In particular, stereolithography is very versatile with respect to the freedom of designing structures and the scales at which these can be built (submicron- to centimeter-sized) [47].

Therefore, stereolithography has been selected as 3D printing technique (Ember DLP® 3D Printer) in the production of the polymeric templates needed to add macropores to the hybrid ceramic foams previously characterized. In fact, the idea of this process is to produce a polymeric template with a defined and precise geometry, which corresponds to the negative of the geometry that we want to obtain in the foam sample. The polymeric template has to be filled with the ceramic slurries. Then, after being left to the traditional curing conditions, the system obtained, composed by the template filled with the consolidated foam, has to be exposed to a thermal treatment in order to burn out the polymeric template and leave inside the solid ceramic foam matrix the desired porosity.

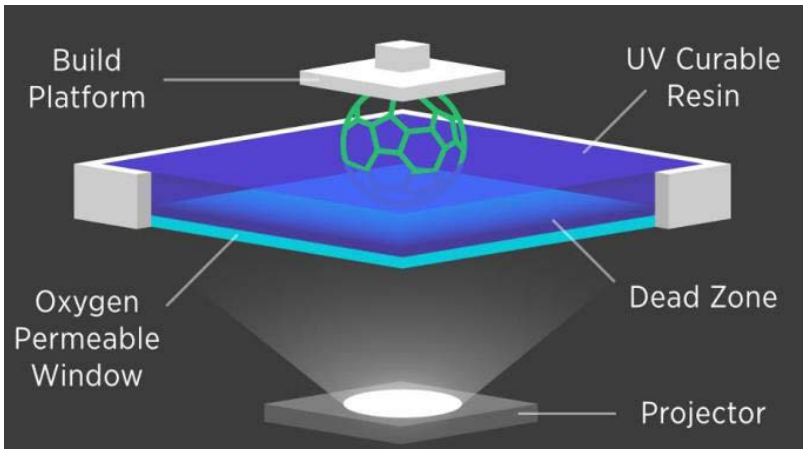

Figure 5.31 Schematic of the working principle of bottom-up approach for SLA [42]

Autodesk Ember 3D-Printer

The printer used for this research activity was reported Figure 5.32. In an Ember printer, the tray (also called the vat) holds the liquid resin that the machine turns into 3D parts. It has a clear window made of glass coated (Figure 5.33) with PDMS (a member of the silicone family), through which 405nm ultraviolet light shines and cures each layer of the print that remains stuck on the printing head (Figures 5.33 and 5.34). The standard tray of the Ember printer needs at least 50 – 100 ml resin so that it can be used for printing.

The window must allow oxygen permeation in order to form a layer that inhibits polymerization which prevents the print to stick to the window.

Figure 5.32 Autodesk Ember 3D-Printer

Figure 5.33 Tray with glass window and build printing head of Ember 3D printer

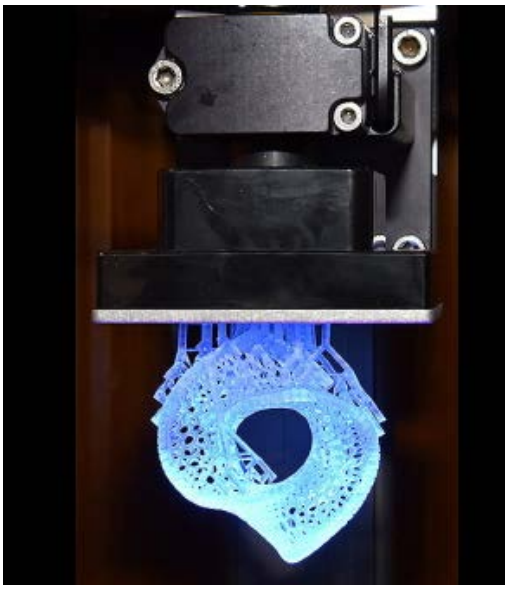

Figure 5.34 Build head of Ember 3D printer after printing process of a part

Design and printing of templates

In figure 5.35 (a) and (b) are reported respectively the drawn model for the polymeric template by AutoCAD and the printed one using the Ember 3D printer.

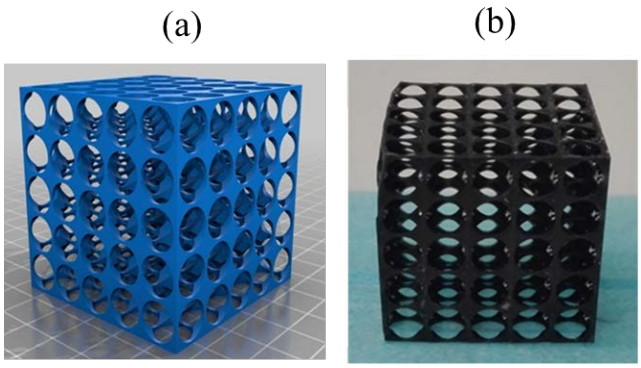

Figure 5.35 Model of template (a) and printed template (b)

The resin used to print templates was a standard resin (Autodesk, PR 48) and it was supplied by the printer producers, who provided the following chemical formulation (all percentages are wt/wt):

• Oligomer: Allnex Ebecryl 8210 39.776%, Sartomer SR 494 39.776%

• Photoinitiator: Esstech TPO+ (2,4,6-Trimethylbenzoyl-diphenylphosphineoxide) 0.400%

• Reactive diluent: Rahn Genomer 1122 19.888%

• UV blocker: Mayzo OB+ (2,2'-(2,5-thiophenediyl)bis(5-tertbutylbenzoxazole)) 0.160%.

5.4 Production of hybrid ceramic foams using 3D printing inverse replica

The hybrid ceramic slurries were poured inside the printed template (see Figure 5.36). The so obtained system was cured at 40°C at room humidity for 24 hours. After curing, the consolidated foams, reported in Figure 5.37, were thermally treated in order to burn out the polymeric template. The samples were slowly (0.5 °C/min) heated at 500°C for 6 hours, in order to avoid the formation of cracks and fractures caused by the polymer burning out.

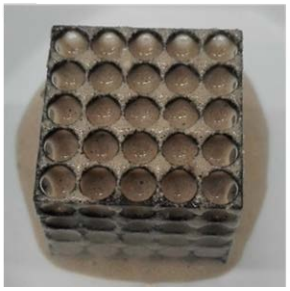

Figure 5.36 3D printed template impregnated with ceramic slurry

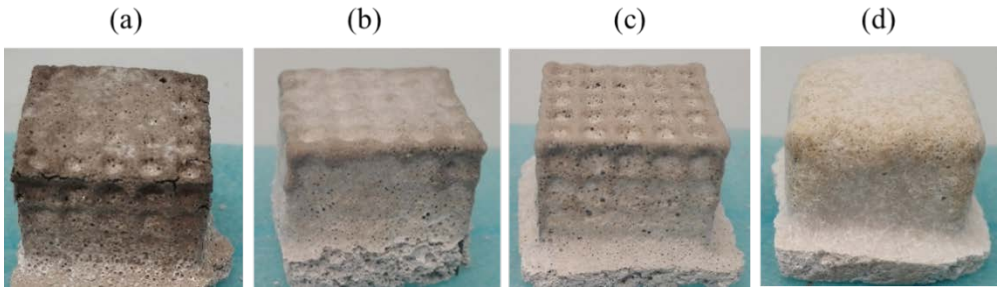

Figure 5.37 Templates with solid foam samples (a) HCF, (b) D-HCF/50, (c) D-HCF/70,(d) D-HCF/100

After the thermal treatment, the foam samples were still solid and did not show any presence of fractures, as it is possible to see from Figure 5.38 in which the D-HCF/100 sample was reported.

Figure 5.38 D-HCF/100 sample after template burn out

Microstructural characterization of ceramic foams produced

In order to investigate the morphology and to verify the presence of different levels of porosity, optical microscopy (Leica Wild M10, Stereo Microscope) and SEM analysis (SEM, LEO 1530, Zeiss) have been performed on all the samples produced.

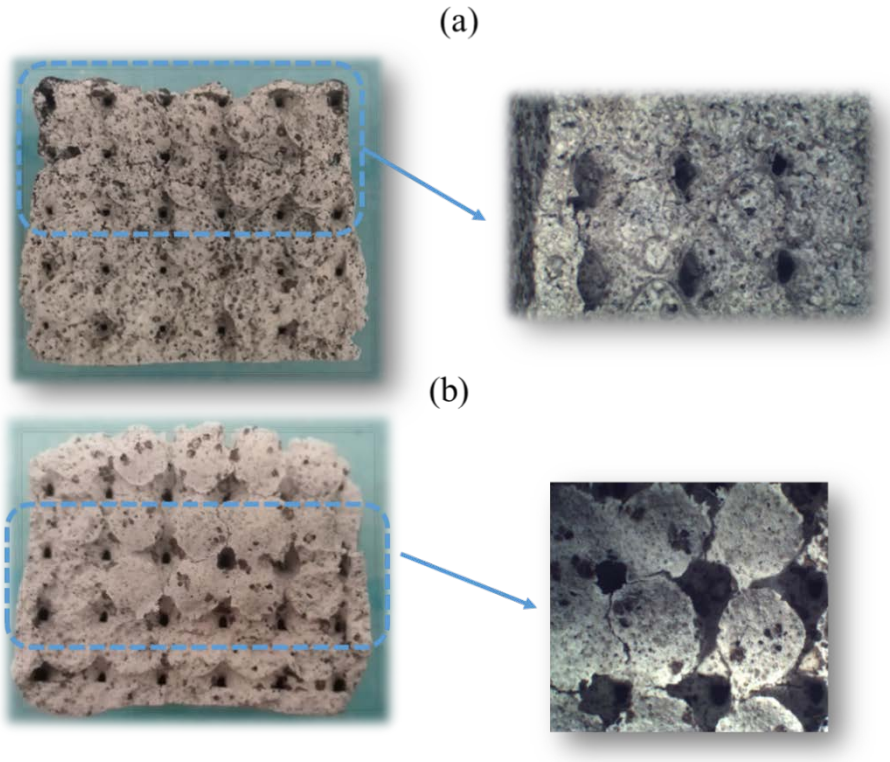

Figure 5.39 Images and Optical microscopies of (a) D-HCF/50 and (b) D-HCF/100 samples

In Figure 5.39 pictures and optical microscopies of D-HCF/50 and D-HCF/100 samples are reported. The images show the presence of the porosity deriving from the template: it

is really evident the periodicity of the pattern of pores originated from the burning out of the polymer resin of the template used. Moreover, in Figure 5.40, that shows a SEM image at very low magnification of D-HCF/70 sample, used as example, it is visible one of the macropores obtained in the foam. It can be easily identified as a template deriving pore either from the size (≈ 0.7 mm) or its regular shape due to the template geometry.

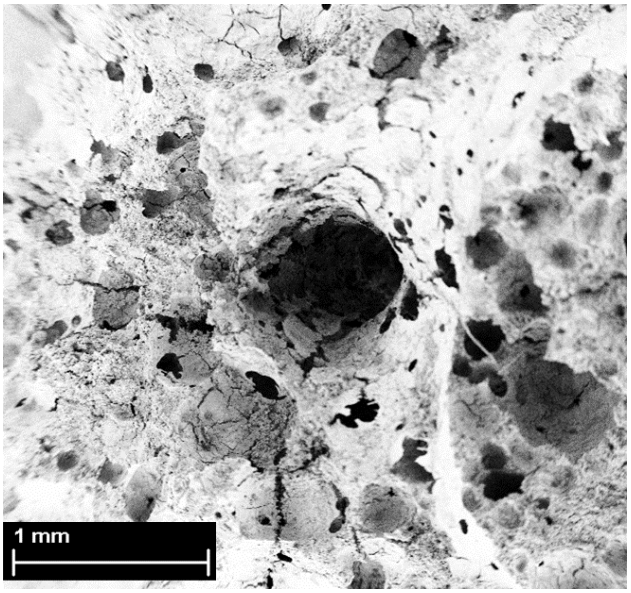

Figure 5.40 SEM image of a macropore of D-HCF/70 sample

SEM images at higher magnifications of D-HCF/50 and D-HCF/100 samples are reported respectively in Figure 5.41(a) and in Figure 5.41(b). From the Figures 5.41, it is possible to see at the same time, both the macropores, produced in the foams using the template, which showed regular and sharp shape with well-defined edges, both the different microstructures of the two different samples. In fact, looking at the structure of the macropore walls, it is possible to see the higher compactness that characterize the D-HCF/100 matrix compared to the D-HCF/50 sample that seems to be characterized by higher heterogeneity.

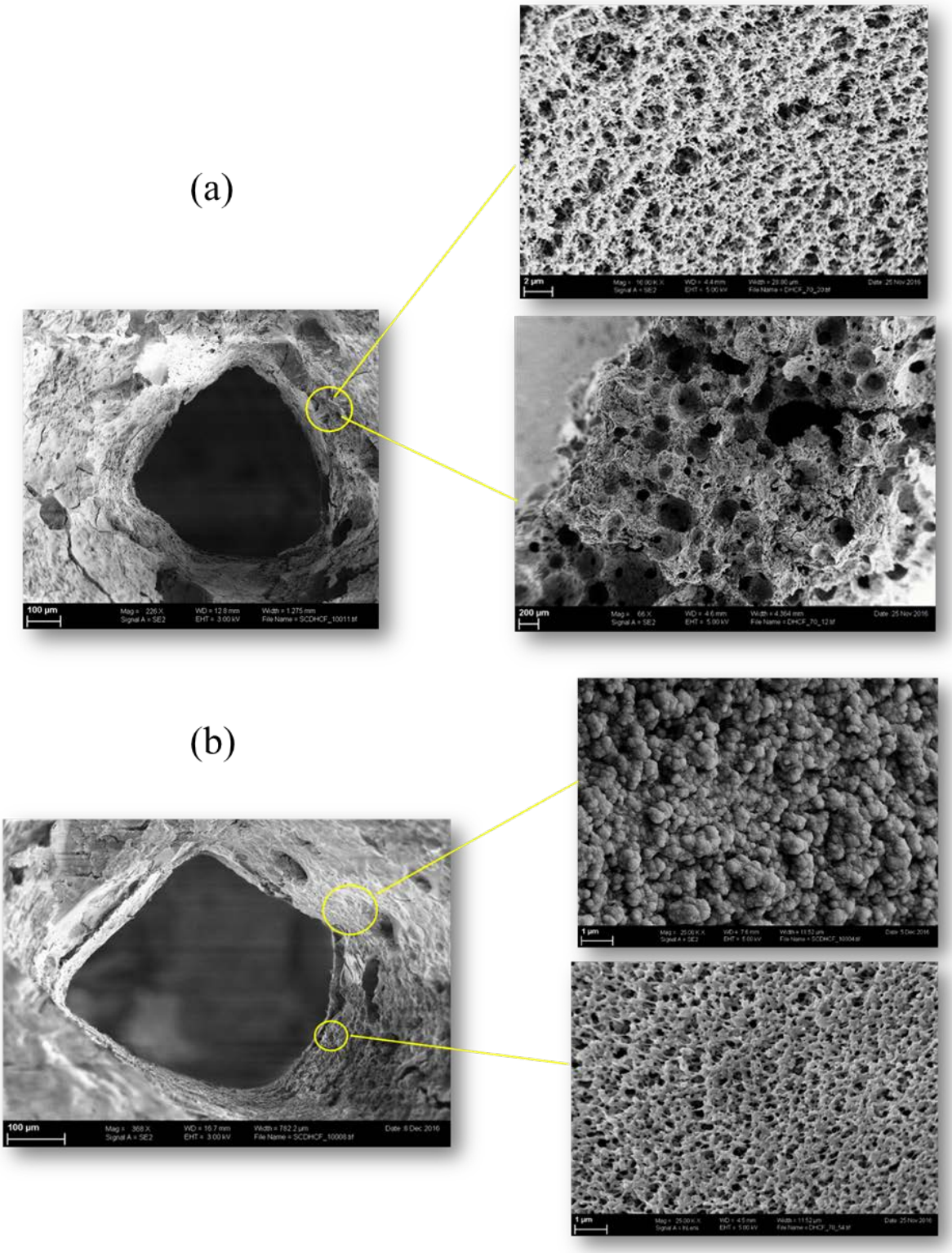

Figure 5.41 SEM images of template deriving porosity for (a) D-HCF/50 and (b) D-HCF/100

Influence of template geometry

In order to investigate the influence of the template geometry on the final microstructure and porosity of the hybrid ceramic foams obtained, different geometries and pore dimensions have been considered, designed and consequently printed and the D-HCF/100 mixture has been selected.

In Figure 5.42, two different AutoCAD models of templates are reported. The template reported in Figure 5.42(a) shows a regular geometry with fixed dimensions of the round openings (3 mm) and square channels (2 mm), while the one reported in Figure 5.42(b) is characterized by a varying dimension of the openings, ranging from 4 to 0.5 mm, along two directions. Figure 5.43 shows the printed versions of the template models reported in Figure 5.42.

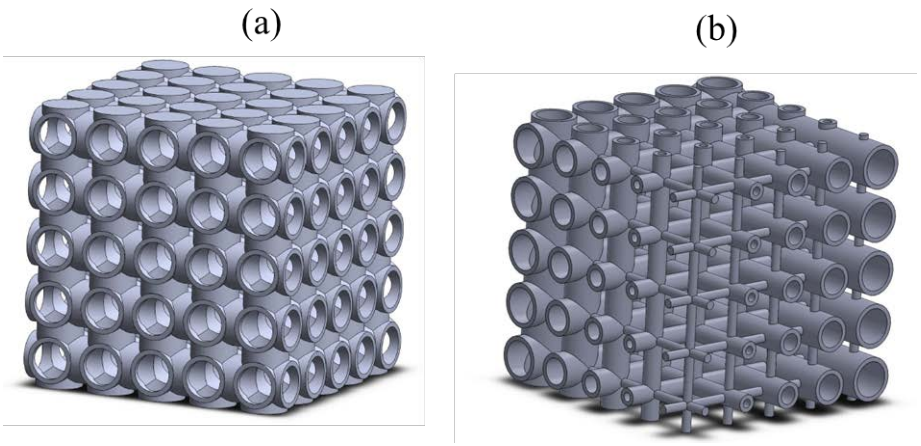

Figure 5.42 AutoCAD models of two different templates with fixed (a) and varying (b) dimensions of the openings

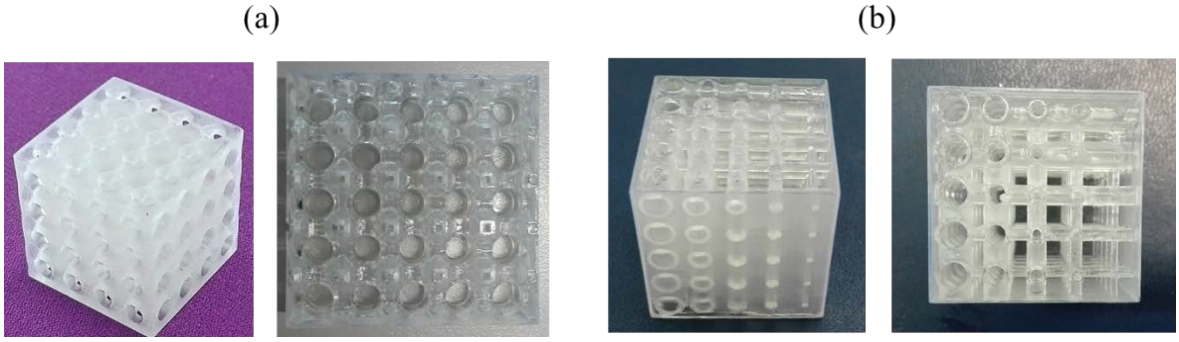

Figure 5.43 Printed versions of the template models reported in Figure 5.38

The D-HCF/100 slurry was poured inside the different printed templates and the so obtained systems were cured at 40°C at room humidity for 24 hours. After curing, the samples of consolidated foam, reported in Figure 5.44, were thermally treated using the same heating cycle previously described. Figure 5.45 shows the final products obtained, which present, even more clearly than first case, a periodic and regular pattern of the pores obtained within the matrix.

Figure 5.44 Templates impregnated with D-HCF/100 foam after curing

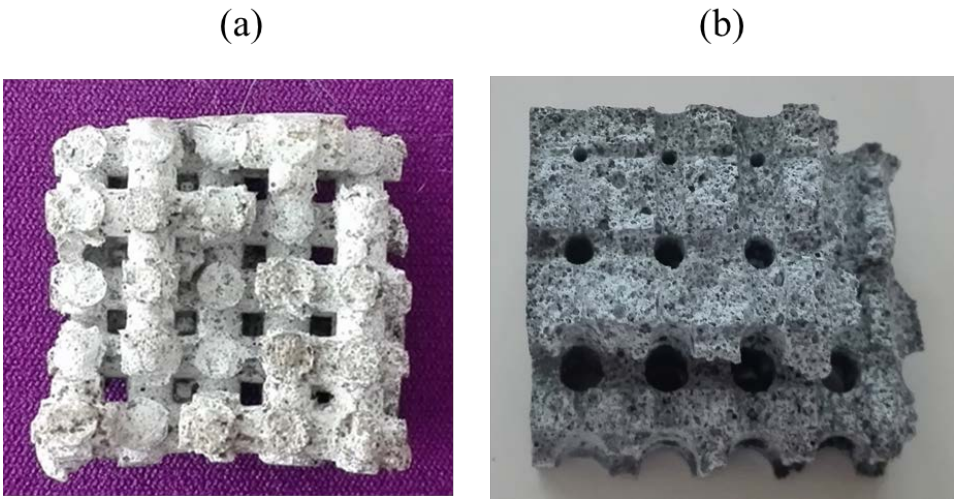

Figure 5.45 D-HCF/100 samples after burn out of the templates

In particular, in Figure 5.45(a) it is possible to easily identify square openings of 2 mm deriving from the square channels present in the template showed in Figure 5.42(a). Figure 5.45(b) reported the ceramic foam obtained with the template showed in Figure 5.42(b) where the presence of round pores with different dimensions (from 1 to 3 mm) was found. All the dimensional ranges of pores obtained in the above foam, included the one of 4 mm that was not visible in the previous figure, are reported in Figure 5.46. The dimension of each pore is underlined by the presence of dimensional markers. Finally,

from Figure 5.47, in which optical and electron microscopies of the two samples of ceramic foam produced are reported, the systematic and periodic pattern of the macropores, due to the use of polymeric templates, is widely showed.

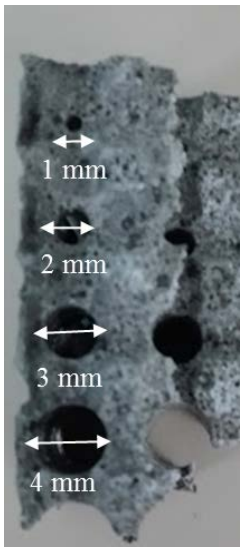

Figure 5.46 D-HCF/100 sample after burn out of the template of Figure 5.38(b) with dimensional markers

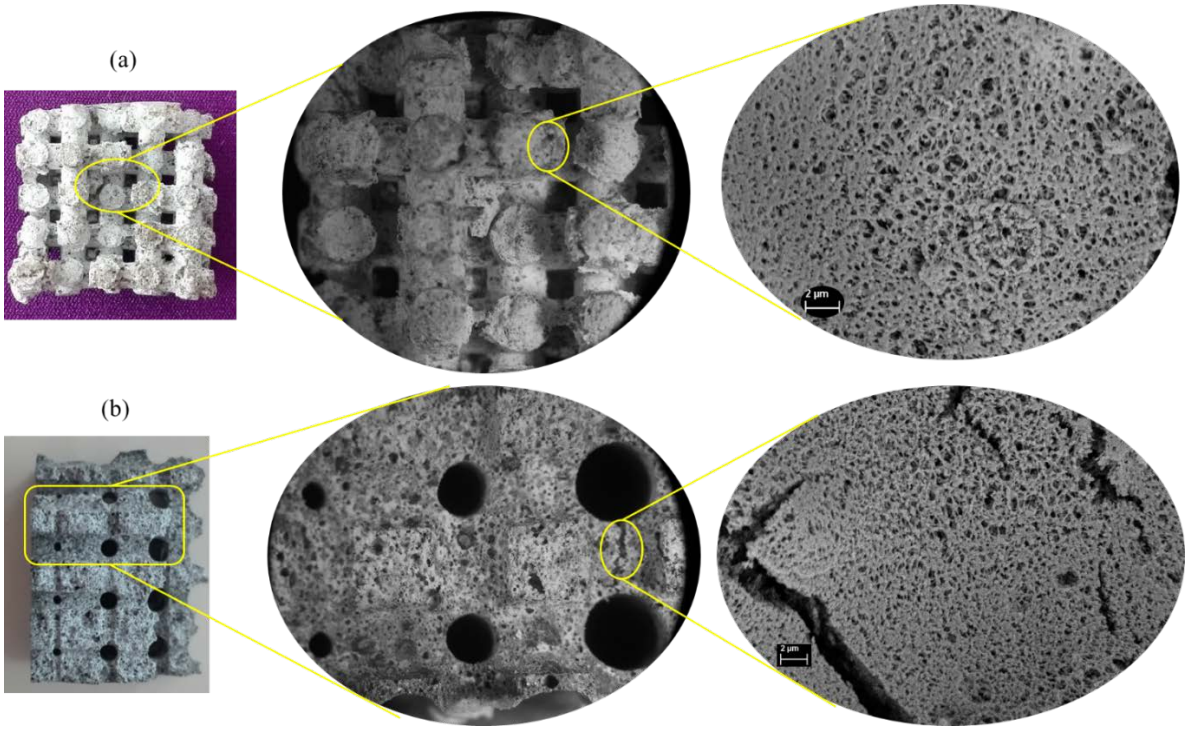

Figure 5.47 Optical and electron microscopies of the two samples of ceramic foam obtained using templates (Figures 5.41(a) and (b))

Bibliography

[1] M. Scheffler, P. Colombo (Eds.), Cellular Ceramics: Structure, Manufacturing, Properties and Applications. John Wiley & Sons (2006). ISBN: 3-527-31320-6.

[2] A.R. Studart, U.T. Gonzenbach, E. Tervoort, L.J. Gauckler, Processing routes to macroporous ceramics: a review, J. Am. Ceram. Soc.89 (2006) 1771–1789.

[3] F. Akhtar, L. Andersson, S. Ogunwumi, N. Hedin, L. Bergström, Structuring adsorbents and catalysts by processing of porous powders, Journal of the European Ceramic Society, 34(7), (2014) 1643-1666.

[4] R. Lakes, Materials with structural hierarchy, Nature 361(6412), (1993) 511-515.

[5]

[6] H. Seitz, W. Rieder, S. Irsen, B. Leukers, C. Tille, Three-dimensional printing of porous ceramic scaffolds for bone tissue engineering, Journal of Biomedical Materials Research Part B: Applied Biomaterials, 74(2), (2005) 782-788.

[7] E. Zanchetta, M. Cattaldo, G. Franchin, M. Schwentenwein, J. Homa, G. Brusatin, P. Colombo, Stereolithography of SiOC ceramic microcomponents. Advanced Materials, 28(2), (2016) 370-376.

[8] P. Yuan, D. Q. Wu, H. P. He, Z. Y. Lin, The hydroxyl species and acid sites on diatomite surface: a combined IR and Raman study, Applied Surface Science, 227(1), (2004) 30-39.

[9] F. A Sterrenburg, R. Gordon, M.A. Tiffany, S.S. Nagy, Diatoms, In Algae and cyanobacteria in extreme environments, Springer Netherlands (2007) 141-172)

[10] T.P. Dolley, Diatomite, Ceramic Bulletin, 70(5), (1991) 860.

[11] R. Leboda, Carbon-mineral adsorbents-new type of sorbents? Part I: The methods of preparation, Mat Chem Phys, 31, (1992) 243-255.

[12] A.C. Aydin and R. Gül, Influence of volcanic originated natural materials as additive on the setting time and some mechanical properties of concrete, Construction and building materials, 21, (2007) 1277-1281.

[13] M. Reguerio, J.P. Calvo, E. Elizaga and V. Calderon, Spanish diatomite geology and economics, Industrial Minerals and Rocks, 306, (1993) 57–67.

[14] J.B. Caillerie, M.R. Aimeur, Y.E. Kortobi, A.P. Legrand, Water adsorption on pyrogenic silica followed by 1h MAS NMR, J. Coll. Interface Sci., 194, (1997) 434-439.

[15] R.K. Iler, The Chemistry of Silica, Wiley, Ed. J. Wiley and Sons, New York, (1979).

[16] H. E. Bergna, Colloid chemistry of silica: an overview, in: H.E. Bergna (Ed.), The Colloid Chemistry of Silica, American Chemical Society, (1994) 1-47.

[17] T. Takei, K. Kato, A. Meguro, M. Chikazawa, Infrared spectra of geminal and novel triple hydroxyl groups on silica surface. Colloids and Surfaces A: Physicochemical and Engineering Aspects, 150(1), (1999) 77-84.

[18] S. Ek, A. Root, M. Peussa, L. Niinisto, Determination of the hydroxyl group content in silica by the thermogravimetry and a comparison with HMAS NMR results, Thermochim. Acta, 379, (2001) 201–212.

[19] C.E. Bronnimann, R.C. Zeigler, G.E. Maciel, Proton NMR study of dehydration of the silica gel surface, J. Am. Chem. Soc., 110, (1988) 2023–2026.

[20] K. Sing, The use of nitrogen adsorption for the characterisation of porous materials, Colloids and Surfaces A: Physicochemical and Engineering Aspects, 187, (2001) 3-9.

[21] M. A. M. Khraisheh, M. A. Al-Ghouti, S.J. Allen, M.N. Ahmad, Effect of OH and silanol groups in the removal of dyes from aqueous solution using diatomite, Water Research, 39(5), (2005) 922-932.

[22] L. Verdolotti, B. Liguori, I. Capasso, A. Errico, D. Caputo, M. Lavorgna, S. Iannace, Synergistic effect of vegetable protein and silicon addition on geopolymeric foams properties, Journal of Materials Science 50(6), (2014) 2459-2466.

[23] P. Colombo, J.R. Hellmann, D.L. Shelleman, Mechanical properties of silicon oxycarbide ceramic foams, Journal of the American Ceramic Society 84(10), (2001) 2245–2251.

[24] L. Verdolotti, M. D'Auria, M. Lavorgna, P. Vollaro, S. Iannace, I. Capasso, B. Galzerano, D. Caputo, B. Liguori, Organic-inorganic hybrid foams with diatomite addition: Effect on functional properties, AIP Conference Proceedings, 1736(1), (2016) 020127.

[25] L. Verdolotti, S. Iannace, M. Lavorgna, R. Lamanna, Geopolymerization reaction to consolidate incoherent pozzolanic soil. Journal of materials science, 43(3), (2008) 865-873.

[26] J. Ortego, J. D., Barroeta, Y., Cartledge, F. K., and Akhter, H., Leaching effects on silicate polymerization. An FTIR and silicon-29 NMR study of lead and zinc in portland cement. Environmental science & technology, 25(6), (1991) 1171-1174.

[27] S. Lucas, M.T. Tognonvi, J-L. Gelet, J. Soro, S. Rossignol, Interactions between silica sand and sodium silicate solution during consolidation process, Journal of Non Crystalline Solids, 357, (2011) 1310-1318.

[28] M.A. Biot, Generalized theory of acoustic propagation in porous dissipative media, Journal of the Acoustical Society of America 34(9A), (1962) 1254-1264.

[29] G. Iannace, C. Ianniello, L. Maffei, R. Romano, Assorbimento acustico di strati di pietrisco sciolto, Proceedings XXVII Convegno Nazionale dell'Associazione Italiana di Acustica, (1999) 116-119.

[30] M. Lavorgna, L. Verdolotti, L. Mascia, Organic–Inorganic Bio-Hybrid Materials by SolGel Processing. In Biofoams: Science and Applications of Bio-Based Cellular and Porous Materials, CRC Press (2015) 39-60.

[31] A. L. Leal-Cruz, M. I. Pech-Canul, In situ synthesis of Si_3N_4 in the Na 2 SiF 6–N 2 system via CVD: Kinetics and mechanism of solid-precursor decomposition. Solid State Ionics, 177(39), (2007) 3529-3536.

[32] UNI EN 13501-1. Fire classification of construction products and building elements. Classification using test data from reaction to fire tests.

[33] 2009/ISO 834. Fire resistance test-elements of building construction, (1999).

[34] ASTM:E119. Standard Test Methods for Fire Tests of Building Construction and Materials.

[35] B. Schartel, T.R. Hull, Development of fire-retarded materials – interpretation of cone calorimeter data, Fire Mater, 31, (2007) 327–54.

[36] V. Babrauskas, R.D. Peacock, Heat release rate: the single most important variable in fire hazard, Fire Safety J, 18, (1992) 255–72.

[37] ISO 5660-1. Reaction-to-fire tests – Heat release, smoke production and mass loss rate – Part 1: Heat release rate (cone calorimeter method), (2002).

[38] S. Bourbigot, F. Samyn, T. Turf, S. Dusquense, Nanomorphology and reaction to fire of polyurethane and polyamide nanocomposites containing flame retardants, Polym Degrad Stab, 95, (2010) 320–6.

[39] ISO 554, Standard atmospheres for conditioning and/or testing–specifications, (2002).

[40] R.V. Petrella, The assessment of full-scale fire hazards from cone calorimeter data, J Fire Sci, 12, (1994) 15–43.

[41] S. M. Peltola, F. P. Melchels, D. W. Grijpma, M. Kellomäki, A review of rapid prototyping techniques for tissue engineering purposes, Annals of medicine, 40(4), (2008) 268-280.

[42] S. H. Huang, P. Liu, A. Mokasdar, L. Hou, Additive manufacturing and its societal impact: a literature review, The International Journal of Advanced Manufacturing Technology, 67(5-8), (2013) 1191-1203.

[43] T.J. Horn, O.L. Harrysson, Overview of current additive manufacturing technologies and selected applications. Sci Prog, 95(3), (2012) 255-82.

[44] A.R. Studart, Additive manufacturing of biologically-inspired materials. Chemical Society Reviews, 45(2), (2016) 359-376.

[45] K. C. Hribar, P. Soman, J. Warner, P. Chung, S. Chen, Light-assisted direct-write of 3D functional biomaterials, Lab on a chip, 14(2), (2014) 268-275.

[46] K. F. Leong, C. M. Cheah, C. K. Chua, Solid freeform fabrication of three-dimensional scaffolds for engineering replacement tissues and organs. Biomaterials, 24(13), (2003) 2363-2378.

[47] F.P.W. Melchels, J. Feijen, D.W. Grijpma, A review on stereolithography and its applications in biomedical engineering. Biomaterials, 31(24), (2010) 6121-6130.

Conclusions

The aim of this PhD research activity is the design and synthesis of hybrid foams with hierarchical porosity starting from a ceramic matrix based on alkali activated alumino-silicate structures. Alkali-bonded ceramic foams have already very interesting applications as thermal and acoustic insulators, catalysts, filters, which can be extended by tailoring their porosity in the nano-to-ultramacro range. In fact, materials with tailored porosity exhibit special properties and features that usually cannot be achieved by their conventional dense counterparts. Moreover, chemical consolidation by geopolymerization can be considered a sustainable alternative to produce ceramic foams with 3D porous architectures without using high temperatures treatments (such as burnout of organics and sintering).

In this work, alkali activated ceramic foams have been produced by using metakaolin and/or diatomite as aluminosilicate source, an aqueous sodium silicate solution as alkali activator and Na_2SiF_6 as a catalyst that promotes the gelification of the entire system. The so obtained system has been foamed using direct foaming. In particular, two different techniques of direct foaming have been coupled, one based on chemical reactions with gas production and the other one based on a mechanical foaming. The chemical foaming was obtained by gaseous hydrogen, H_2, produced through the redox reaction of Si powder in the alkaline media. The mechanical foaming was performed by the addition of a natural surfactant (vegetable protein) within the matrix, previously foamed. This approach allows to tailor the chemical–physical properties and density of the resulted hybrid foams. Three different ceramic foams were prepared. All of the three ceramic foams are based on the same starting mixture, the only difference consisted in the pore forming agent used to generate porosity inside the geopolymeric matrix. The first foam, was prepared using only the silicon powder as pore forming agent, the second one was prepared by adding a ‘‘meringue’’ type foam, obtained from the whipping of the vegetable protein . Finally, the third foam was prepared using simultaneously the Si powder and the whipped protein, adding both of them to the starting mixture. The so produced foams were characterized from mechanical, morphological and chemical point of view. In particular, the mechanical characterization has been carried out through flexural and compressive tests, the chemical one using FT-IR spectroscopy and the scanning electron microscopy (SEM) has been used to look at the morphology and porosity of the produced foamed systems.

It was found out that the synergistic effect of the two different foaming agents, leads to an hybrid ceramic foam characterized by more interconnected and open porosity with homogeneous pore size distribution (ranging from 200 to 700 μm) and a low density preserving, at the same time, mechanical properties mediated between ceramic and polymeric foams. So, the hybrid foam obtained has been selected as the best candidate for further investigations in order to be used as possible innovative inorganic material for thermal and acoustic insulation.

The following step, in order to be able to tailor the porosity of the hybrid geopolymeric foam, has been the addition of two other levels of hierarchical porosity. The idea was to add porosity on both nanometric and macrometric scale to the expanded system.

The nano-porosity has been included into the system using diatomite, a sedimentary rock composed of rigid cell walls, called frustules ranging from less than 1 to more than 100 μm and characterized by protuberances and pores close to 100 nm, as partial or total (5, 10, 50, 70 and 100% by weight) replacement of the metakaolin in the starting geopolymeric matrix.

The macropores have been added to the hybrid ceramic foams by a 3D printed polymeric template (3D printing inverse replica method).

The produced foams have been mechanically, chemically, physically and morphologically characterized. Moreover, their acoustic and thermal properties, in terms of thermal stability and conductivity, and also their fire behavior have been investigated.

The addition of diatomite, changed the microstructure, porosity and functional properties of the ceramic foam according to the different amounts added to the starting mixtures. In particular, the mechanical properties increase with the increasing of diatomite and the dimensions of pores seem to decrease with the increasing of diatomite content, while their finesse and homogeneous distribution seem to increase with the increasing of diatomite. The difference in the microstructures can be ascribed to the different chemical mechanism of consolidation of the foams. For the samples with lower percentages of diatomite, in fact, the consolidation and hardening processes are consequences of a typical geopolymeric reaction. For the foams produced with higher amounts of diatomite, the consolidation process, changed from geopolymerization to a silicate polycondensation mechanism. The replacement of diatomite, in fact, leads to a consolidation process due to

the formation of a polysilicate on the surface of diatomite. In particular, the polycondensation of sodium silicate as glassy materials produced bridges between grains and, ensuring higher cohesion, resulted in a more homogeneous microstructure and, as a consequence, in better mechanical properties.

Moreover, the addition of diatomite causes a reduction in the thermal conductivity of the foams obtained, starting from a value of 0.128 W/m·K, for the metakaolin based hybrid foam, to a value of 0.074 W/m·K for the ceramic foam produced using only diatomite. Cone calorimeter results, performed in order to find out the fire behavior properties of the ceramic foams, showed that samples in the condition of external heat flux do not burn, so that they can be considered not flammable, regardless of the content of diatomite. The presence of diatomite affects the acoustic absorption behavior of hybrid foams, widening the range of sound absorption frequencies. This kind of features, makes these materials really interesting and promising in the field of thermal and acoustic insulation.

The last part of this research activity has been focused on the addition of a further level of hierarchical porosity to the already studied hybrid expanded ceramic systems. In particular, the addition of macropores, in the range of millimetric dimensions, has been performed using the 3D printing inverse replica method. Polymeric templates with different geometries have been used in order to generate periodic and regular pattern of millimetric pores within the matrix.

In conclusion, it is possible to assess that the coupled use of different foaming methods and starting raw materials, combined to the use innovative manufacturing techniques, like 3D printing process, leads to the possibility of producing macroporous hybrid ceramic foams with different porous architectures ranging from three orders of magnitudes: macro (sacrificial template or 3D inverse replica), micro (pores obtained by chemical and/or mechanical foaming) and nano (diatomite).

Data collected in this this experimental work, focused on the combined use of innovative production methods (3D printing) and sustainable innovative materials (hybrid geopolymeric and ceramic foams) result to be really promising and drive to further investigations in this field. Firstly, a deeper investigation of the influence of template geometry, using more complex shapes and different materials in the template production, is necessary. The most ambitious and interesting idea could be the direct 3D printing of the ceramic foams produced, directly using the ceramic slurries as ink in the 3D printing process in order to attain defined and specific designed final geometries and structures

which properly fit and satisfy the final properties wanted. This kind of approach would request a deepened study of the rheology of the expanded systems produced.